

EARTHQUAKE FOCAL MECHANISMS IN THE
SOUTHEASTERN UNITED STATES

A THESIS

Presented to

The Faculty of the Division of Graduate
Studies

By

Stewart Allen Guinn

In Partial Fulfillment


of the Requirements for the Degree
Master of Science in Geophysical Sciences

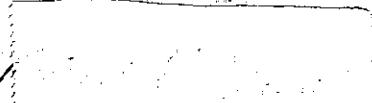
Georgia Institute of Technology

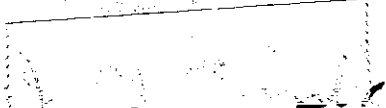
December, 1977

EARTHQUAKE FOCAL MECHANISMS IN
THE SOUTHEASTERN UNITED STATES

Approved:


L. Timothy Long, Chairman


Robert P. Lowell


J. Marion Wampler

Date approved by Chairman

Oct 10 1977

ACKNOWLEDGMENTS

The author wishes to express his thanks and appreciation to those persons who gave freely of themselves during the course of this research. Special recognition is given to Dr. Leland Timothy Long, who served as the major director of this research. Dr. Long's ideas, guidance and support throughout this study are greatly appreciated. Dr. R. P. Lowell and Dr. J. M. Wampler served on my thesis reading committee. Their suggestions provided clarity and continuity to the manuscript. Their efforts are greatly appreciated.

I wish to thank Mrs. Mary K. Wharton of the United States Geological Survey, Branch of Earthquake Hazards, Mr. Charles W. Krapp of the Savannah River Plant Laboratories, Dr. Pradeep Talwani of the University of South Carolina at Columbia, Mr. T. N. Hodge of the Oak Ridge National Laboratory, Tennessee, and Dr. G. A. Bollinger of the Virginia Polytechnic Institute. These persons provided much of the data, in both published and unpublished forms, used in this thesis. Their efforts have been of great help.

The Duke Power Company and the Law Engineering Testing Company provided data from the Jocassee Reservoir area in South Carolina. Thanks and appreciation go out to these organizations for being so cooperative.

Some of my fellow classmates have been instrumental in helping to solve various problems (e.g. field work, computer programs, etc.) encountered during the course of this study. They are (alphabetically) Mr. D. M. Dunbar, Mr. Helmut Y.A. Hsiao, Mr. G. E. Marion and Mr. W. R. (Bill) Volz.

A special note of thanks is given to my wife, Laurie, whose benevolence and love helped me accomplish the goal I set forth.

This research was supported mainly by a grant from the Georgia Power Company and in part by the Nuclear Regulatory Commission, grant number AT (49-24)-0210, and the National Science Foundation, Earth Science Section, NSF grant number DES 75-15756. I also want to thank the American Oil Company (New Orleans Division) for allowing me the time I needed to complete this study.

TABLE OF CONTENTS

	Page
ACKNOWLEDGMENTS	ii
LIST OF TABLES	vi
LIST OF ILLUSTRATIONS	vii
SUMMARY	xii
Chapter	
I. INTRODUCTION	1
II. THEORY	5
Early Observations Concerning the P Wave Motion	
Mathematical Model of Earthquake Foci	
III. DISCUSSION OF COMPUTER METHODS.	11
Description of Analysis Technique	
Method	
Grid Formulation	
Testing Procedure	
Examples	
IV. DISCUSSION OF DATA	26
Data Preparation	
The Conasauga, Tennessee Area	
The Maryville, Tennessee Area	
The Englewood, Tennessee Area	
The Clark Hill Reservoir Area	
The Jocassee Reservoir Area	
The Bowman, South Carolina Area	
The Charleston-Summerville, South Carolina Area	
The Reidsville, Georgia Area	
The Barnwell, South Carolina Area	
V. OVERALL DISCUSSION	122
VI. CONCLUSIONS	127
VII. RECOMMENDATIONS	129

TABLE OF CONTENTS (Continued)

	Page
APPENDIX	131
1 COMPUTER PROGRAM	134
BIBLIOGRAPHY	145

LIST OF TABLES

Table	Page
1. First Motion Data for the February 4, 1976 Conasauga, Tennessee Earthquake	30
2. First Motion Data for the Englewood, Tennessee Earthquake of July 27, 1977	45
3. First Motion Data for the August 2, 1974 Clark Hill Reservoir Area Earthquake	52
4. First Motion Data for 12 Clark Hill Reservoir Area Earthquakes of March 26, 1977	65
5. First Motion Data for Two Clark Hill Reservoir Area Earthquakes of April 14, 1977	69
6. First Motion Data for Two Clark Hill Reservoir Area Earthquakes of March 26, 1977	70
7. First Motion Data for the Bowman, South Carolina Earthquake of May 28, 1974	91
8. First Motion Data for the Bowman, South Carolina Earthquake of November 22, 1976	94
9. First Motion Data for the Charleston-Summerville, South Carolina Earthquake of April 28, 1975	101
10. First Motion Data for the Reidsville, Georgia Earthquake of December 27, 1976	114
11. First Motion Data for the Barnwell, South Carolina Earthquake of June 5, 1977.	118

LIST OF ILLUSTRATIONS

Figure	Page
1. Regional Map of Southeastern United States	4
2. Source Models	8
3. B Axis Grids	16
4. First Motion Plot of Test Data	21
5. Focal Mechanism Solutions of Test Data for Zero Errors	22
6. Focal Mechanism Solutions of Test Data for Several Errors.	23
7. First Motion Plot of North Atlantic Earthquake	24
8. Focal Mechanism Solutions for North Atlantic Earthquake.	25
9. Location Map and Intensity Data for the Conasauga, Tennessee Earthquake	28
10. First Motion Plot for the Conasauga, Tennessee Earthquake.	31
11. Focal Mechanism Solutions for the Conasauga, Tennessee Earthquake	32
12. Location Map and Historical Earthquake Epicenter for the Maryville, Tennessee Area	34
13. Geologic Map with November 30, 1973 Maryville, Tennessee Earthquake Sequence	36
14. First Motion Plot for the Maryville, Tennessee Area Earthquake of November 30, 1973	38
15. Focal Mechanism Solutions for the Maryville, Tennessee Area Earthquake of November 30, 1973.	39
16. Composite First Motion Plot of 14 Maryville, Tennessee Area Aftershocks	41
17. Focal Mechanism Solutions for 14 Composite Maryville, Tennessee Area Aftershocks for 4 Errors.	42
18. Focal Mechanism Solutions for 14 Composite Maryville, Tennessee Area Aftershocks for 7 Errors.	43

LIST OF ILLUSTRATIONS (Continued)

Figure	Page
19. First Motion Plot for the Englewood, Tennessee Area Earthquake of July 27, 1977	46
20. Focal Mechanism Solutions for the Englewood, Tennessee Area Earthquake of July 27, 1977	47
21. Geologic Map of the Clark Hill Reservoir Area	49
22. First Motion Plot for the August 2, 1974 Clark Hill Reservoir Area Earthquake	53
23. Focal Mechanism Solutions for the August 2, 1974 Clark Hill Reservoir Area Earthquake	54
24. First Motion Plot for an April 14, 1977 Clark Hill Reservoir Area Microearthquake.	55
25. Focal Mechanism Solutions for an April 14, 1977 Clark Hill Reservoir Area Microearthquake.	56
26. Composite First Motion Plot (case 1) for the Clark Hill Reservoir Area	58
27. Composite First Motion Plot (case 2) for the Clark Hill Reservoir Area	59
28. Focal Mechanism Solutions (case 1) for the Clark Hill Reservoir Area	60
29. Focal Mechanism Solutions (case 2) for the Clark Hill Reservoir Area	61
30. Composite First Motion Plot (case 1 and 2) for the Clark Hill Reservoir Area	62
31. Focal Mechanism Solutions (case 1 and 2) for the Clark Hill Reservoir Area	63
32. Composite First Motion Plot of 12 Clark Hill Reservoir Area Microearthquakes of March 26, 1977	67
33. Focal Mechanism Solutions for 12 Composite Clark Hill Reservoir Area Microearthquakes of March 26, 1977	68

LIST OF ILLUSTRATIONS (Continued)

Figure	Page
34. Composite First Motion Plot for 2 Clark Hill Reservoir Area Microearthquakes of April 14, 1977	71
35. Composite First Motion Plot of 2 Clark Hill Reservoir Area Microearthquakes of March 26, 1977	72
36. Focal Mechanism Solutions for 2 Clark Hill Reservoir Area Microearthquakes of April 14, 1977	73
37. Focal Mechanism Solutions for 2 Clark Hill Reservoir Area Microearthquakes of March 26, 1977	74
38. Geologic Map of the Jocassee Reservoir Area	78
39. Composite First Motion Plot (All Data) for Events at the Jocassee Reservoir Area	81
40. Focal Mechanism Solutions (All Data) for Events at the Jocassee Reservoir Area	82
41. Composite First Motion Plot for Events Beneath the Deep Portion of the Jocassee Reservoir	84
42. Focal Mechanism Solutions for Events Beneath the Deep Portion of the Jocassee Reservoir	85
43. Composite First Motion Plot for Events Outside the Bounds of the Jocassee Reservoir	86
44. Focal Mechanism Solutions for Events Outside the Bounds of the Jocassee Reservoir	87
45. First Motion Plot for the Bowman, South Carolina Earthquake of May 28, 1974	92
46. Focal Mechanism Solutions for the Bowman, South Carolina Earthquake of May 28, 1974	93
47. First Motion Plot for the Bowman, South Carolina Earthquake of November 22, 1976	96
48. Focal Mechanism Solutions for the Bowman, South Carolina Earthquake of November 22, 1976	97

LIST OF ILLUSTRATIONS (Continued)

Figure	Page
49. Simple Bouguer Gravity Map of the Summerville, South Carolina Area	100
50. First Motion Plot for the Charleston-Summerville, South Carolina Area Earthquake of April 28, 1975	102
51. Focal Mechanism Solutions for the Charleston-Summerville South Carolina Area Earthquake of April 28, 1975	103
52. Composite First Motion Plot for Events in the Charleston-Summerville, South Carolina Area.	105
53. Focal Mechanism Solutions for Events in the Charleston-Summerville, South Carolina Area for 11 Errors.	106
54. Focal Mechanism Solutions for Events in the Charleston-Summerville, South Carolina Area for 12 Errors.	107
55. Composite First Motion Plot for the November 22, 1974 Charleston-Summerville Area Earthquake and Aftershock . . .	108
56. Focal Mechanism Solutions for the November 22, 1974 Charleston-Summerville Area Earthquake and Aftershock for 4 Errors	110
57. Focal Mechanism Solutions for the November 22, 1974 Charleston-Summerville Area Earthquake and Aftershock for 5 Errors	111
58. Intensity Map of the Reidsville, Georgia Earthquake	112
59. First Motion Plot for the Reidsville, Georgia Earthquake ..	115
60. Focal Mechanism Solutions for the Reidsville, Georgia Earthquake for 1 Error	116
61. Focal Mechanism Solutions for the Reidsville, Georgia Earthquake for 2 Errors.	117
62. First Motion Plot for the Barnwell, South Carolina Earthquake of June 5, 1977	120
63. Focal Mechanism Solutions for the Barnwell, South Carolina Earthquake of June 5, 1977	121

LIST OF ILLUSTRATIONS (Continued)

Figure	Page
64. Southeastern United States Map Showing Focal Mechanism Solutions	125
65. Flowchart of Main Program	133

SUMMARY

Given a finite number of P wave first motions there exists a domain of valid focal mechanism solutions which satisfies the requirements set forth by the theory of the double couple without moment earthquake source. An analysis technique, adapted for computer application, which determines the domain of valid focal mechanism solutions in terms of the orthogonal pressure, tension, and null axis directions is developed. Focal mechanism solutions using the proposed analysis technique are determined for nine epicentral areas in the southeastern United States from published and new focal mechanism data. Focal mechanisms are proposed from the solutions and other geologic and geophysical data. In general, the focal mechanism solutions indicate that southeastern intraplate seismic activity does not appear to be the result of a single dominant stress direction. Many of the solutions support nearly vertical fault planes suggesting a low level compressional to tensional environment for the Southeast.

CHAPTER I

INTRODUCTION

Earthquakes in the southeastern United States have been reported by inhabitants since the early 1700's (see Bollinger (1975) and Moneymaker (1954,55,57)). However, accurate locations and focal mechanism solutions for these have not been possible until recently because of a sparsity of instrumental data. Earthquake activity in the southeast is sparse, about one event per year of intensity IV or larger. Most of the recent data comes from studies made on intensity IV earthquakes or microearthquakes recorded by portable seismometers.

This paper is an analysis of focal mechanism data (P wave first motions) obtained from recent southeastern United States earthquakes. It is also a review and analysis of published focal mechanism solutions and focal mechanism data for the southeastern United States. In general, the maximum number of usable P wave first motions for an intensity IV or larger earthquake in the southeast is about twenty. Because of this sparsity of first motion data, a technique adapted for computer application was developed. The technique finds focal mechanism solutions by defining the domain of valid pressure (P), tension (T), and null (B) axes over the focal sphere. The objective is to characterize focal mechanisms in the southeast and perhaps define the operative stress field using the results from the computer adapted technique.

Major areas of earthquake activity such as the Circum Pacific Belt receive considerable attention since the numbers and magnitudes of earth-

quakes allow researchers from many seismic observatories world-wide to study their seismic implications. Focal mechanisms and tectonic theories may be constrained and tested with data from such earthquake prone areas. For example, actual ground breakage resulting from a magnitude $M = 6.7$ (i.e. Richter magnitude scale) earthquake, which occurred in the Varto area of eastern Turkey, has been observed and related to focal mechanism data (Wallace, 1968). Reliable, consistent, stress directions have been obtained from focal mechanism solutions involving earthquakes of intermediate to deep focus.

Focal mechanism solutions are difficult to obtain in the southeast because the number of recording stations and their distribution are limited. Attempts to determine focal mechanism solutions often give ambiguous results. Published focal mechanism solutions for the southeast, although sparse, generally are developed from composite first motion data due to limited station distributions around epicenters. The focal mechanism solutions often show ambiguous fault plane orientations, direction of faulting, and principle stress directions, and hence are ambiguous in their tectonic implications. Focal mechanism solutions preceding or contemporaneous with this study have not been related to any known faults, although there are numerous faults near many of the epicenters. The major faults in the Southeast are generally believed to be aseismic.

Focal mechanism solutions are usually determined from the direction of the P wave first onset as determined from vertical component seismometers and are often constrained with S wave polarization (McKenzie, 1969). Also focal mechanism solutions may be obtained from surface waves (Brune,

1961) and from the amplitudes of free oscillations (Gilbert and MacDonald, 1961). However, according to McKenzie (1969) these solutions are typically less reliable than solutions obtained from P wave first motions.

The analysis of focal mechanism data presented here utilizes the P wave first motion as recorded by regional observatories and by portable microearthquake recorders. New focal mechanism data and published focal mechanism solutions from both macroearthquakes and microearthquakes are evaluated.

In this study focal mechanism solutions are determined for earthquakes in three physiographic provinces in the southeastern United States; the Valley and Ridge Province, the Crystalline Piedmont Province, and the Coastal Plain Province. Focal mechanism solutions are determined for 9 epicentral areas; the Conasauga, Tennessee area (CTA), the Maryville, Tennessee area (MTA), the Englewood, Tennessee area (ETA), the Clark Hill Reservoir area (CHRA), the Jocassee Reservoir area (JRA), the Bowman, South Carolina area (BSCA), the Charleston-Summerville, South Carolina area (CSSCA), the Reidsville, Georgia area (RGA), and the Barnwell, South Carolina area (BASCA) (figure 1).

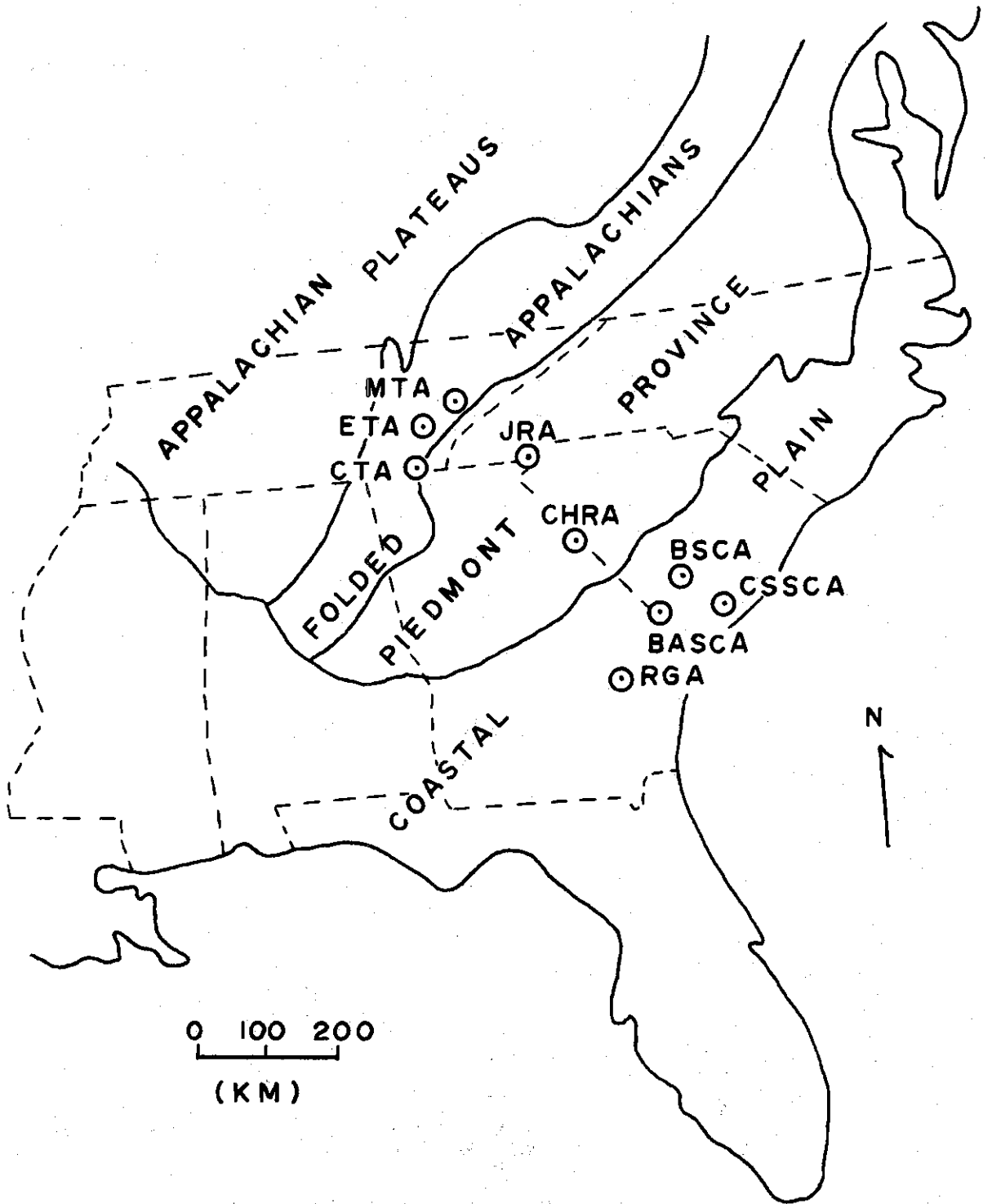


Figure 1. Regional Map of Southeastern United States Showing Data Areas (Raisz, 1970).

CHAPTER II

THEORY

Early Observations Concerning The P Wave First Motion

In the early days of seismology the first impulse of a P wave was noted to consistently be either upward or downward on the record for earthquakes occurring in certain regions. According to Stauder (1962b), Galitzin (1909) was probably the first to systematically use these motions as a method of locating earthquake epicenters by constructing vector diagrams from motions read from three component seismometers. He noted that an upward ground displacement was a compression and the resultant motion pointed away from the epicenter. If the ground displacement was downward, the motion was a rarefaction and pointed toward the epicenter.

Byerly (1926) first proposed that P wave first motions could be used to determine the forces acting at an earthquake source. Byerly's insight is confirmed by Nakano's (1923) analysis of displacements and accelerations in an infinite, elastic, homogeneous medium due to the action of various types of point sources. Nakano (1923) determined that a source consisting of two oppositely directed forces would give rise to alternate compressions and dilatations in quarter spaces separated by two orthogonal null planes.

The initial objective of focal mechanism studies was to determine nodal planes separating regions of compression and dilatation as resolved from P wave first motions and to interpret the nodal planes relative to

the displacements or forces at a given source (Stauder, 1962b).

Mathematical Model of Earthquake Foci

The basic theory of point sources was derived by Love (1904) and has been properly adapted to focal mechanisms. The formulation of a mathematical model for force systems, described below, follows Stauder (1962b).

Single and Double Force Systems

Let $r(x, y, z, t)$ be the resultant of the body forces per unit mass acting within a certain region A of an infinite elastic space. The displacement of any point in space is some integral effect of all the forces in A . If the limit concept is applied by assuming all linear dimensions of A reduce to zero and also r increases without limit such that the integral over A remains finite, then the force function is

$$R(t) = \lim_{A \rightarrow 0} \iiint \rho r(x, y, z, t) \, dx \, dy \, dz \quad (1)$$

where ρ is the density of the medium. The function $R(t)$ represents the simplest point source, a single force acting at a point in space. Keilis-Borok et al. (1957), in their analysis of point sources, chose a rectangular coordinate system in which the focus coincided with the origin and the force $R(t)$ acted along the positive X axis. The displacements of the longitudinal and transverse waves at large distances are given by

$$\begin{aligned} U_{\alpha}(q) &= \frac{1}{4\pi\rho} \frac{xq}{\alpha^2 L^3} R(t-L/\alpha) \\ U_{\beta}(q) &= \frac{1}{4\pi\rho} \frac{1}{\beta^2} \frac{\partial^2 L}{\partial x \partial q} R(t-L/\beta) \end{aligned} \quad (2)$$

where α , β , γ denote the P wave velocity, S wave velocity, (x,y,z) , and $L = \sqrt{x^2+y^2+z^2}$.

Sources of higher order may be obtained from the force function $R(t)$ by letting two forces $\pm \frac{1}{e} R(t)$ act at the points $(0, \pm \frac{e}{2}, 0)$ as shown in figure 2a. Then the displacement at any point will be the sum of displacements of each force acting separately. As $e \rightarrow 0$ the displacements may be written

$$\begin{aligned} U_{\alpha}^{(q)} &= -C \frac{\partial}{\partial y} \left\{ \frac{xq}{\alpha^2 L^3} R(t-L/\alpha) \right\} \\ U_{\beta}^{(q)} &= -C \frac{\partial}{\partial y} \left\{ \frac{1}{\beta^2} \frac{\partial^2 L}{\partial x \partial q} R(t-L/\beta) \right\} \end{aligned} \quad (3)$$

where C is the constant from (2). This force system represents the dipole with moment or the type I force system of Honda (1957) and requires two orthogonal nodal planes in its application. Byerly's method assumes the type I source in which the nodal planes represent two possible planes of fracture, an auxiliary plane and the actual fault plane. The type I force system may be subdivided into two groups depending on the moment direction which produces either clockwise (Type Ia) or counter clockwise (Type Ib) rotation (figure 2b).

By superimposing two dipoles of opposite moment the double couple without moment model or type II force system of Honda (1957) may be obtained as shown in figures 2c and 2d. The displacements are given by adding the contribution from each dipole as given below:

$$\begin{aligned} U_{\alpha}^{(q)} &= C \left\{ -\frac{\partial}{\partial y} \left(\frac{xq}{\alpha^2 L^3} R(t-L/\alpha) \right) - \frac{\partial}{\partial x} \left(\frac{yq}{\alpha^2 L^3} R(t-L/\alpha) \right) \right\} \\ U_{\beta}^{(q)} &= C \left\{ -\frac{\partial}{\partial y} \left(\frac{1}{\beta^2} \frac{\partial^2 L}{\partial x \partial q} R(t-L/\beta) \right) - \frac{\partial}{\partial x} \left(\frac{1}{\beta^2} \frac{\partial^2 L}{\partial y \partial q} R(t-L/\beta) \right) \right\} \end{aligned} \quad (4)$$

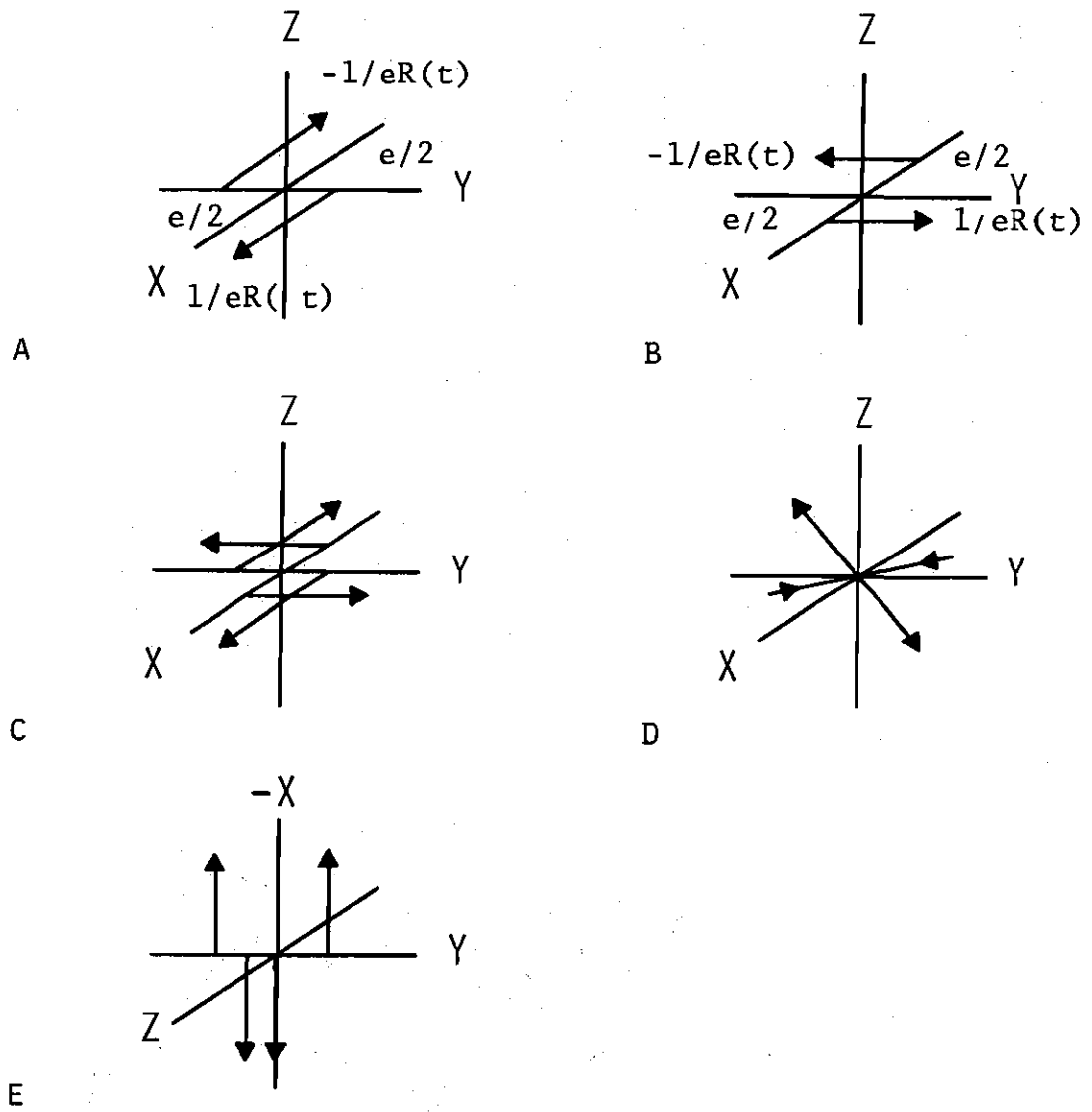


Figure 2. Single and Double Force Systems (after Stauder, 1962).

In the type II source model the nodal planes separate regions of compressive stress from regions of tensile stress.

The order of the source is determined by the number of differentiations. Then for n differentiations the order is $n + 1$. Figure 2e represents a third order source or the double couple with moment model. The displacements given by Keilis-Borok et al. (1957) are:

$$\begin{aligned} U_{\alpha}^{(q)} &= c \frac{\partial^2}{\partial y^2} \left\{ \frac{xq}{\alpha^2 L^3} R(t-L/\alpha) \right\} \\ U_{\beta}^{(q)} &= c \frac{\partial^2}{\partial y^2} \left\{ \frac{1}{\beta} \frac{\partial^2 L}{\partial x \partial q} R(t-L/\beta) \right\} \end{aligned} \quad (5)$$

From this and more involved work two basic questions concerning focal mechanisms arose in the early 60's: 1) Which model, the type I or type II force systems, if either, represents an earthquake focus? 2) Assuming a type I source, which of the two nodal planes is the fault plane? Honda (1961) pointed out that the radiation patterns from the two models were identical for the P wave, but different for the S wave.

Steketee (1958) has shown that the mechanism of fault production is analogous with the theory of dislocations on a much smaller scale (i.e. solid state physics). The fundamental concept of dislocation theory is that there exists a local discontinuity in the displacement vector or a center of dislocation. Two types of dislocation centers are found. The first type is a discontinuity in displacement normal to the surface. The second type is a discontinuity in displacement parallel to the surface. The first type is related to dilatational stress and the second type is related to two shearing couples (Garland, 1971). The dislocation theory requires that the body be in static equilibrium at each point, before and

after failure. Therefore a two couple system is required. According to Garland (1971), it is this strong reason that the double couple model is favored over the single couple model. In general, the double couple without moment model of the earthquake source is used in the interpretation of P and S wave data (Herrmann, 1975). All focal mechanisms presented in this thesis assume the double couple without moment model.

CHAPTER III

DISCUSSION OF COMPUTER METHODS

A number of computer techniques for determining focal mechanism solutions utilizing body waves have been developed in recent years. Programs using P waves have been developed by Knopoff (1961), Kasahara (1963), Wickens and Hodgson (1967), and Keilis-Borok et al. (1972). Programs using S wave polarization angles have been developed by Udias (1964), Hirasawa (1966), and Stevens (1967). Keilis-Borok et al. (1972) developed a program which utilizes the directions of the SH and SV first motions. Programs using P and S wave data have been developed by Udias and Baumann (1969), Chandra (1971), and Dillinger, Pope and Harding (1972).

Of these methods, the technique described by Dillinger et al. (1972) is most similar in concept to the program presented here. Two main differences, which affect the final solutions, exist between their technique and the one presented here. The technique presented here uses only P wave first motions whereas the technique given by Dillinger et al. (1972) uses P and S wave data. The second main difference is that the P and S wave observations are combined in the technique by Dillinger et al. (1972) to give a maximum likelihood solution using the likelihood functions given by Pope (1972). According to Pope (1972) the solution is determined by generating likelihoods over a discrete grid covering the parameter space. The likelihood values are then contoured to show regions of maximum likelihood. By an appropriate calibration of the contours of the regions,

they may be interpreted as fiducial regions which express the quality of the focal mechanism solution. A good solution is one in which the fiducial regions are small, and a poor solution is one in which the fiducial regions are large and distorted (Pope, 1972). The method herein does not employ statistical relations as does the technique given by Dillinger et al. (1972) or attempt to find a single solution, but rather maps out the domain of valid focal mechanism solutions in terms of the pressure, tension, and null axis directions (PTB) as warranted by the first motion data.

The combination of P wave first motions and S wave polarization data at teleseismic distances generally provides well constrained focal mechanism solutions. However, the epicentral distances investigated in this study are within about 500 Km and as Nuttli (1961) points out, S wave particle motion at distances less than 44° is nonlinear, i.e. the vertical, radial and tangential components of the S wave at the free surface are not linear with respect to one another due to the free surface effect.

Description of Analysis Technique

The analysis technique developed in this study (see appendix 1 for computer program listing) is an iterative search for the domain of valid focal mechanism solutions allowed by the P wave first motions. A 5 x 5 grid of B axes is generated and used to cover the focal sphere. For each B axis position possible solutions are tested in accordance with the double couple without moment model. The spacing of the grid depends on the increment angle employed. The B axis and data are referenced to a right-handed rectangular coordinate system which is defined such that the

positive (x_1, x_2, x_3) axes are north, east and down, respectively. The B axes are then used to define new coordinate systems in which the x_3 axis corresponds to the B axis. The first motions are then transformed to the new system. The data are rotated about the x_3 axis of the new system in increments and the data are systematically checked in each increment for the total number of points lying the proper quadrants. The number of inconsistent first motions (for each increment) is defined in advance. A solution is found when the total number of first motions in the proper quadrants is less than or equal to this predefined value. This procedure is repeated for all of the B axes in the 5×5 grid. Finally, all of the solutions (PTB) are plotted on the lower half of the focal sphere on a Wulff net projection. The resulting domain size and shape depend on the distribution and number of observations. The dependence of the domain on single data points may be determined by allowing additional inconsistent first motions. In so doing the relative change in the domain size gives an indication as to how dependent the solutions are on one or a few of the observations.

Method

First motion data are defined for input in spherical coordinates assuming a focal sphere radius of unity. The data are mapped into reference coordinate system by the following

$$\begin{aligned}
 x_1^0 &= R \cos \theta \sin i_h \\
 x_2^0 &= R \sin \theta \sin i_h \\
 x_3^0 &= R \cos i_h
 \end{aligned}
 \tag{1}$$

where θ is the azimuth of the ray leaving the focus, i_h is the angle of incidence of the ray leaving the focus, and $R = 1$. The superscript zero denotes the reference or geographic coordinate system.

The B axis or null direction represents the intersection of the two nodal planes. The B axis may be used to form a new right-handed coordinate system, $X^i = (x_1^i, x_2^i, x_3^i)^T$, such that the i th B axis coincides with the i th x_3 axis. If the first motion data are transformed with respect to each new system, the determination of focal mechanism solutions is simply carried out by measuring the number and sign of the first motions lying in each quadrant. In the new system the nodal planes are given by the $(x_1^i, 0, x_3^i)$ and $(0, x_2^i, x_3^i)$ planes. A 3×3 transformation matrix which transforms data in the reference coordinate system to an i th coordinate system may be determined by knowing the trend (τ_3) and plunge (ϕ_3) of any B axis on the focal sphere. Let \bar{A}^i be the i th transformation matrix for the i th coordinate system. Then in matrix notation the transformation is accomplished by

$$X^i = \bar{A}^i X^0 \quad (2)$$

The relation which defines the direction cosines \bar{A}^i as given by Herrmann (1975) is

$$\begin{bmatrix} x_1^i \\ x_2^i \\ x_3^i \end{bmatrix} = \begin{bmatrix} \cos(\tau_1) \cdot \cos(\phi_1) & \sin(\tau_1) \cdot \cos(\phi_1) & \sin(\phi_1) \\ \cos(\tau_2) \cdot \cos(\phi_2) & \sin(\tau_2) \cdot \cos(\phi_2) & \sin(\phi_2) \\ \cos(\tau_3) \cdot \cos(\phi_3) & \sin(\tau_3) \cdot \cos(\phi_3) & \sin(\phi_3) \end{bmatrix} \begin{bmatrix} x_1^0 \\ x_2^0 \\ x_3^0 \end{bmatrix} \quad (3)$$

where τ_3 is measured clockwise in degrees from north and ϕ_3 is measured downward from the horizontal in degrees. The remaining arguments of the matrix are defined by;

$$\tau_1 = \tau_3 - \pi \quad \tau_2 = \tau_3 - \pi/2 \quad (4)$$

$$\phi_1 = \pi/2 - \phi_3 \quad \phi_2 = 0$$

The transformation matrix \bar{A}^i given in equation (2) and defined in equation (3) imparts a superfluous rotation of τ_3 . The unwanted rotation is removed by a rotational transformation matrix R^i and the rotation corrected transformation matrix A^i is found by matrix multiplication

$$A^i = R^i \bar{A}^i \quad (5)$$

where

$$R^i = \begin{bmatrix} -\cos(\tau_3) & \sin(\tau_3) & 0 \\ -\sin(\tau_3) & -\cos(\tau_3) & 0 \\ 0 & 0 & 1 \end{bmatrix} \quad (6)$$

Grid Formulation

The grid contains 25 B axis positions arranged in an equidistant 5 x 5 array. In the search for valid PTB axes the data are successively transformed into new coordinate systems with the B axis corresponding in each case to the X_3 axis. Figure 3 shows the B axis grid for an angle increment of 5, 10, 15 and 20 degrees. The distortion is due to the line printer display of the grid.

The transformation matrix, C^1 , to get to the first B axis (corner)

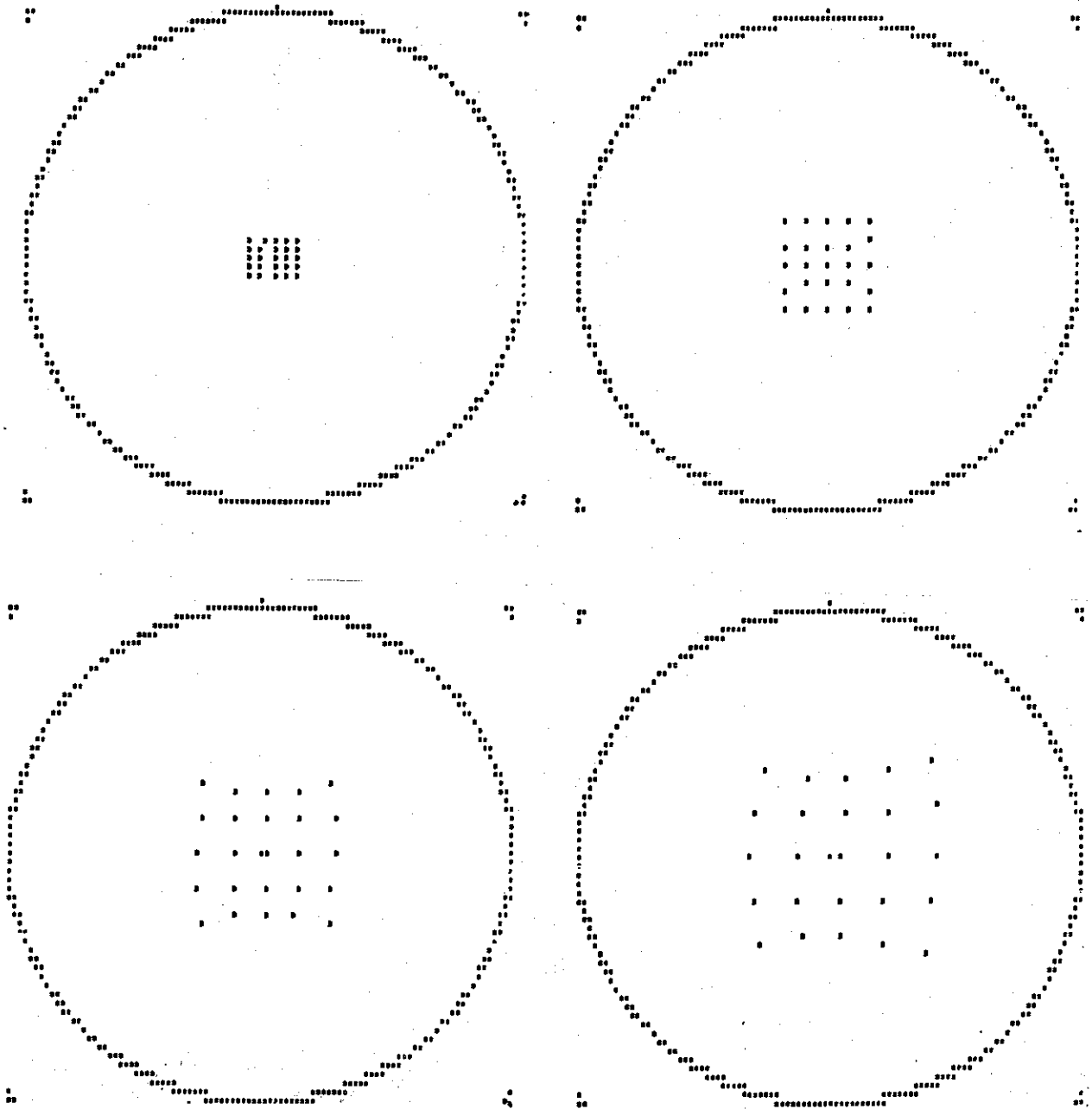


Figure 3. B Axis Grid for an Angle Increment of 5 Degrees, 10 Degrees, 15 Degrees, and 20 Degrees.

position in the grid, is determined for a $\tau_3 = \pi/4$ and $\phi_3 = \pi/2 - \sqrt{8} \Delta$, where Δ is the angle interval. The matrix C^1 is computed in the same manner as matrix A^i (corrected for rotation) from (5). The transformation matrix D^m , which transforms the first motion vectors from the reference coordinate system to the first grid position is given by

$$D^m = C^1 A^i \quad (m=i=1) \quad (7)$$

Then the first motions are transformed to the new system by

$$X^i = D^m X^0 \quad (m=i=1) \quad (8)$$

and searched for valid P and T axes. The remaining four B axis coordinate systems in the first row are reached by transforming the data successively to coordinate systems defined by a B axis with a trend of $\pi/2$ and a plunge of $\pi/2 - \Delta$. D^m , where $m = 2, 3, 4, 5$, represent the transformation matrices, corrected for rotation, for the remaining four positions. Then the first motion data transformed to the last grid position in the first row has the form

$$X^i = D^m X^{i-1} \quad (m=i=5) \quad (9)$$

Let E^1 be the transformation matrix, corrected for rotation, which transforms the fifth B axis position to the sixth B axis position (second row). E^1 is determined for a $\tau_3 = 104$ degrees and a $\phi_3 = \pi/2 - \sqrt{17} \Delta$. Then the transformation matrix F^n , which transforms the first motion vectors from the coordinate system given in (9) to the new system is given by

$$F^n = E^1 D^{n-1} \quad (n=6) \quad (10)$$

and the first motions are transformed to the first B axis position of the second row by

$$x^i = F^n x^{i-1} \quad (n=i-6) \quad (11)$$

The remaining four B axis positions of the second row are determined the same way as the first row of 4 remaining B axis positions were determined. The next row is reached in the same manner as the second row was reached. The above procedure is repeated until all 25 B axis positions are found and all first motion data are transformed to each new coordinate system.

Testing Procedure

After each transformation of first motion data to a new coordinate system as defined by the B axis, the data are tested for valid focal mechanism solutions. The test is performed by rotating the data in cylindrical coordinates about the x_3^i axis in increments (typically 5 degrees) for a total of 90 degrees. Since the nodal planes are orthogonal, 90 degrees of rotation is sufficient for testing because of the symmetry involved. The relation for testing the first motion data is given by

$$S = \left| \sum_{L=1}^{NM} \text{sgn}\{\arctan(X_1^i(L)/X_2^i(L) + \Delta\theta)\} \cdot \text{sgn}(Q) \right| \quad (12)$$

where the superscript i denotes the stage of transformation, NM represents the number of first motions, L indicates the L th first motion, $\Delta\theta$ represents the cumulative value of rotation, and Q represents the first motion direction as determined from seismograms, $Q = +1$ for compression and $Q = -1$ for dilatation. For each iteration S is compared against $NERR$, the number of errors allowed. If $S < NM - 2 \cdot NERR$ then that orientation does

not correspond to a solution and the data are rotated 5 degrees and checked again. If $S \geq NM-2$ NERR then that orientation satisfies the criteria for a solution and a set of P and T axes can be defined. The P and T axes in the i th coordinate system may be defined by

$$\begin{aligned} T^i &= (\sin(\theta^i), \cos(\theta^i), 0) \\ P^i &= (-\cos(\theta^i), \sin(\theta^i), 0) \end{aligned} \quad (13)$$

where $\theta^i = \text{sgn}(S) \frac{\pi}{4} - \Delta\theta$.

After the data have been rotated through 90° the P and T axes are saved in the i th coordinate system. The P and T axes are transformed back to the reference coordinate system by using the transpose of the i th transformation matrix and forming the product

$$\begin{aligned} P^0 &= (A^i)^T P^i \\ T^0 &= (A^i)^T T^i \end{aligned} \quad (14)$$

The transformation back to the reference coordinate system using $(A^i)^T$ is equivalent to using the inverse $(A^i)^{-1}$ since the transformation for mutually orthogonal normal vectors is a unitary matrix.

The B axis is required by theory to be orthogonal to the P and T axis so that the corresponding B axes may be found from the cross product

$$B^0 = T^0 \times P^0 \quad (17)$$

With all of the P and T axes computed for the entire focal sphere and saved, the corresponding B axes are then found and saved. The domain of valid focal mechanism solutions (the P T B axes) is then plotted on the lower hemisphere of a Wulff net projection.

Examples

In order to illustrate the method, fictitious data representing strike-slip faulting were analyzed. The plotted data (figure 4) contain no inconsistent readings and are designed to allow only one solution. The focal sphere was searched for possible solutions. The domain of valid focal mechanism solutions, determined for zero errors, is shown in figure 5. This example illustrates data that are tightly constrained, allowing only one solution. In the next example the domain of valid focal mechanism solutions for the 16 fictitious data points were determined for a maximum of 6 errors (figure 6). This example illustrates data that are poorly constrained, allowing no meaningful interpretation.

Another example is an earthquake which occurred in the North Atlantic on November 17, 1963. The data for this event (figure 7) were taken directly from Udias and Baumann (1969). This example allows comparison of two independent techniques. Udias and Baumann (1969) found a solution (see figure 7) by combining P and S wave data for one inconsistent P wave first motion. They also computed a solution using P wave data for no errors. The domain of valid focal mechanism solutions for the P wave data for no inconsistent readings is shown in figure 8. The domain is defined by nearly fifty solutions. The small size of the domains indicates data which give well constrained results. The published focal mechanism solution (figure 7) is seen to be a member of the domain.

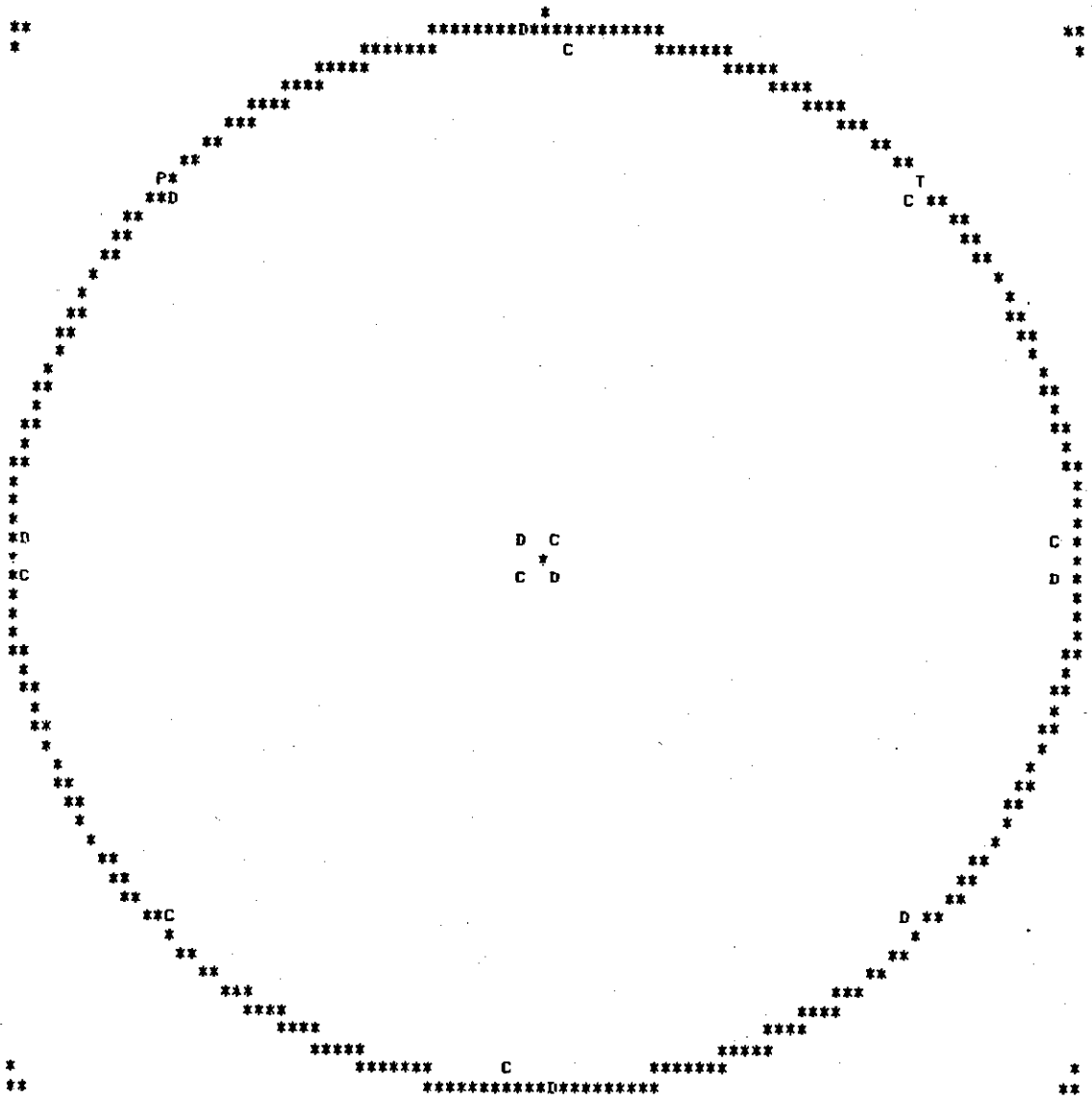


Figure 4. Test Data for Illustration.

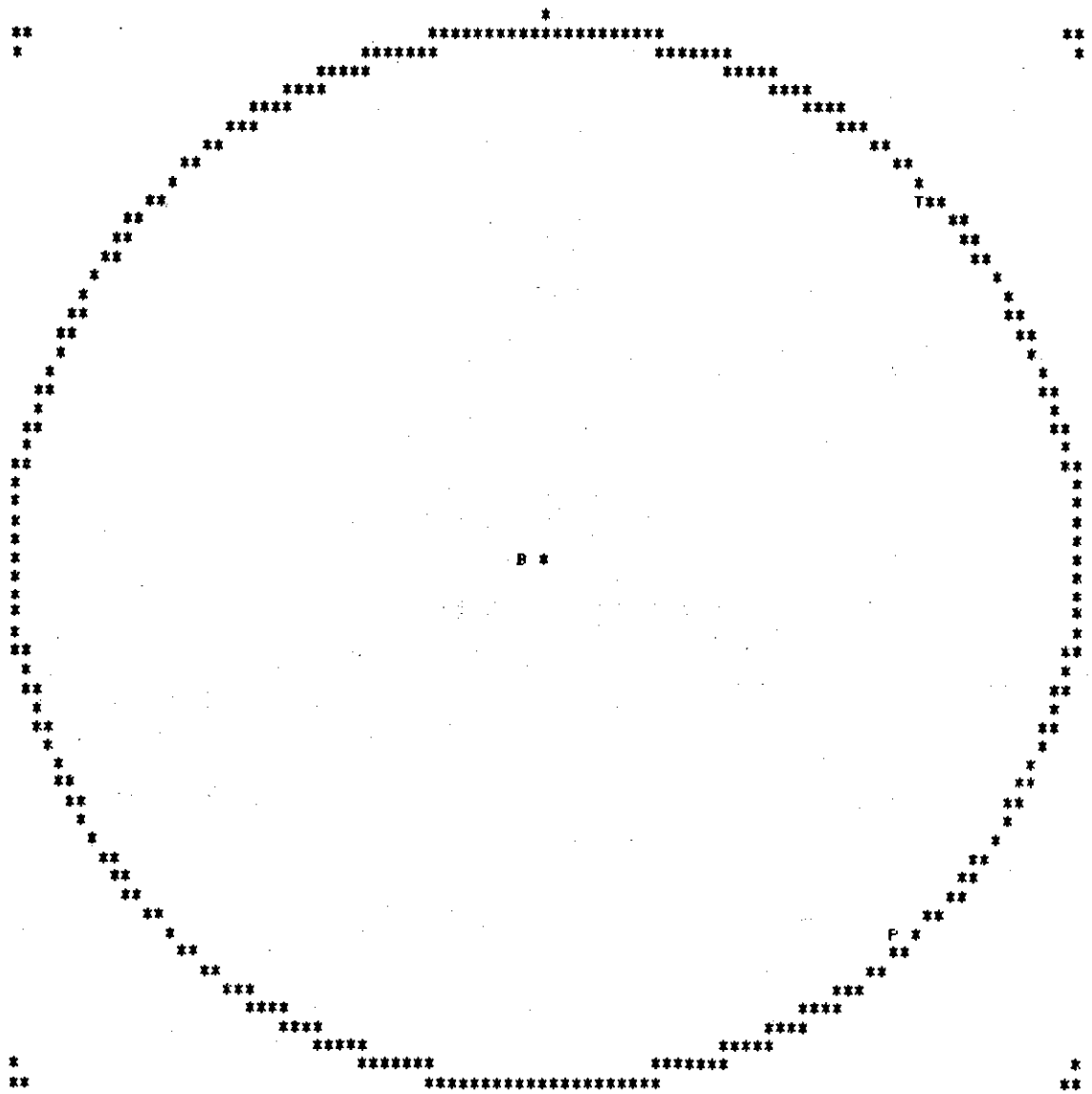


Figure 5. The Domain of Valid Focal Mechanism Solutions for No Errors for the Test Data.

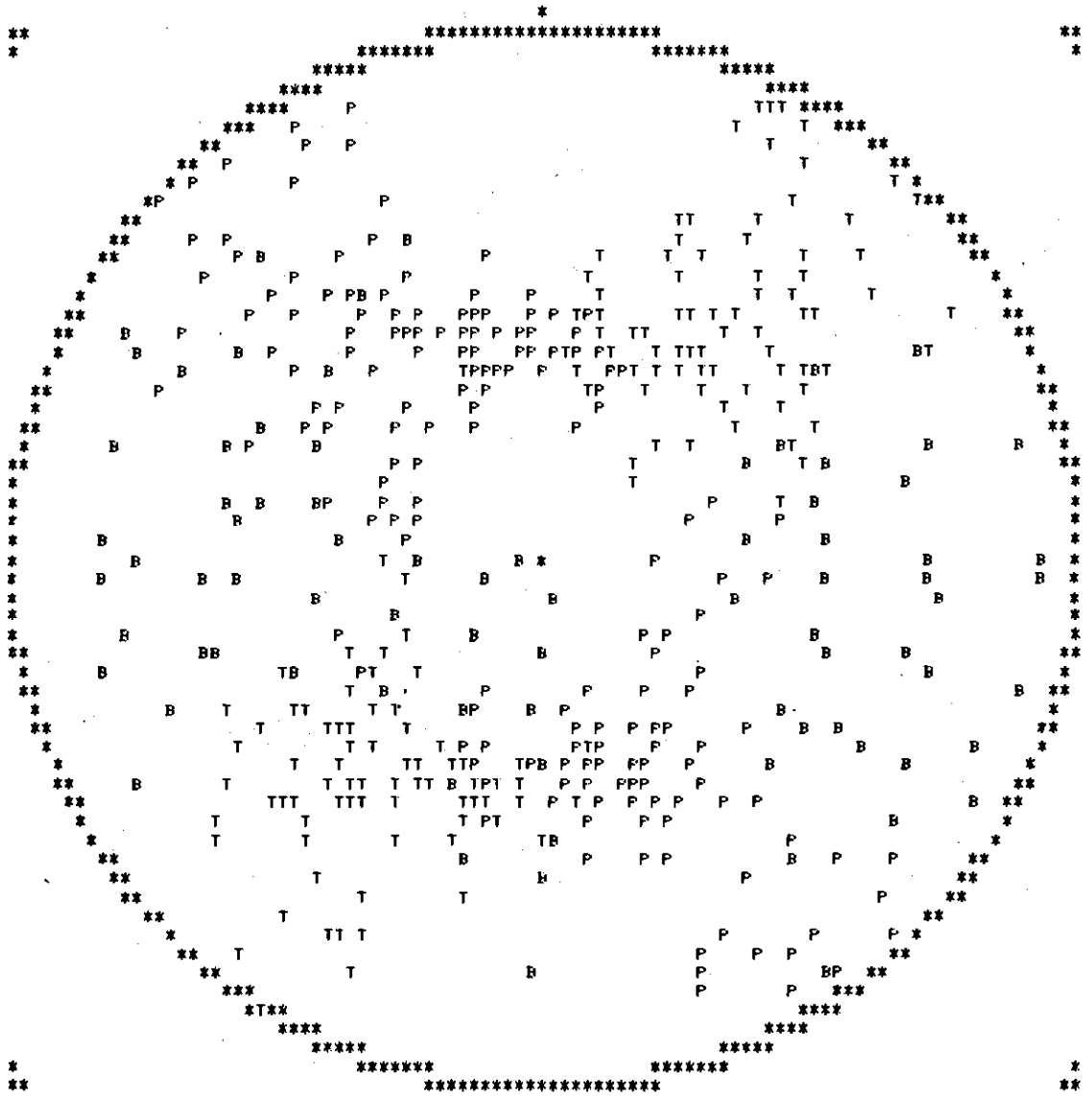


Figure 6. The Domain of Valid Focal Mechanism Solutions for a maximum of Six Errors for the Test Data. An Example of Poorly Constrained Data.

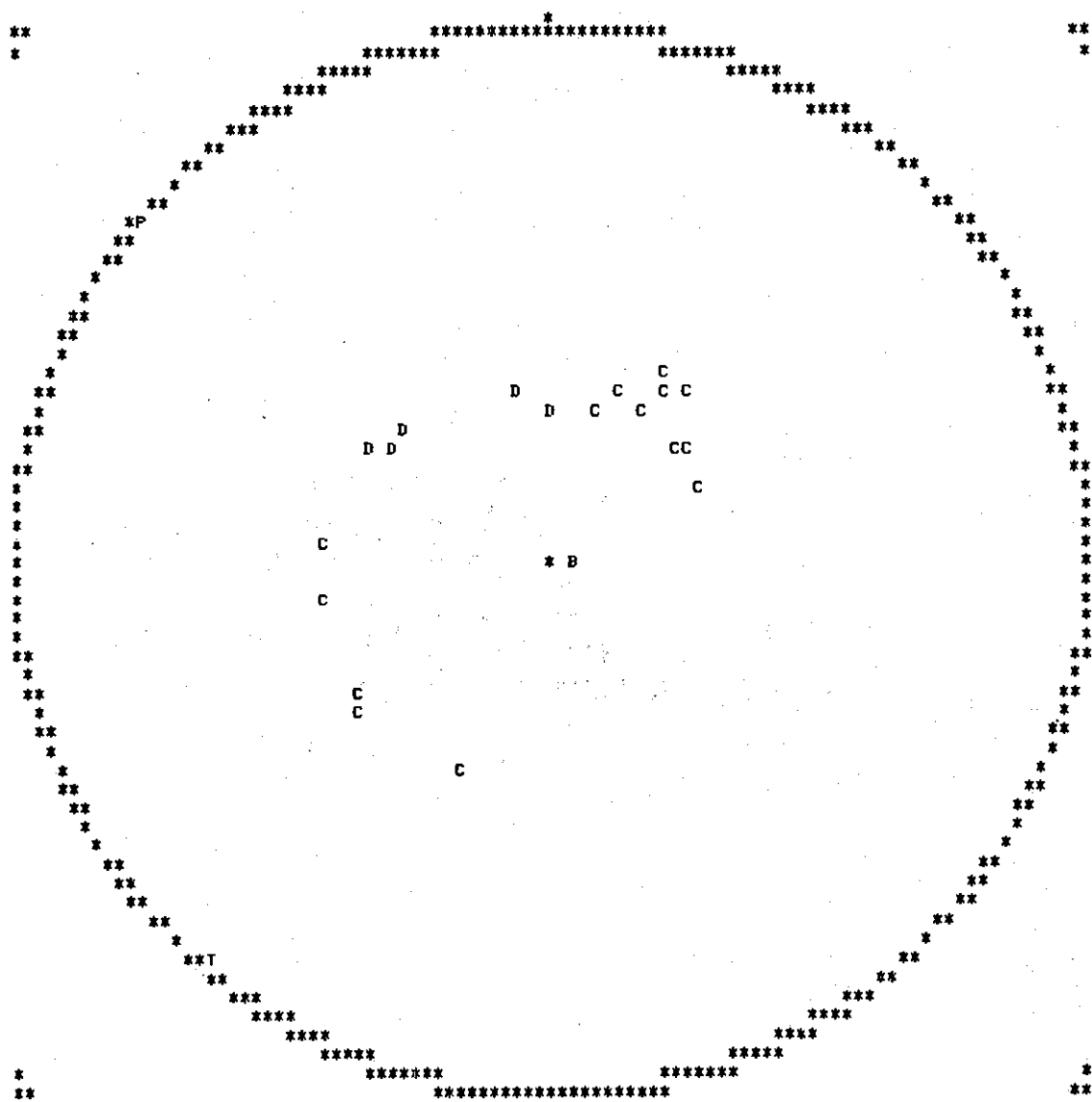


Figure 7. First Motion Data and Focal Mechanism Solution for the North Atlantic Earthquake of November 17, 1963 (after Udias and Baumann, 1969).

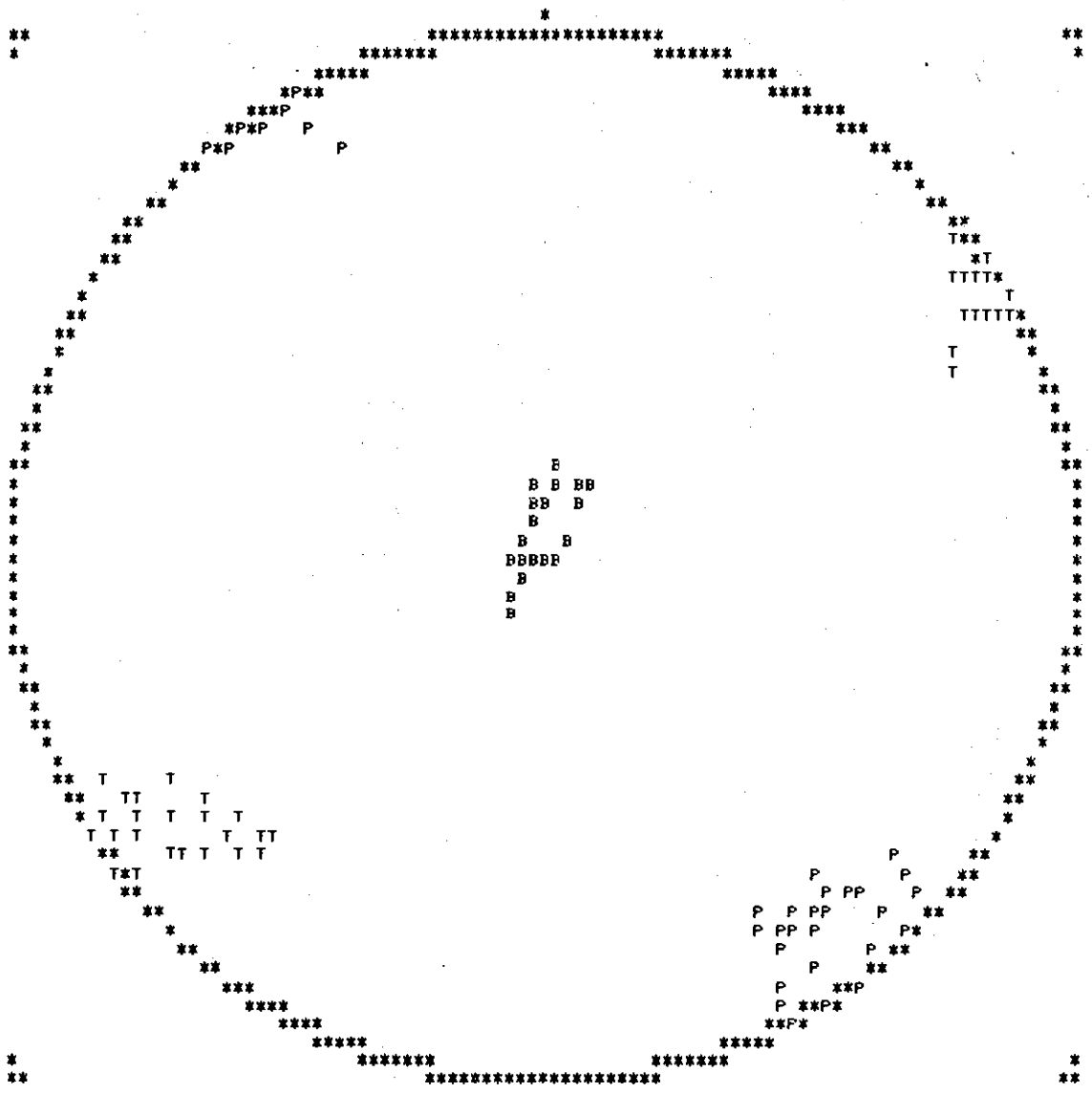


Figure 8. The Domain of Valid Focal Mechanism Solutions for Zero Errors for the North Atlantic Earthquake of November 17, 1963.

CHAPTER IV

DISCUSSION OF DATA

Data Preparation

The focal mechanism data analyzed in this study were accumulated from the literature from microearthquake surveys at the CHRA and JRA, and from regional seismic nets.

In order to prepare the data for analysis the following parameters must be determined; hypocentral locations, observation station locations, epicentral distances, accurate first motion readings, azimuths from epicenters, instrument ground motion responses, and angles of incidence at the sources. In general, all of these parameters can be obtained with sufficient accuracy except for angles of incidence at the sources. For large epicentral distances the angles of incidence were taken from published tables by Pho and Behe (1972). For intermediate epicentral distances (75 to 600 Km) regional travel times curves were used. For distances less than 75 Km local travel time curves were used, such as the one prepared by Dunbar (1977) for the CHRA. Angles of incidence were also estimated with reasonable precision from other geophysical survey methods.

The Conasauga Tennessee Area

On February 4, 1976 at 19:53:54.6 Universal Time an earthquake occurred in the vicinity of Conasauga, Tennessee near the Georgia-Tennessee border. The event was located about 44 Km north of the Carters Dam, Geor-

gia (CDG) seismic station. The main shock registered a local magnitude $M_{LSE} = 3.1$ as determined from the ATL (WWSS) seismograms. The hypocenter was determined from seismic arrival times at the CDG, CPO, and ORT observatories. The hypocenter, determined by several location techniques, was $35.01^{\circ}N$ and $84.67^{\circ} \pm 5$ Km with an approximate depth of 4 Km. No foreshocks have been satisfactorily identified, however, three aftershocks consistent with the main event were detected on the CDG seismogram. An aftershock study was initiated using portable microearthquake recorders, but the survey yielded no data consistent with the main event. Figure 9 shows the location of the February 4, 1976 main shock along with nearby seismic stations and intensity data. The main event was felt in parts of northwest Georgia and southeast Tennessee. Felt reports obtained from the surrounding area indicated a maximum intensity of VI (MM). A more detailed account of this earthquake sequence has been presented by Long and Guinn (1976), who included a historical seismicity evaluation. From the evaluation it was concluded that the area was probably active prior to this event.

The epicentral area is located in the Valley and Ridge Province of southeast Tennessee and northwest Georgia. The rock types range from Precambrian elastics to lower Paleozoic marine sedimentary sequences. The Precambrian rocks consist of sandstone, graywacke, arkose, and conglomerate, while the lower Paleozoic (Cambrian-Ordovician) rocks consist of sequences of sandstone, limestone, and shale. The epicentral area is cut by the Great Smoky Thrust Fault, where rocks of Precambrian age were thrust over Ordovician rocks. The area contains numerous folds and is cut by smaller northeast and northwest striking faults. The hypocenter

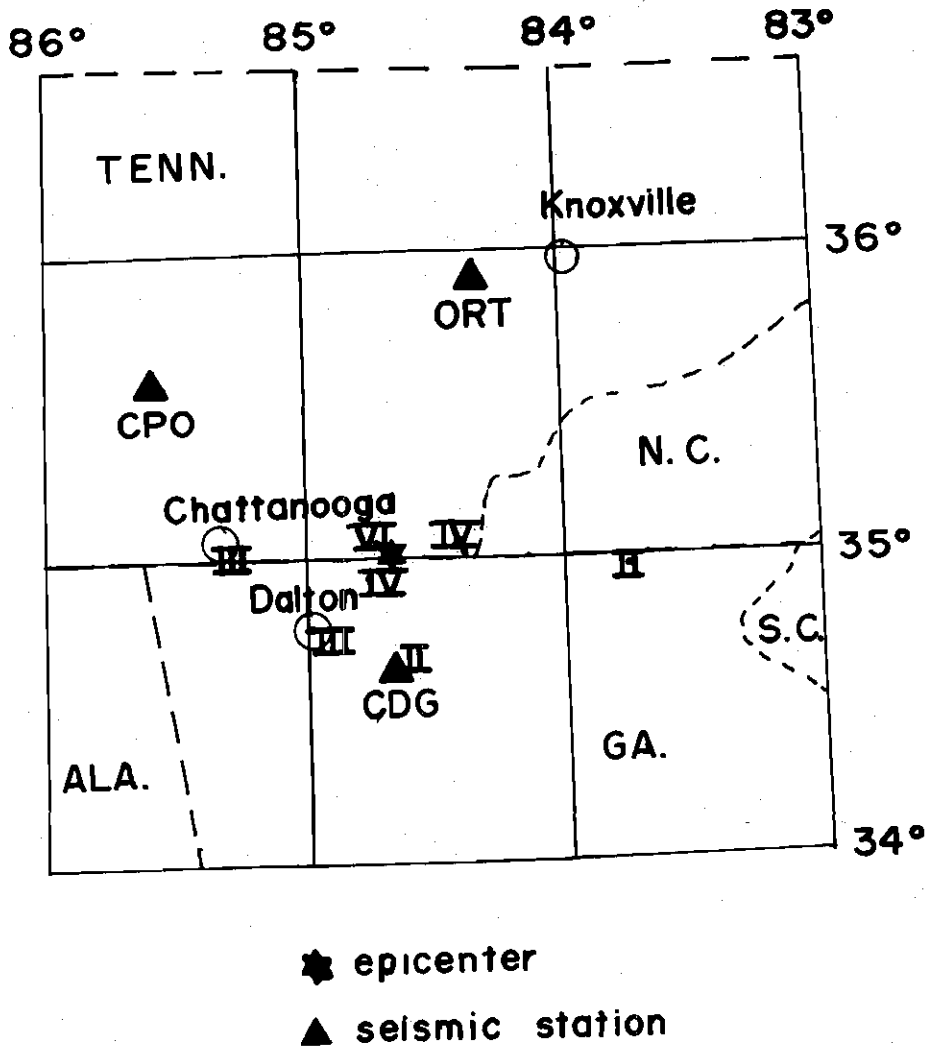


Figure 9. Location Map of the February 4, 1976 Conasauga, Tennessee Earthquake along with Nearby Intensity Data (MM) and Seismic Observatories.

at a depth of 4 Km lies below the Precambrian Sandsuck Formation in the vicinity of the Great Smoky Thrust Fault.

The P wave first motion data for the February 4, 1976 CTA main event are given in table 1. The plotted first motions are shown in figure 10. Although only 8 first motions were obtained the first motion plot shows data present in the 4 geographic quadrants. The domain of valid focal mechanism solutions for zero errors indicates many solutions are valid (figure 11). However, the pressure axes or maximum principal stress directions are constrained to northeast trends and vary in plunge from horizontal to about 60° . The tension axes or minimum principle stress directions are seen to vary more, but are more dense in the southern quadrant. The B axes or intermediate stress directions occur in three zones.

An S wave polarization angle, ϵ , was also determined for the main event using the short period records from the ATL (WWSS) seismic station. The amplitudes, U , of the S wave were read from the north (U_n), east (U_e) and vertical (U_v) component seismograms for the same instant of time. However, due to the free surface effect as discussed earlier the vertical S wave component cannot be measured directly. Nevertheless, the polarization angle, ϵ , can be estimated using the relation employed by Stauder and Bollinger (1964),

$$\tan \epsilon = \tan \gamma \cos j_o \quad (1)$$

where $\tan \gamma = (-U_T/U_R)$ and j_o is the S wave angle of incidence at the free surface. U_R and U_T are the radial and tangential components of the S wave motion and according to Herrmann (1975) they may be obtained by

Table 1. First Motion Data for the February 4,
1976 Conasauga, Tennessee Area Earthquake

No.	Station	Phase-Arrival Time	Dist (Km)	Azimuth	Take Off Angle
1	CDG	PC 19:54:01.0	46.0	196.0	50.0
2	CPO	PC 19:54:11.1	115.0	306.0	50.0
3	ORT	PD 19:54:11.5	116.0	11.0	50.0
4	ATL	PC 19:54:21.3	178.0	175.0	50.0
5	GSC	PD 19:54:21.5	165.0	90.0	50.0
6	JSC	PNC 19:54:40.4	320.0	105.0	50.0
7	CH5	PNC 19:54:30.5	258.0	125.0	50.0
8	CH6	PNC 19:54:33.5	231.0	124.0	50.0

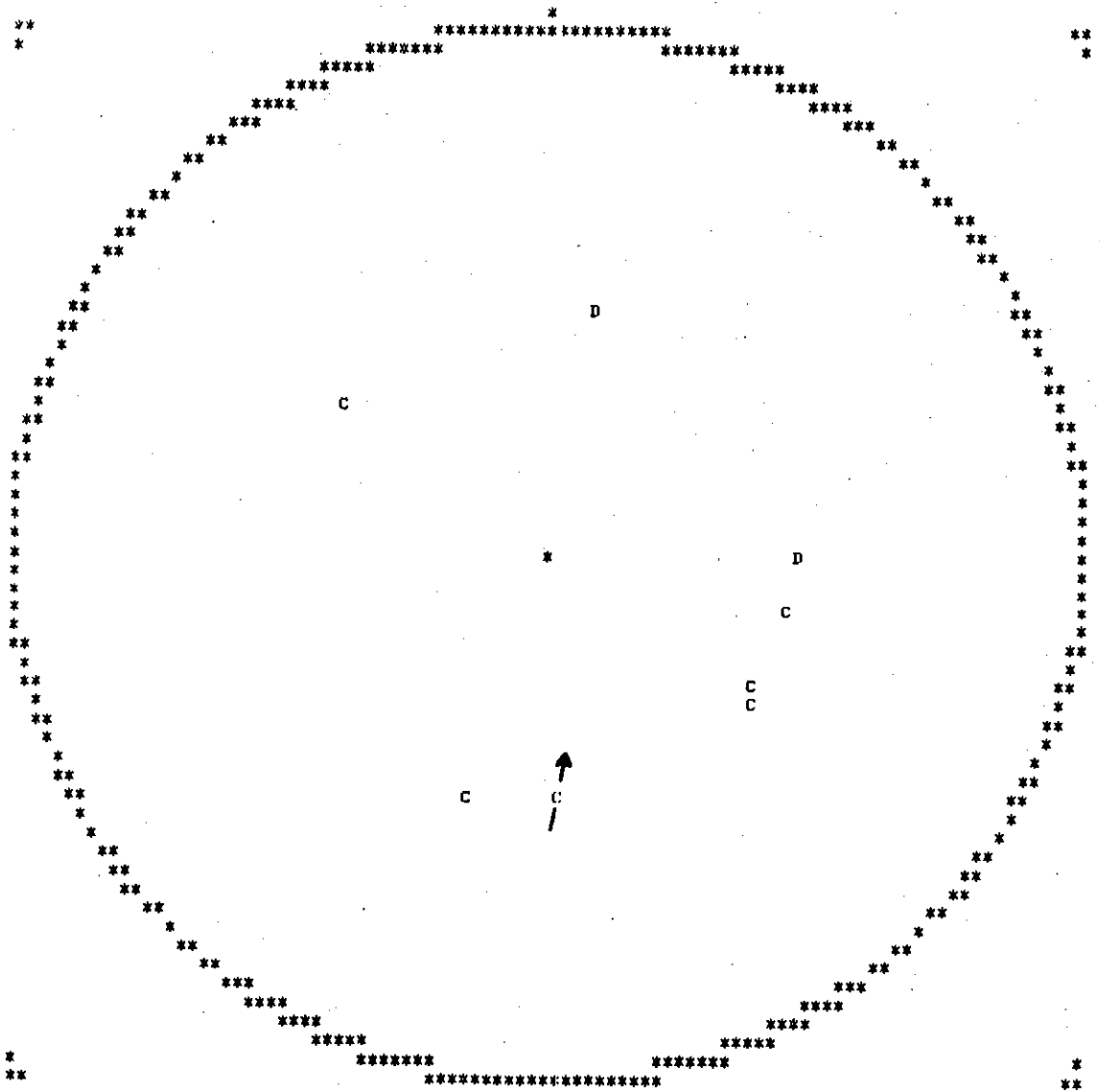


Figure 10. First Motion Plot for the Conasauga, Tennessee Area (CTA) Earthquake of February 4, 1976. The Arrow Indicates S Wave Polarization Angle.

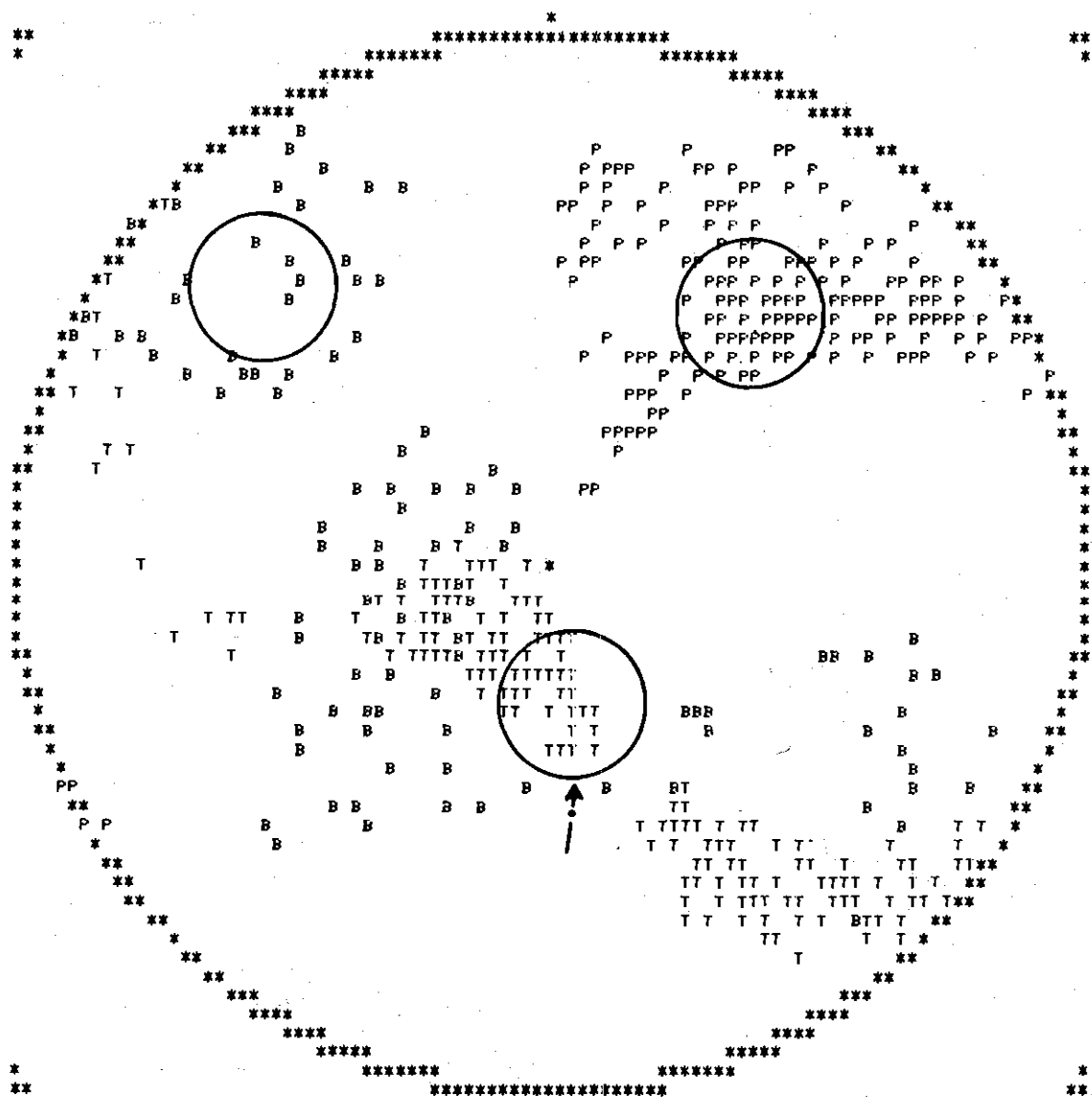


Figure 11. The Domain of Valid Focal Mechanism Solutions for Zero Errors for the Conasauga, Tennessee Area Earthquake of February 4, 1976. The Arrow Indicates S Wave Polarization Angle and Circles Indicate Solutions Constrained by the S Wave Data.

the following transformations

$$\begin{aligned} U_r &= -\cos \sigma U_n - \sin \sigma U_e \\ U_T &= \sin \sigma U_n - \cos \sigma U_e \end{aligned} \quad (2)$$

where σ is the azimuth from the station to the epicenter and U_n and U_e are taken to be positive in the north and east directions. The polarization angle was determined, using the above relations, to be $12^\circ \pm 10^\circ$ (see figure 11). Since S wave polarization angles converge at the P and T axes and are normal to the nodal planes the one determined for this event provides an additional constraint on the possible solutions determined from the P wave data.

The preferred fault plane, as suggested by the S wave polarization angle and P wave data, is one which strikes to the northwest with reverse type movement. This orientation suggests recent faulting may be perpendicular to the predominant northeast structural trends of the Appalachians.

The Maryville Tennessee Area

The Maryville, Tennessee area (MTA) is located in the Valley and Ridge Province, about 25 kilometers south of Knoxville, Tennessee. Recent seismicity and historical earthquakes around the twin cities of Alcoa and Maryville have been researched in detail and compiled by Bollinger et al. (1976). The historical earthquake epicenters are shown in figure 12. The largest known historical event, intensity VII (MM), occurred in the Knoxville area, causing considerable fright to inhabitants and damage to structures (Moneymaker, 1957). Bollinger et al. (1976) noted that many of the historical earthquakes occurred in multiples, several events per

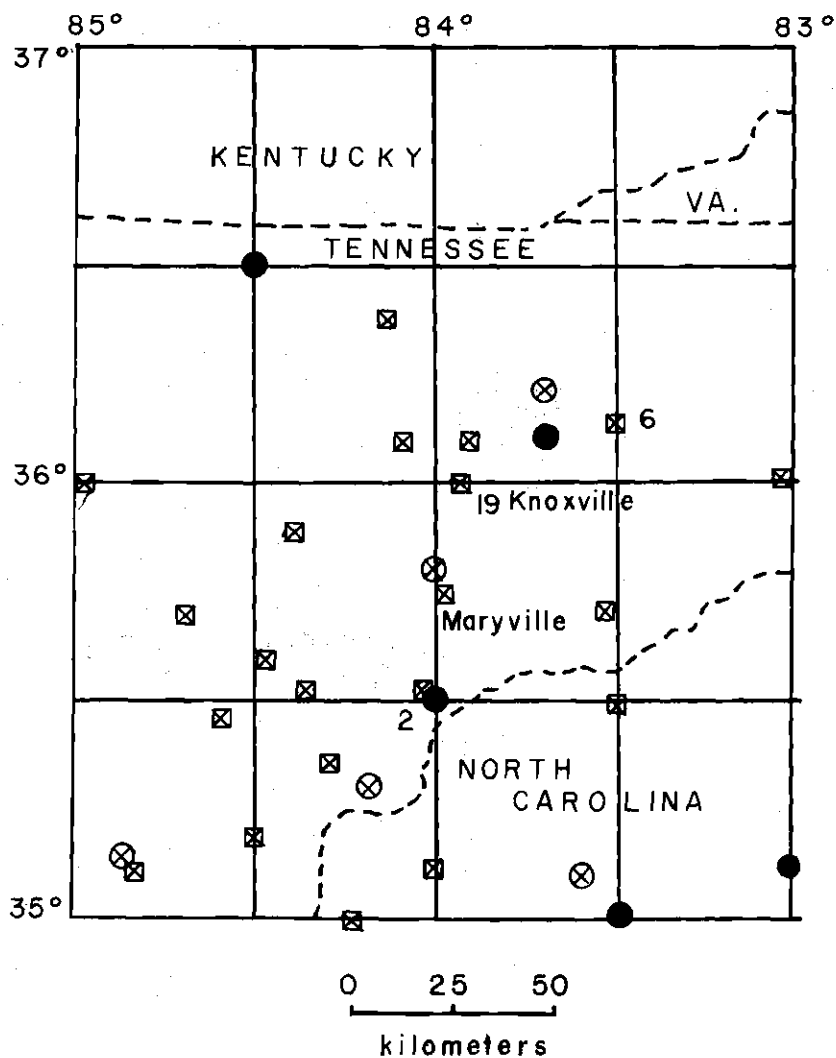


Figure 12. Historical Seismicity in the Knoxville, Tennessee Area. Number Indicates Multiple Occurrences.

- -- Instrumental Epicenter
 - ⊗ -- Epicenter from Isoseismal Map
 - ⊠ -- Felt Reports
- (after Bollinger et al., 1976)

year. From 1829 through 1969 58 earthquakes occurred in the region of which 22 were assigned to the Knoxville-Alcoa-Maryville area. These events are proposed by Bollinger (1973) to be part of the general low level seismic energy release associated with eastern Tennessee and western North Carolina.

The MTA geology, which is similar to the CTA geology, consists of marine elastics and carbonate sedimentary rocks (dolomite, chert, shale, sandstone and limestone) which range in age from Cambrian through Mississippian. In general, the area is characterized by numerous tightly folded synclines, anticlines and thrust faults which trend and strike northeast-southwest. Several thrust faults cut through the MTA and a series of very tightly folded anticlines and synclines in Cambrian shale and limestone are present in the Alcoa area (Cattermole, 1962). In contrast to the well-known northeast Appalachian trend, two major northwest striking fault zones, the Jacksboro and Emory River fault zones are located about 50 Km northwest of Knoxville. The Jacksboro fault zone forms the southern boundary of the Pine Mountain overthrust block. The Emory River fault zone forms the northeastern limit of the Cumberland Plateau overthrust (Rodgers, 1970). The sense of motion on these fault zones is strike-slip. Watkins (1964), using aeromagnetic data, and Staub and Johnson (1970), using gravity data, have concluded that basement rocks were not involved in Valley and Ridge thrust faulting.

On November 30, 1973 at 07:48:41.2 Universal Time an earthquake of magnitude $m_b = 4.6$ (U.S.G.S., 1974) occurred in the MTA (figure 13). The main shock was preceded by one $m_b = 3.4$ foreshock which came on October 30, 1973 at 22:58:39.0 Universal Time. More than 30 aftershocks

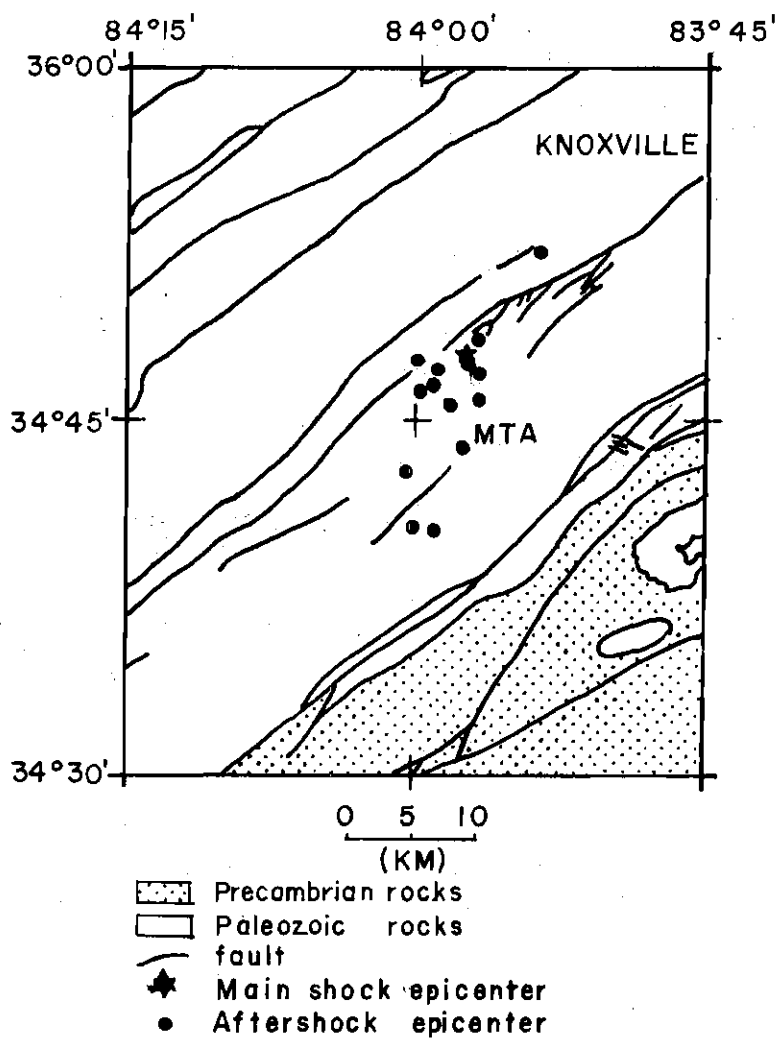


Figure 13. Map of Main Shock Epicenter, Aftershock Epicenters and Geology (after Bollinger et al., 1976).

were recorded and 342 felt reports resulted from the main event.

Focal mechanism solutions for the November 30, 1973 main event and aftershock sequence have been prepared by Bollinger et al. (1976). Seventeen P wave first motions were obtained for the main shock (16 of Pn type). An angle of incidence of 47° was used to obtain focal mechanism solutions for the MTA main event using the objective technique of Dillinger et al. (1972). The analysis by Bollinger et al. (1976) indicated that two equally valid solutions existed for two inconsistent readings, and the solutions were interpreted as a northwest striking reverse fault and a northeast striking normal fault.

The first motion data for the main event were taken from the paper by Bollinger et al. (1976) and solutions were recomputed in order to determine the domain of valid focal mechanism solutions. The first motion plot for the main event (figure 14) shows a minimum of three first motions in the 4 geographic quadrants. The recomputed focal mechanism solutions indicate first of all that the earlier proposed solutions are members of the domain of valid focal mechanism solutions and secondly that the PTB axes occur in discrete zones (figure 15). The majority of the pressure axes trend west. The majority of the tension axes trend south and most of the B axes trend east-northeast. The pressure and tension axis positions are only about 20° wide. The recomputed focal mechanism solutions indicate a larger domain exists for the northeast fault plane interpretation, whereas only one solution was found for the northwest fault plane interpretation. Thus, the analysis shows that more than two possible solutions are valid. The ambiguity as to which fault orientation is correct remains, yet the maximum and minimum principal stress orientations are viable indicators

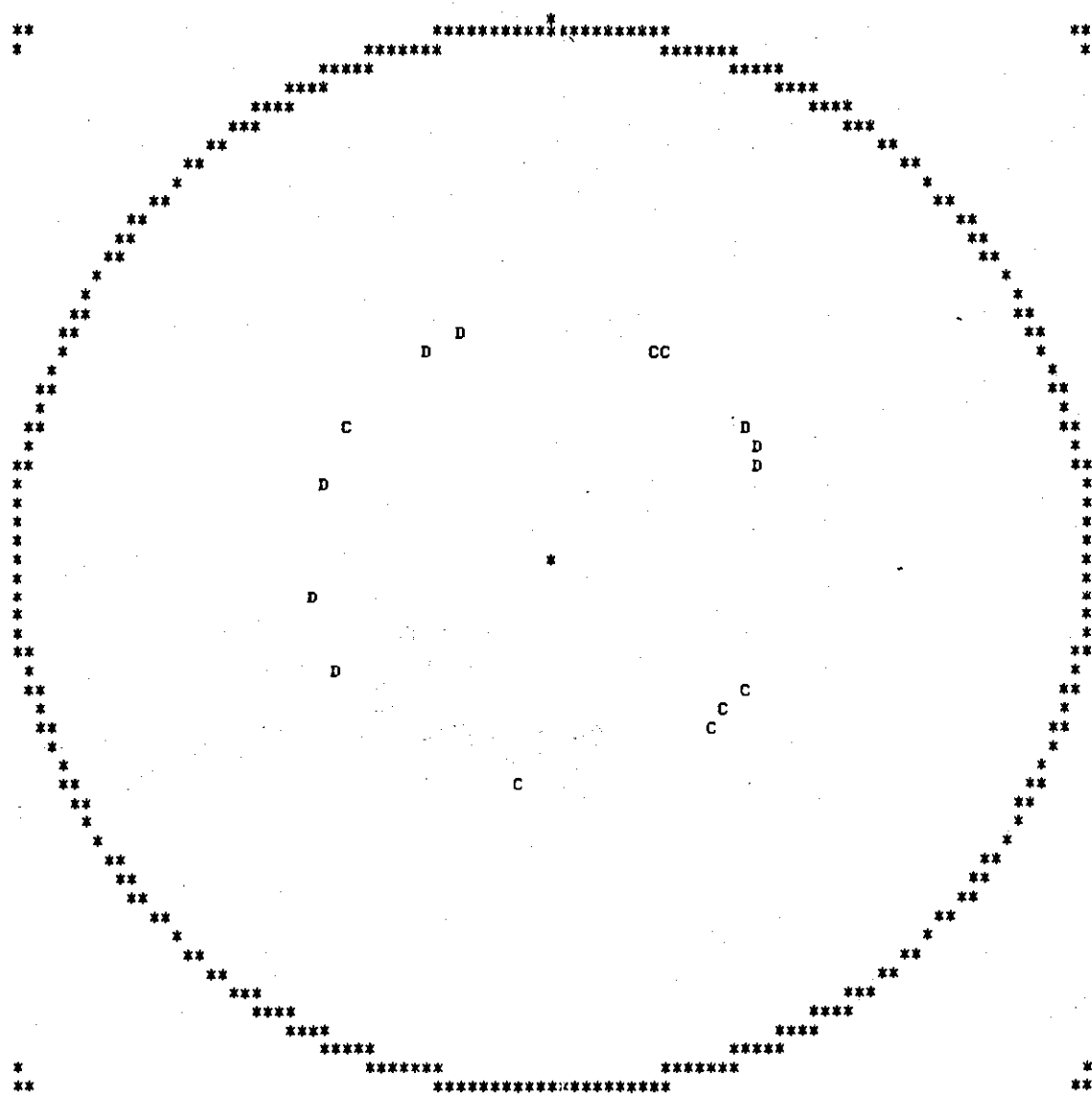


Figure 14. First Motion Plot for the Maryville, Tennessee Area (MTA) Main Shock of November 30, 1973 (after Bollinger et al., 1976).

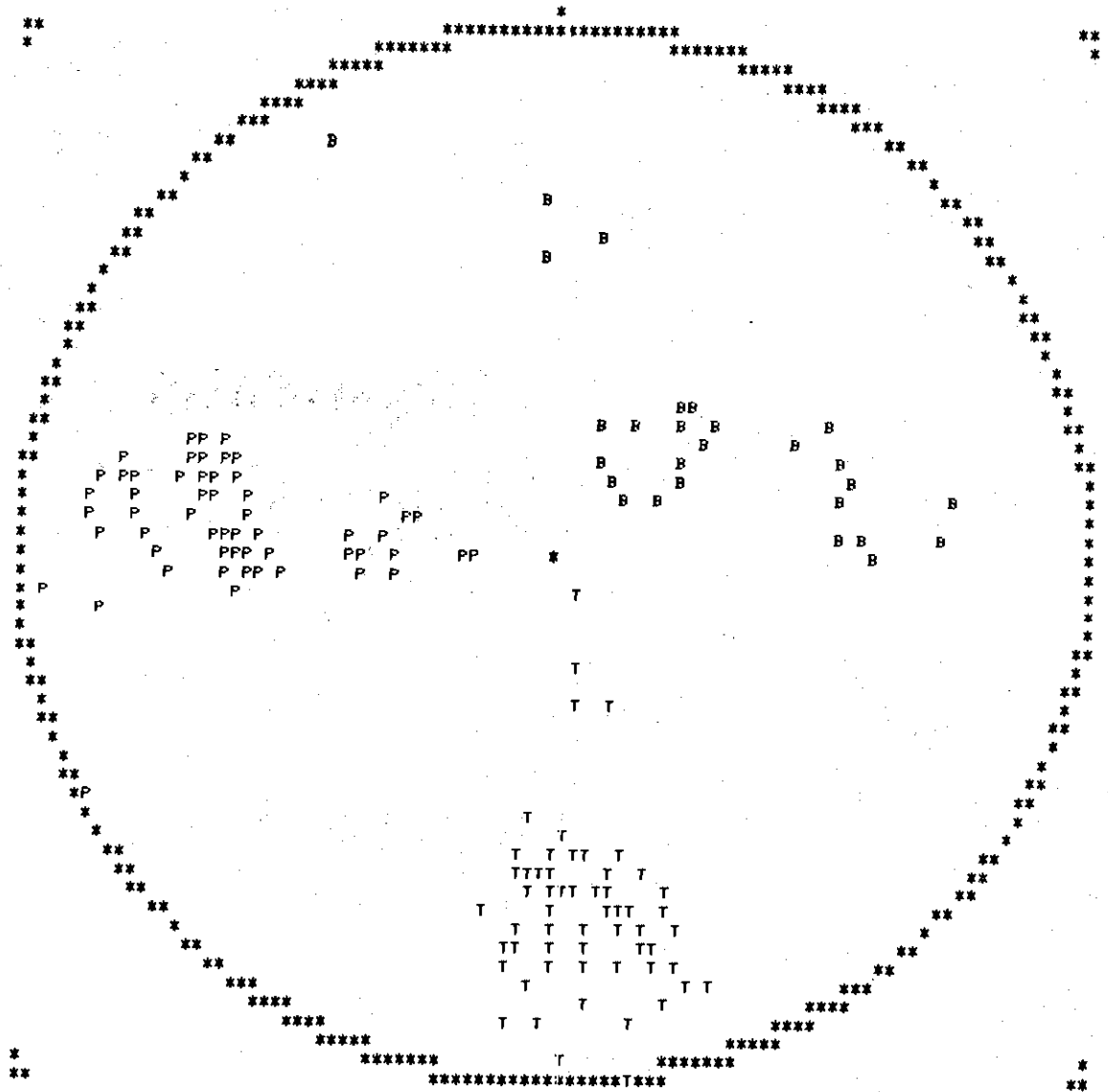


Figure 15. The Domain of Valid Focal Mechanism Solutions for Two and Three Errors for the MTA Main Shock of November 30, 1973.

as to possible force directions. Bollinger et al. (1976) on the basis of epicentral trends and hypocentral crosssections have suggested the main event resulted from reverse type movement on a northwest striking fault.

Bollinger et al. (1976), using composite aftershock first motions, found that composite focal mechanism solutions (CFMS) were not consistent with the main event focal mechanism solutions. They proposed that either the criteria for CFMS were not met or multiple mechanisms resulted from the energy release associated with the November 30, 1973 main shock. According to Bollinger et al. (1976) the composite aftershock first motion data indicated dip-slip faulting along a near vertical east-west striking fault or strike-slip motion along a near horizontal north-south striking fault. The aftershock first motion data for 14 aftershocks, taken from Bollinger et al. (1976) are shown plotted in figure 16. The domain of valid focal mechanism solutions for the minimum of 4 errors is shown in figure 17. The solutions are tightly constrained by the first motion data and indicate the previously published solution is a member of the domain of valid focal mechanism solutions. The domain of valid focal mechanism solutions for a maximum of 7 errors is shown in figure 18. The additional errors were introduced to determine how dependent the solutions were on one or more P wave first motions. The solutions show a wider variation in domain size but are compatible with the solutions shown in figure 17. The main result is that none of the composite aftershock pressure axes overlap with the main event pressure axes, suggesting multiple mechanisms may have been involved.

With the possible exception of the northeast fault plane interpre-

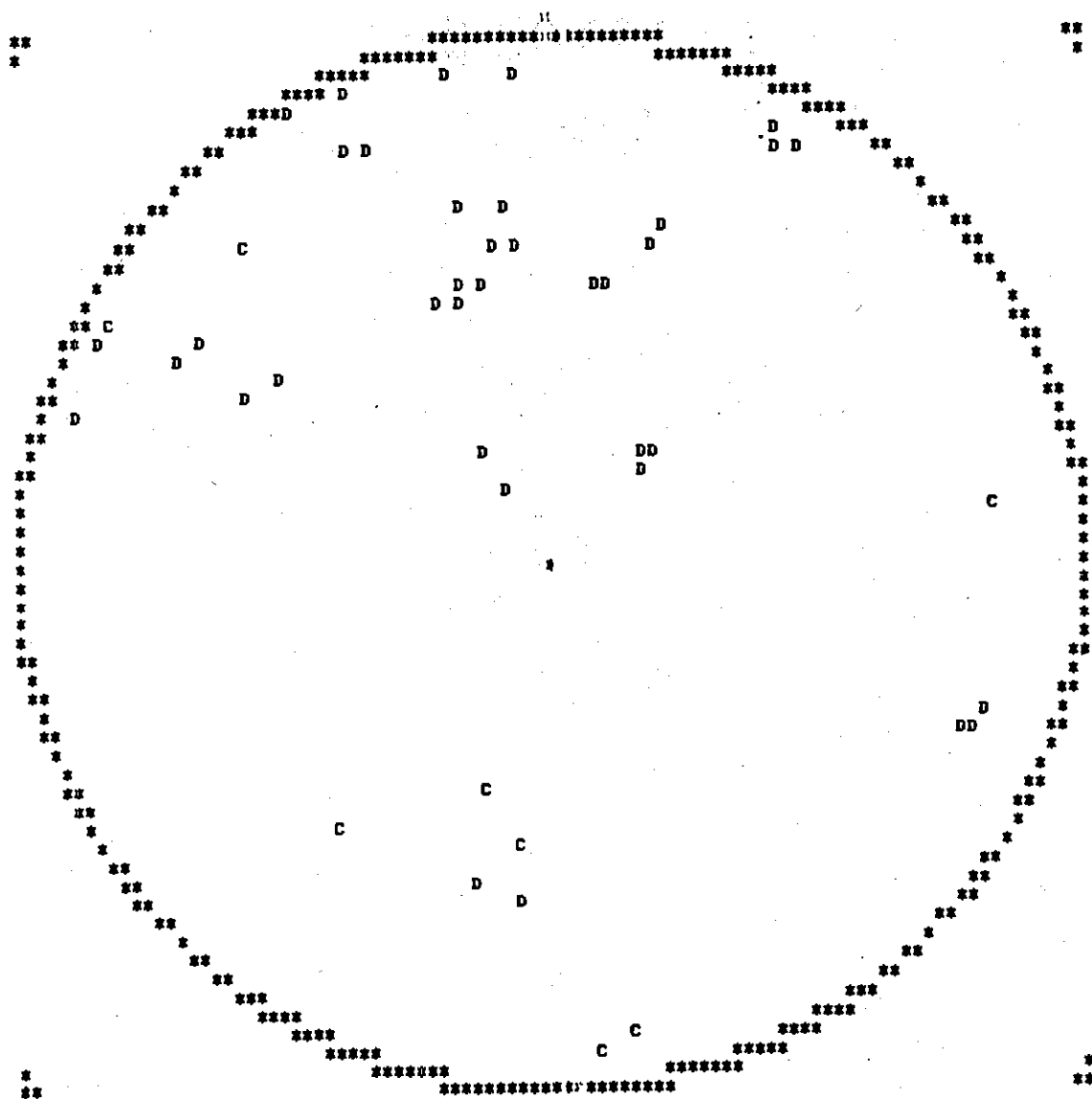


Figure 16. Composite First Motion Plot of 14 Aftershocks Associated with the November 30, 1973 Maryville, Tennessee Area (MTA) Main Shock (after Bollinger et al., 1976).

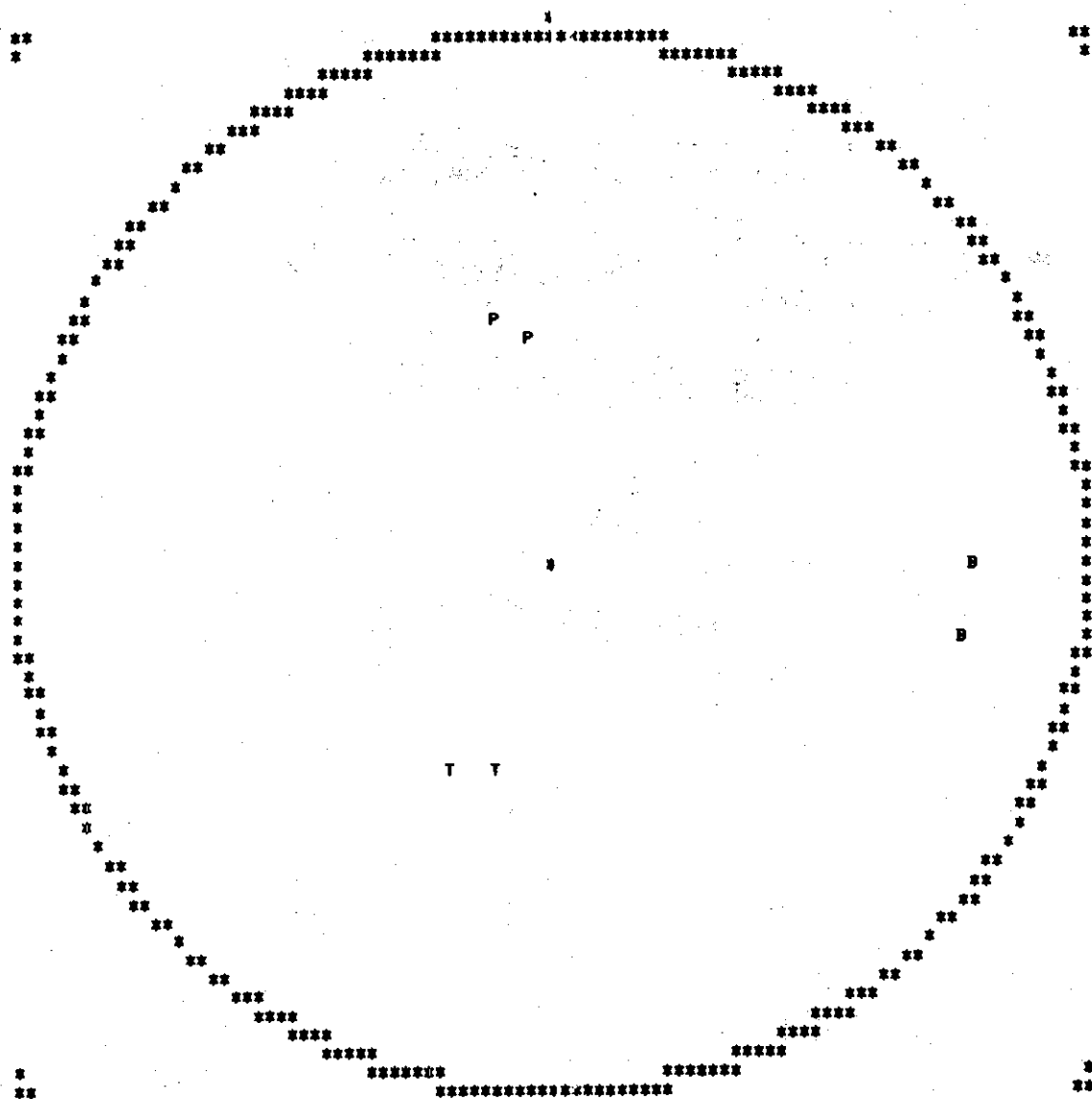


Figure 17. The Domain of Valid Focal Mechanism Solutions for Four Errors from Composite Aftershock First Motions for the Maryville, Tennessee Area (MTA).

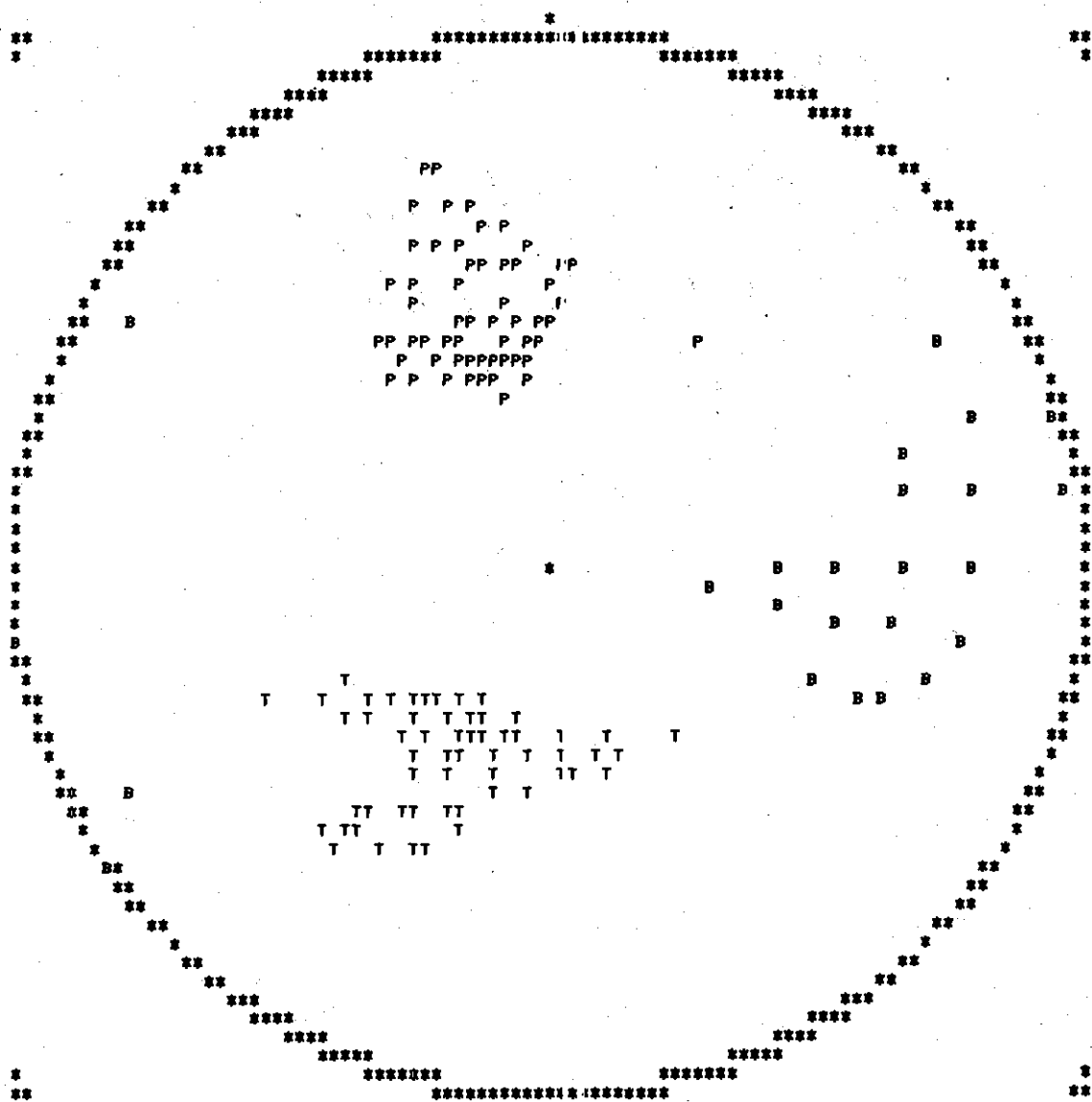


Figure 18. The Domain of Valid Focal Mechanism Solutions for Seven Errors from Composite Aftershock First Motions for the Maryville, Tennessee Area (MTA).

tation for the MTA main event, the focal mechanism solutions indicate fault planes which are not parallel to the structural trends of the Appalachians.

The Englewood Tennessee Area

The Englewood, Tennessee Area (ETA) is located in the Valley and Ridge Province about 50 Km southwest of the MTA and about 60 Km northeast of the CTA. On July 27, 1977 an earthquake of magnitude $M_{LSE}=3.5$ occurred at 22:03:21.1 Universal Time near the Englewood, Tennessee area. The earthquake was located at $35^{\circ}29'24''N$ and $84^{\circ}22'12''N$ at an approximate depth of 4 to 5 Km.

The P wave first motions are given in table 2 and are shown plotted in figure 19. The first motion plot indicates a near absence of data northwest and southwest of the epicenter. The domain of valid focal mechanism solutions for no inconsistent readings is shown in figure 20. The large domain size indicates the need for data from the northwest and southwest. The pressure axes are constrained to north-northeast trends and vary in plunge from horizontal to near vertical. The tension axes vary more but are in general constrained to the southern quadrant. Although a variety of possible fault plane orientations exists, the solutions are quite similar to the solutions given for the CTA (figure 11). Based on this similarity, a northwest striking fault with reverse movement for the ETA earthquake of July 27, 1977 may be valid.

The Clark Hill Reservoir Area

The Clark Hill Reservoir area (CHRA) is located along the Savannah River at the Georgia-South Carolina border. The reservoir extends from

Table 2. First Motion Data for the Englewood, Tennessee Area
Earthquake of July 27, 1977

No.	Station	Phase	Dist (Km)	Azimuth	Take Off Angle
1	ATL	PnC	229.0	187.0	50.0
2	CHF	PnC	243.0	131.0	50.0
3	ORT	P D	50.0	17.0	69.0
4	PRM	PnD	248.0	128.0	50.0
5	SRPM	PnC	358.0	131.0	50.0
6	HBF	PnC	471.0	126.0	50.0
7	PBS	PnC	457.0	120.0	50.0
8	LHS	PnC	353.0	108.0	50.0
9	WDG	PnC	266.0	153.0	50.0
10	ETG	PnC	265.0	157.0	50.0
11	CPO	P*C	109.0	277.0	60.0
12	BH	PnD	194.0	55.0	50.0
13	RM	PnD	194.5	54.0	50.0
14	KTS	PnC	144.0	115.0	50.0

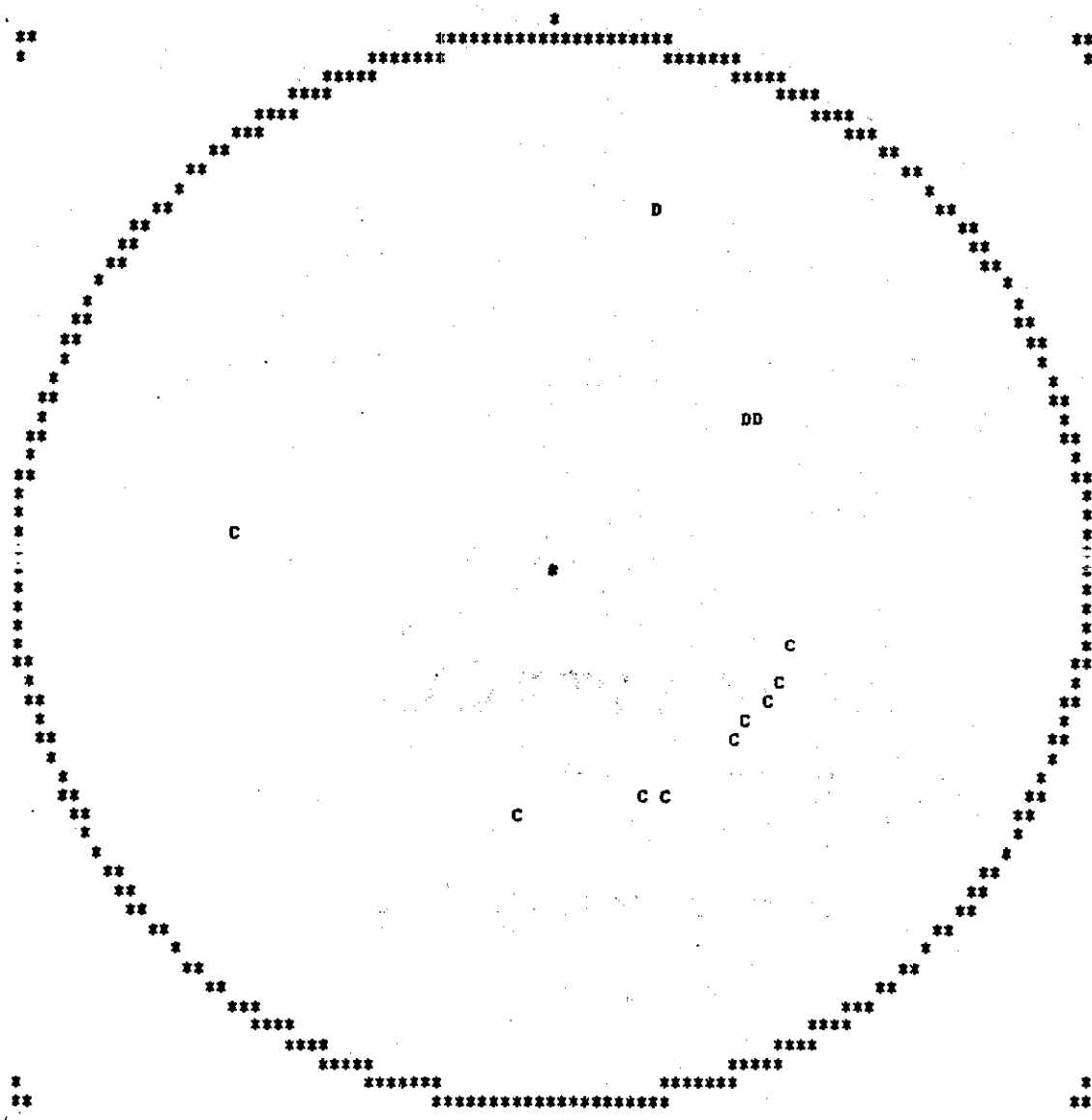


Figure 19. First Motion Plot for the Englewood, Tennessee Area (ETA) Earthquake of July 27, 1977.

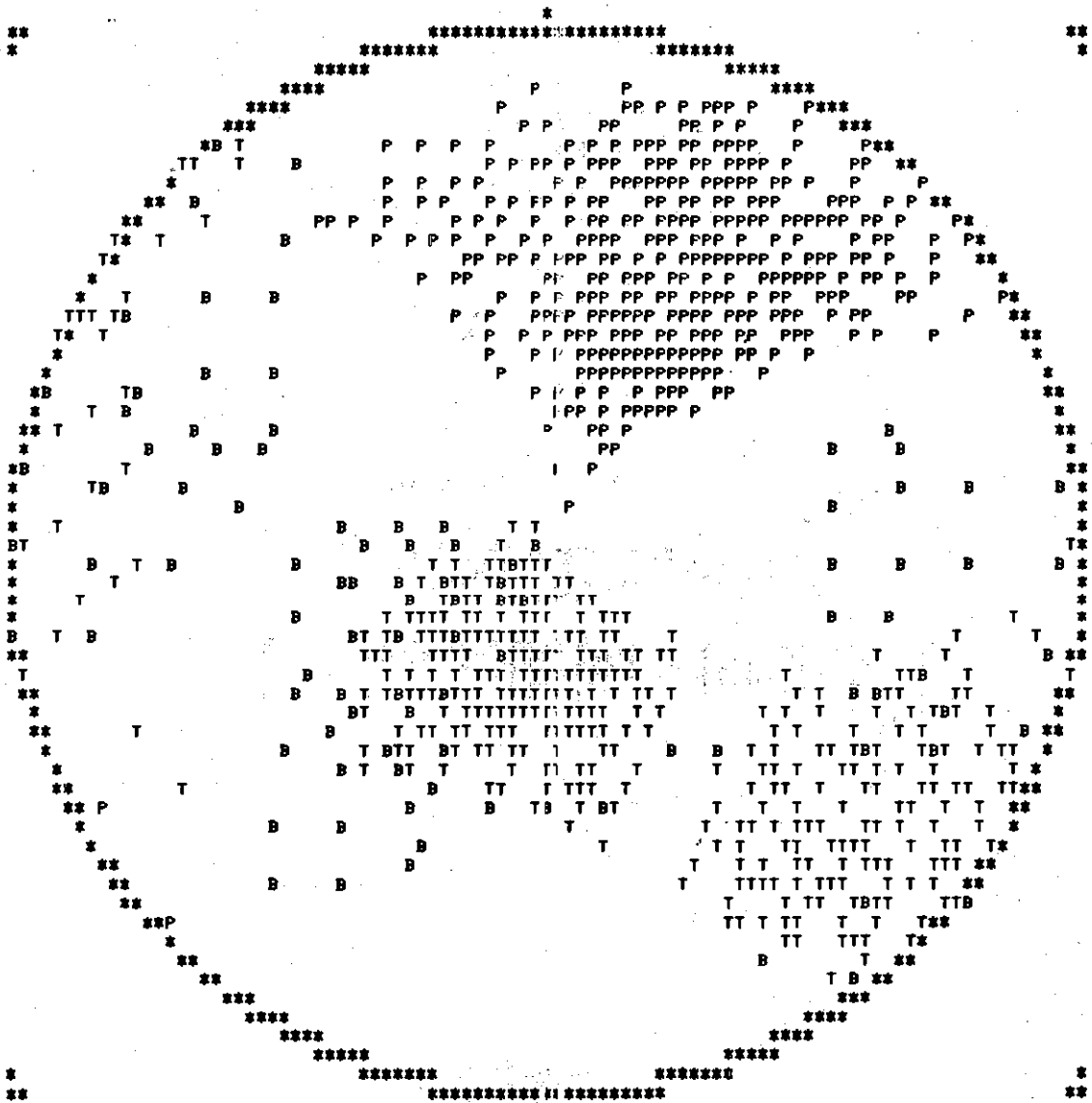


Figure 20. The Domain of Valid Focal Mechanism Solutions for Zero Errors for the Englewood, Tennessee Area (ETA) Earthquake of July 27, 1977.

33.67°N, 82.16°W to 34.0°N, 82.6°N and is located in the Crystalline Piedmont Province.

The only earthquake reported as being felt in the CHRA prior to the August 2, 1974 main shock occurred on November 1, 1875, with an intensity of VI (MM) (Bridges, 1975). According to the Earthquake Data Reports (EDR No. 62-74, U.S.G.S.), an earthquake of magnitude $m_b = 4.3$ occurred on August 2, 1974 at 8:52 Universal Time with maximum intensities of VI (MM) (Bridges, 1975 and Talwani, 1976). The main shock was felt over 36,000 square kilometers in the Piedmont (Benson and Fogle, 1974) and resulted in slight damage to the Bobby Brown State Park in Georgia. Investigation of ATL (WSS) seismograms from 1963 up to the time of the August 2, 1974 event indicated numerous earthquakes consistent with the CHRA (Long, 1974). A detailed aftershock study has been presented by Bridges (1975) for the August 2, 1974 event.

The geology of the CHRA (figure 21) is characteristic of the Crystalline Piedmont Province. The rock types are both metamorphic and igneous. The metamorphic rocks are Precambrian to Paleozoic and consist of both metasedimentary and metaigneous rocks. The area has been intruded by granitic plutons and by smaller gabbroic bodies. The area contains numerous metamorphosed extrusive flows and northwest trending diabase dikes. In the August 2, 1974 epicentral area the rocks are coarse grained gneisses. This epicentral area is further characterized by many fractures or joints, and numerous pegmatite, quartzite, and diabase dikes. Many of the dikes in the main event epicentral area have been displaced 2 to 6 centimeters along fractures. The major joint directions are N35°N and N55°N with nearly vertical dips at the surface. The overall structural

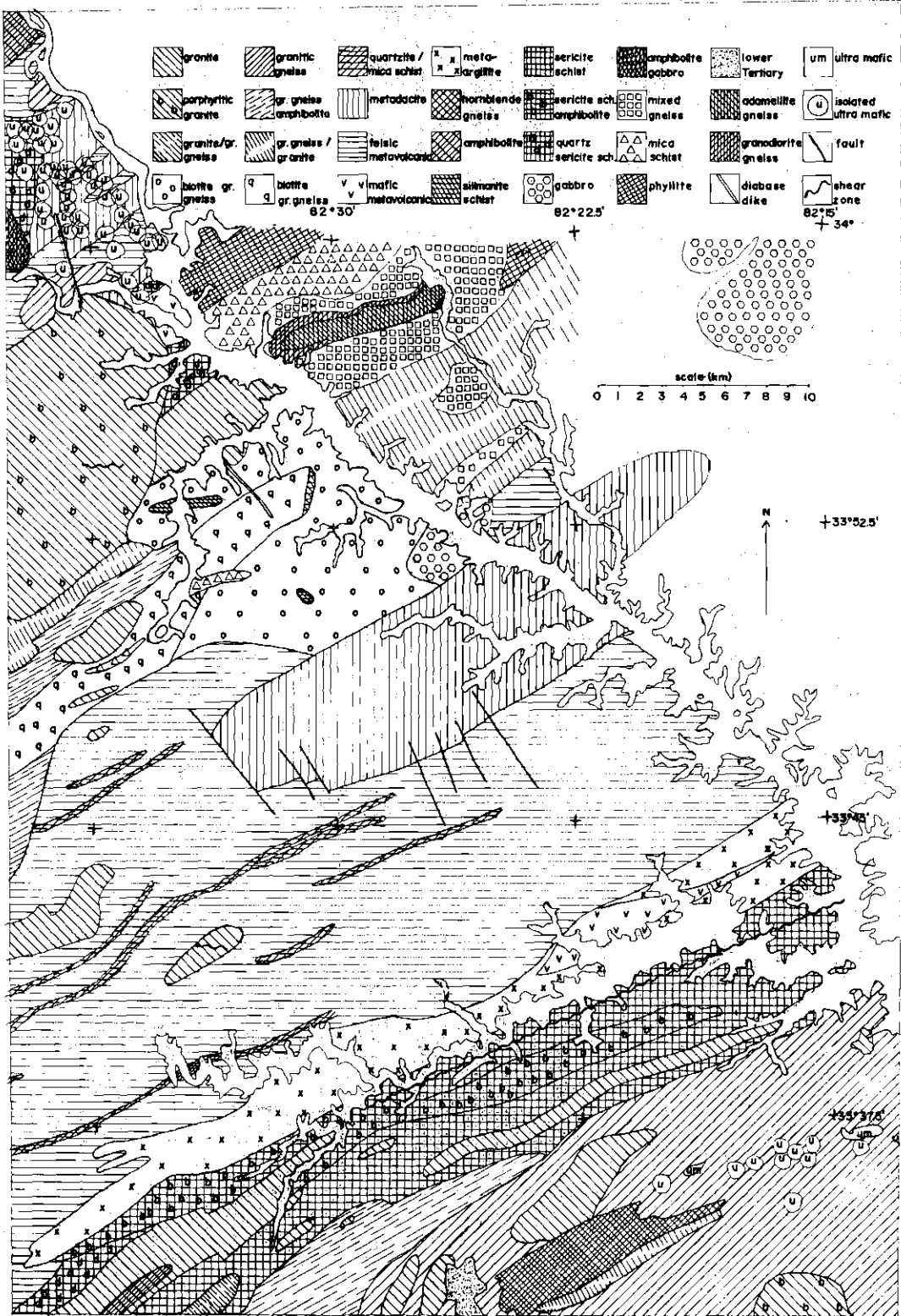


Figure 21. Geology Map of the Clark Hill Reservoir Area. Geologic Map of Georgia, Georgia Geological Survey, 1976.

trend is northeast-southwest.

Since the early 1970's numerous workers have investigated the implications of seismic activity in the CHRA. Denman (1974) and Scheffler (1976) have undertaken geologic and geophysical studies of the area. The petrography of part of the area has been examined by Paris (1976). Secor (1974) carried out detailed geologic mapping in the epicentral area. The U. S. Corps of Engineers (1977) has investigated the area as part of the seismic evaluation for the Richard B. Russell Dam Project. Dunbar (1977) has recently completed a close-in velocity survey of the northern portion of the reservoir area, near the epicentral area. Marion (1977) has presented the spectral characteristics of CHRA microearthquakes. Talwani (1976) has proposed possible focal mechanism solutions from composite first motion data and suggested possible earthquake mechanisms for the CHRA. Detailed gravity surveys have been compiled by Long et al. (1976).

New focal mechanism data have been collected for this area, including the August 2, 1974 event. The new data and analyses are correlated with previous work in order to further constrain any interpretations made concerning earthquake mechanisms at the CHRA.

The results presented here for the CHRA represent one of the most extensive attempts to interpret focal mechanism solutions for a southeastern epicentral area. The solutions are given for the main shock of August 2, 1974, for a microearthquake, and for composites of numerous events recorded for intermittent periods of nearly 3 years.

The focal mechanism solutions presented for the August 2, 1974 main event represent the first analysis not relying on composite data for the CHRA. Sixteen P wave first motions were obtained for the main event

(Table 3). The plotted first motions are shown in figure 22. The domain of valid focal mechanism solutions indicates that more than one focal mechanism solution exists for zero errors (figure 23). However, all the possible solutions are related to one small set of T axes which vary in trend and plunge by about $\pm 20^\circ$ and 30° respectively. The pressure axes occur in two dominant groups, one to the east and one to the south. The B axes are seen to vary the most. Hence, two possible focal mechanisms are indicated. The first focal mechanism implies fault planes striking northwest and northeast dipping respectively to the southwest and southeast and having reverse movement. The second focal mechanism implies east-west striking faults, one having a nearly horizontal dip and other near vertical. In the second case the vertical plane is preferred and indicates normal or high angle reverse movement.

Six first motions were obtained for a CHRA microearthquake which occurred on April 14, 1977 at 12:53:32.01 Universal Time. The first motion plot consists of only dilatational readings which are distributed (one-sided) in the northern quadrant (figure 24). Even though the number of first motions and their distribution are limited, the domain of valid focal mechanism solutions can be defined (figure 25). The pressure axes are tightly grouped and have an overall trends to the north. The solutions for this indicate similar possible fault plane orientations to those given for the August 2, 1974 main event (see figure 23). Although similar fault planes appear valid, the pressure and tension axes are completely reversed. This indicates an opposite sense of movement along the fault planes. The preferred solutions for this microevent and the main event are those which give fault planes striking northwest and northeast.

Table 3. First Motion Data for the August 2, 1974

CHRA Earthquake

No.	Station	Phase	Dist (Km)	Azimuth	Take Off Angle
1	ATL (WSS)	IPND	180.0	252.0	50.0
2	AMG	IPND	264.0	217.5	50.0
3	CPO	PND	331.0	303.5	50.0
4	EUR (WSS)	PC	3612	292.0	28.0
5	ALQ (WSS)	PC	2200	283.0	36.0
6	OXF (WSS)	PNC	635.0	278.0	50.0
7	LASA ARRAY	PC	2800	310.0	30.0
8	PBS	PND	224.0	111.5	50.0
9	HBF	PND	226.0	119.0	50.0
10	SMA	PND	204.0	99.0	50.0
11	SGS	PND	201.0	113.5	50.0
12	VCS	PND	178.0	131.0	50.0
13	OSC	PND	160.0	105.5	50.0
14	GBS	PD	71.0	124.0	75.0
15	TUC (WSS)	PC	2550.0	278.0	31.0
16	PAL (WSS)	PNC	1100.0	40.0	50.0

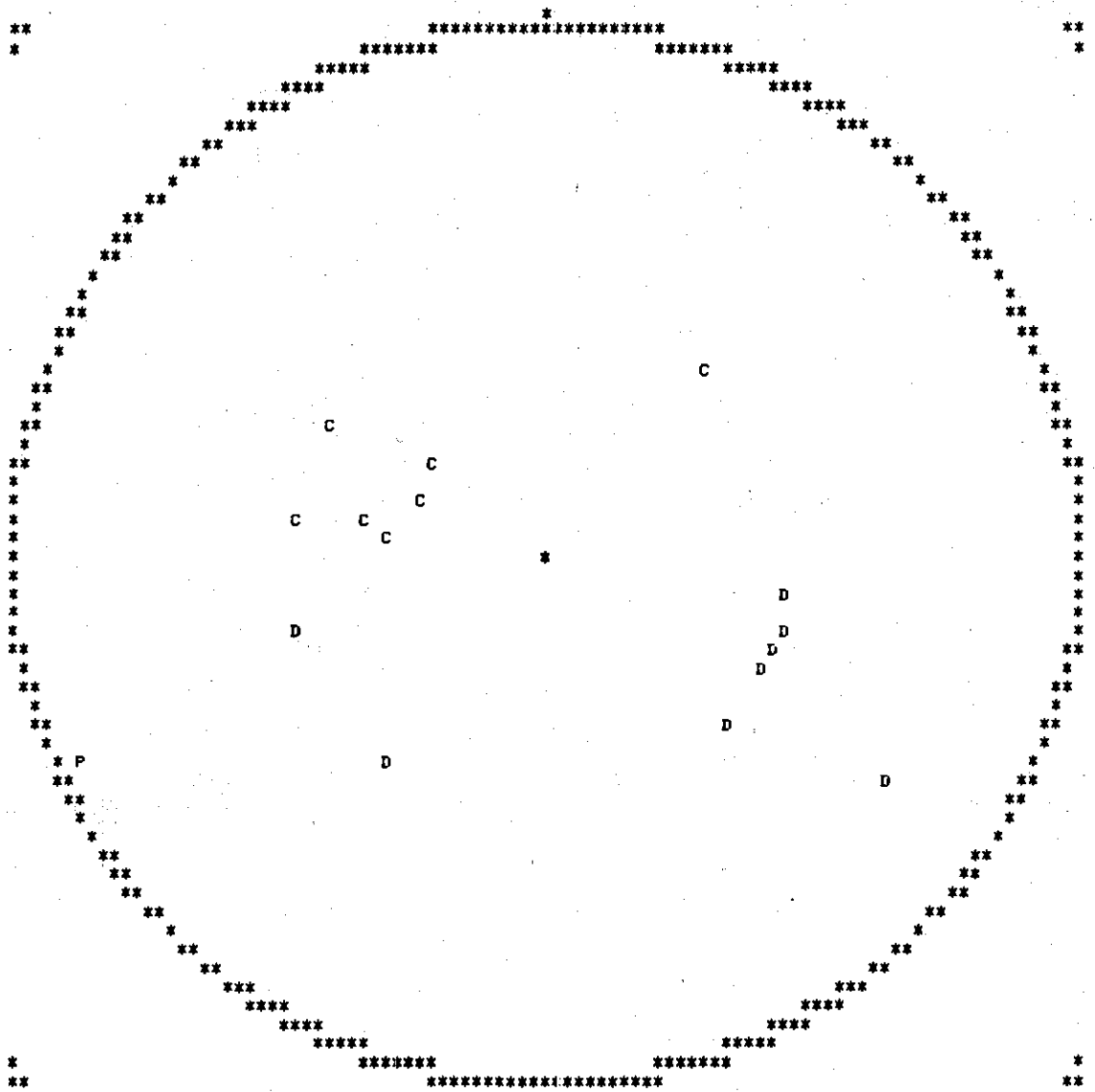


Figure 22. First Motion Plot for the August 2, 1974 Clark Hill Reservoir Area (CHRA) Main Shock.

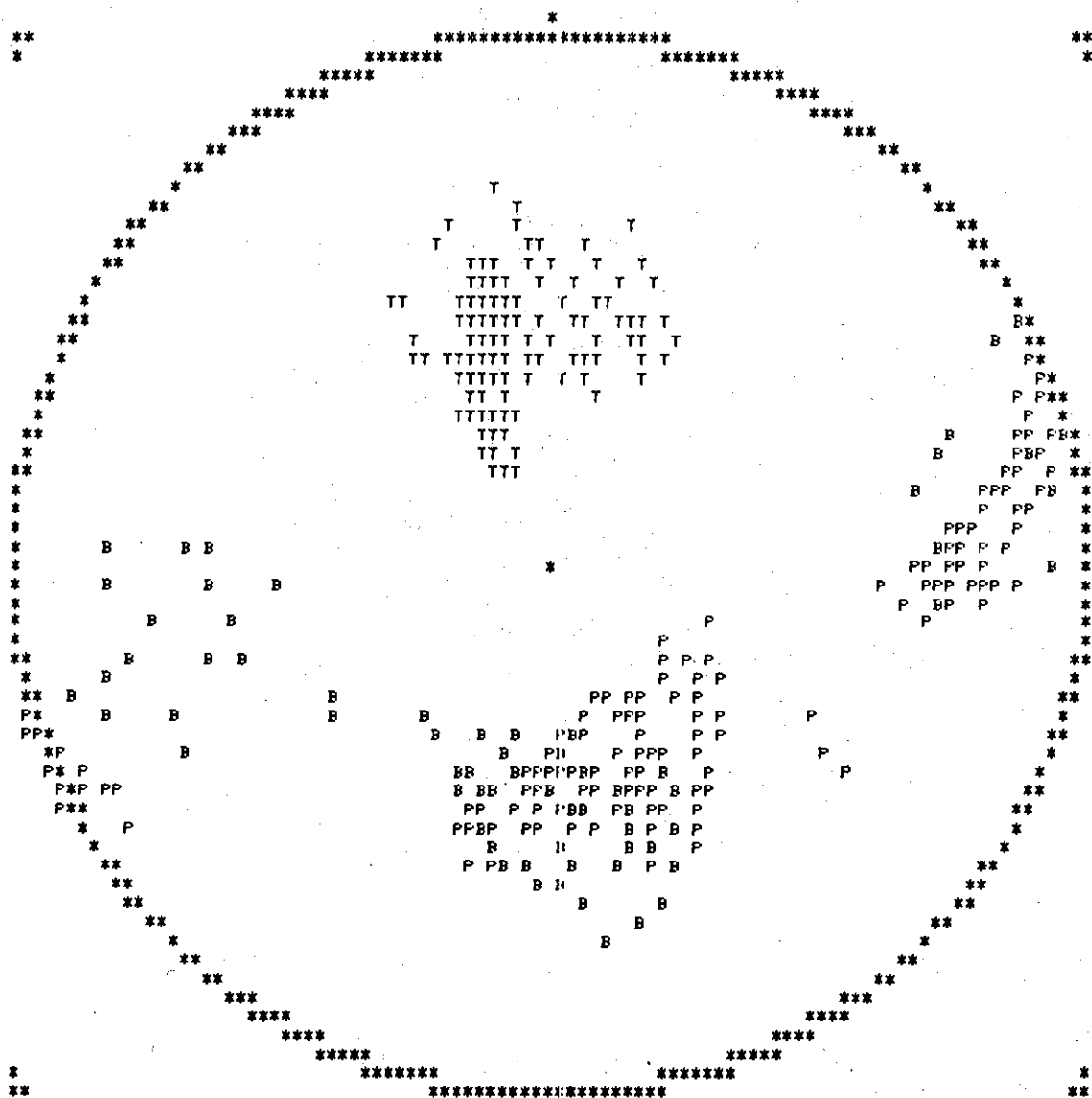


Figure 23. The Domain of Valid Focal Mechanism Solutions for Zero Errors for the August 2, 1974 CHRA Main Shock.

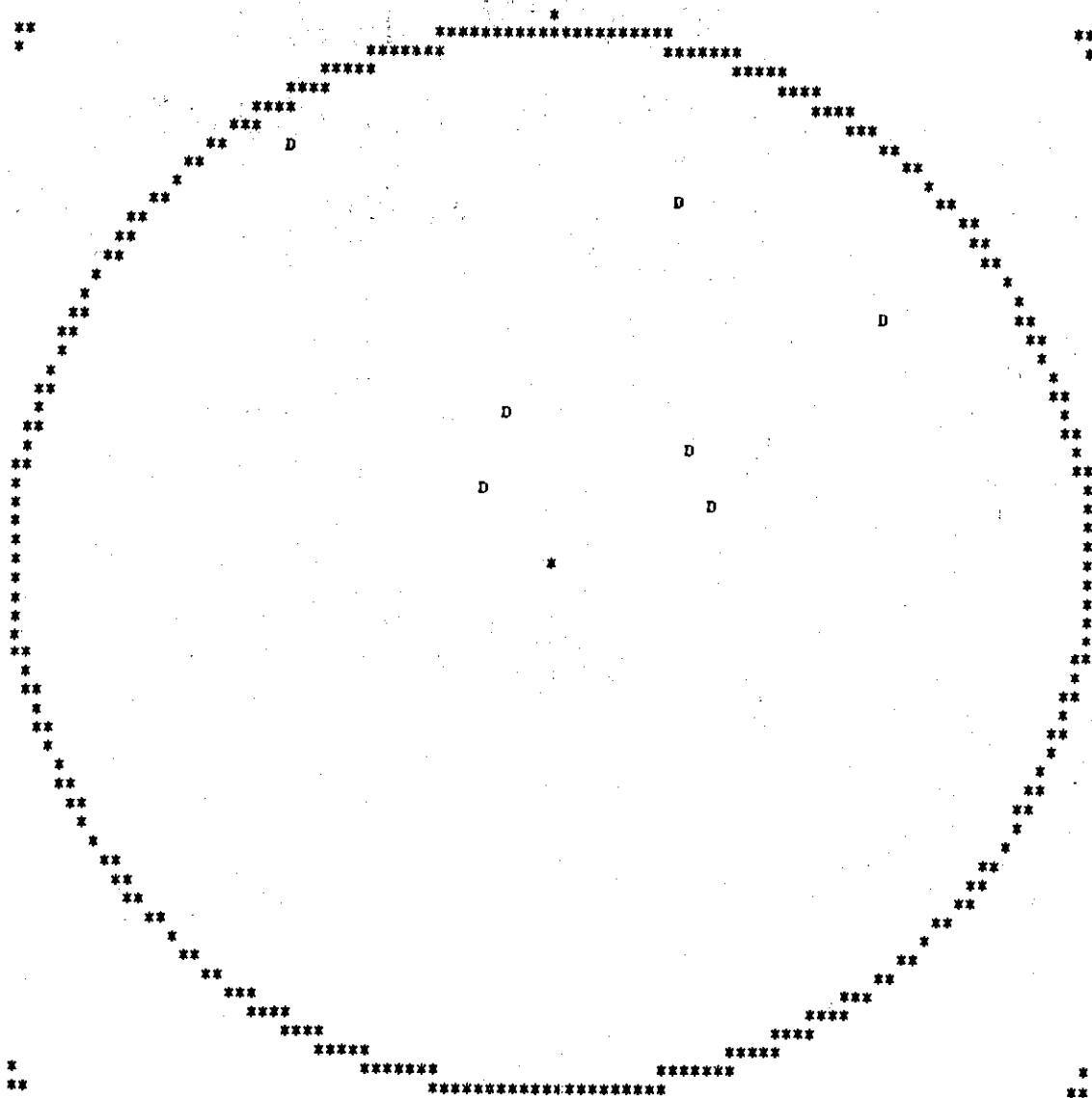


Figure 24. First Motion Plot for an April 14, 1977 CHRA Microearthquake.

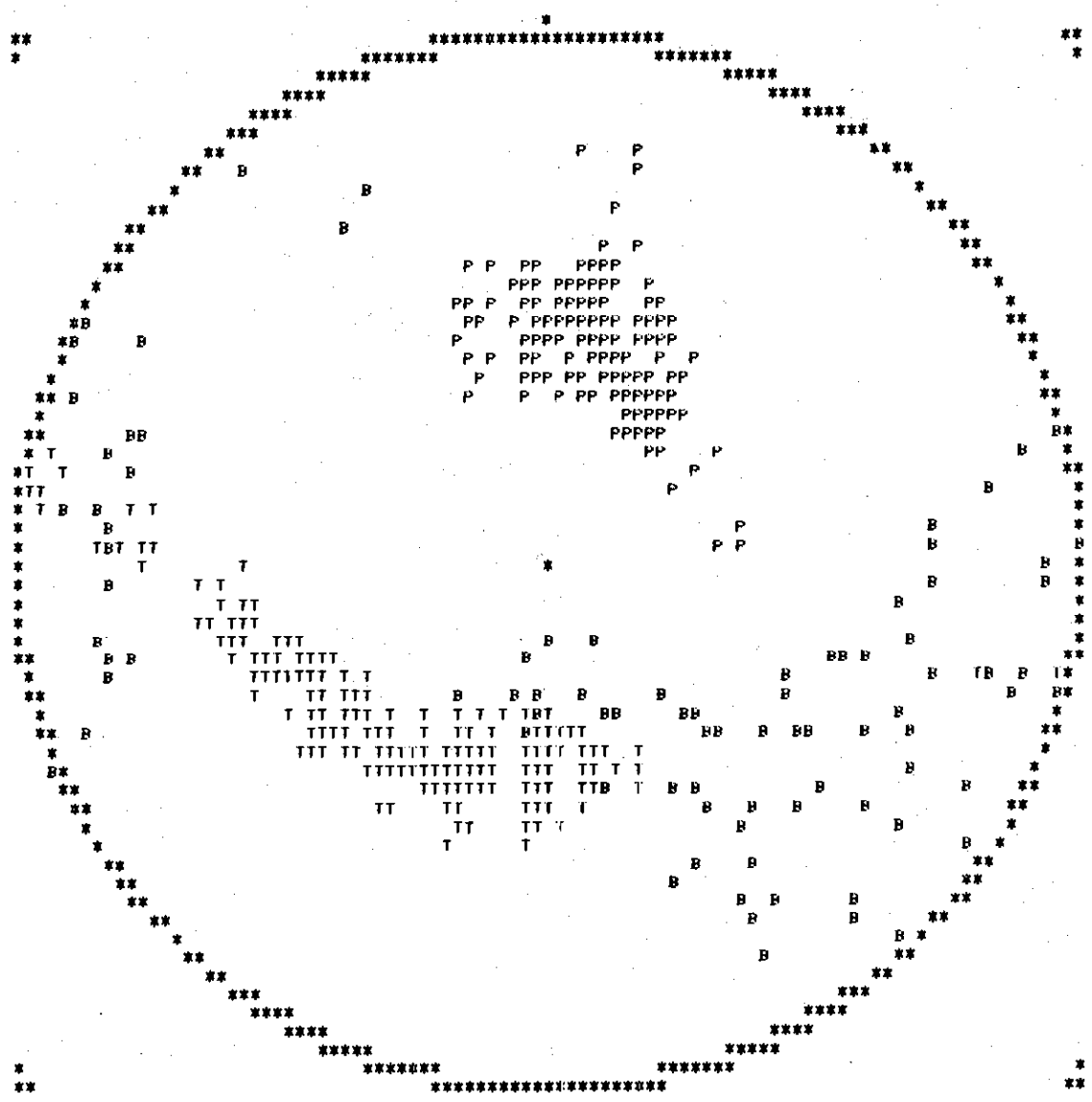


Figure 25. The Domain of Valid Focal Mechanism Solutions for Zero Errors for the April 14, 1977 CHRA Microearthquake.

Figure 26 and 27 show CHRA composite first motions plotted for the case 1 and case 2 taken from Talwani (1976). According to Talwani (1976) the combination of the two cases yielded no clear separation of compressional and dilatational motion, but instead supported two possible fault plane interpretations. Two-thirds of the data supported case 1, left lateral strike-slip motion with nodal planes striking $N20^{\circ}E$ to $N40^{\circ}W$. The remainder, case 2, supported dip-slip motion with nodal planes striking northeast and dipping northwest and southeast. Figures 28 and 29 represent the recomputed focal mechanism solutions for case 1 and case 2. The recomputed solutions indicate the initial published solutions are members of the domain of valid focal mechanism solutions. Since the first motions were composites, the recomputed solutions were determined first for a minimum number of errors and then for additional errors in order to check the dependency of the results on one or several P wave first motions. The results did not appear to be dependent on several additional errors. The case 1 results are more constrained and appear similar to the solutions obtained for the single April 14, 1977 microearthquake and thus a similar interpretation appears valid. The case 2 solutions (figure 29) support fault planes striking northeast, but indicate more variation in trend and plunge. The results for case 2 do not agree with the April 14, 1977 microearthquake focal mechanism solutions. However, the case 2 solutions do appear similar to the main shock solutions. The first motions and solutions for the combination of case 1 and 2 are shown in figures 30 and 31. Although a maximum of 34 errors out of 103 first motions were allowed, the solutions in general show some overlap with the solutions found for case 1 and 2. This result probably represents an averaging of the two cases.

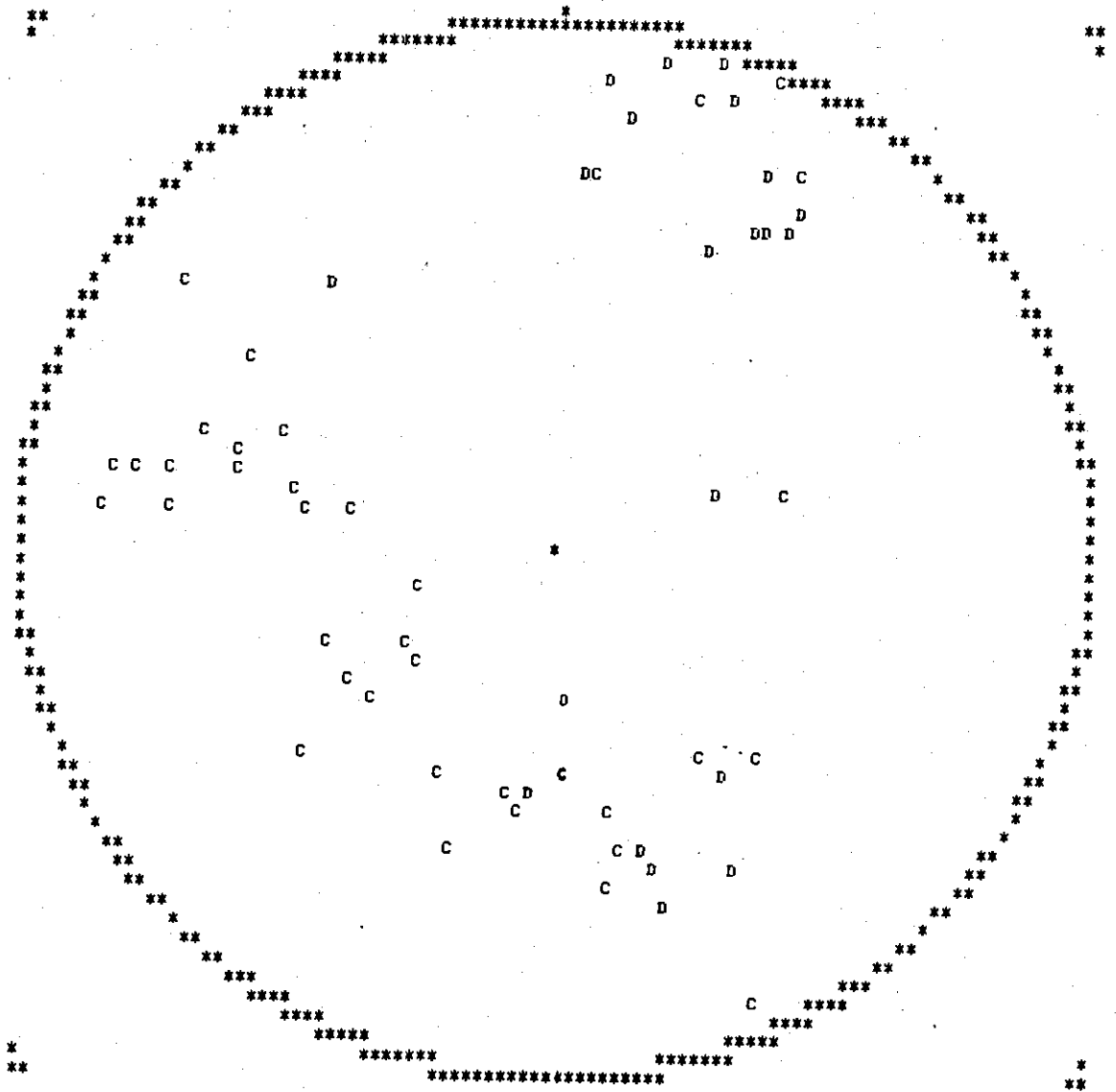


Figure 26. Composite First Motion Plot (Case 1) for the CHRA (after Talwani, 1976).

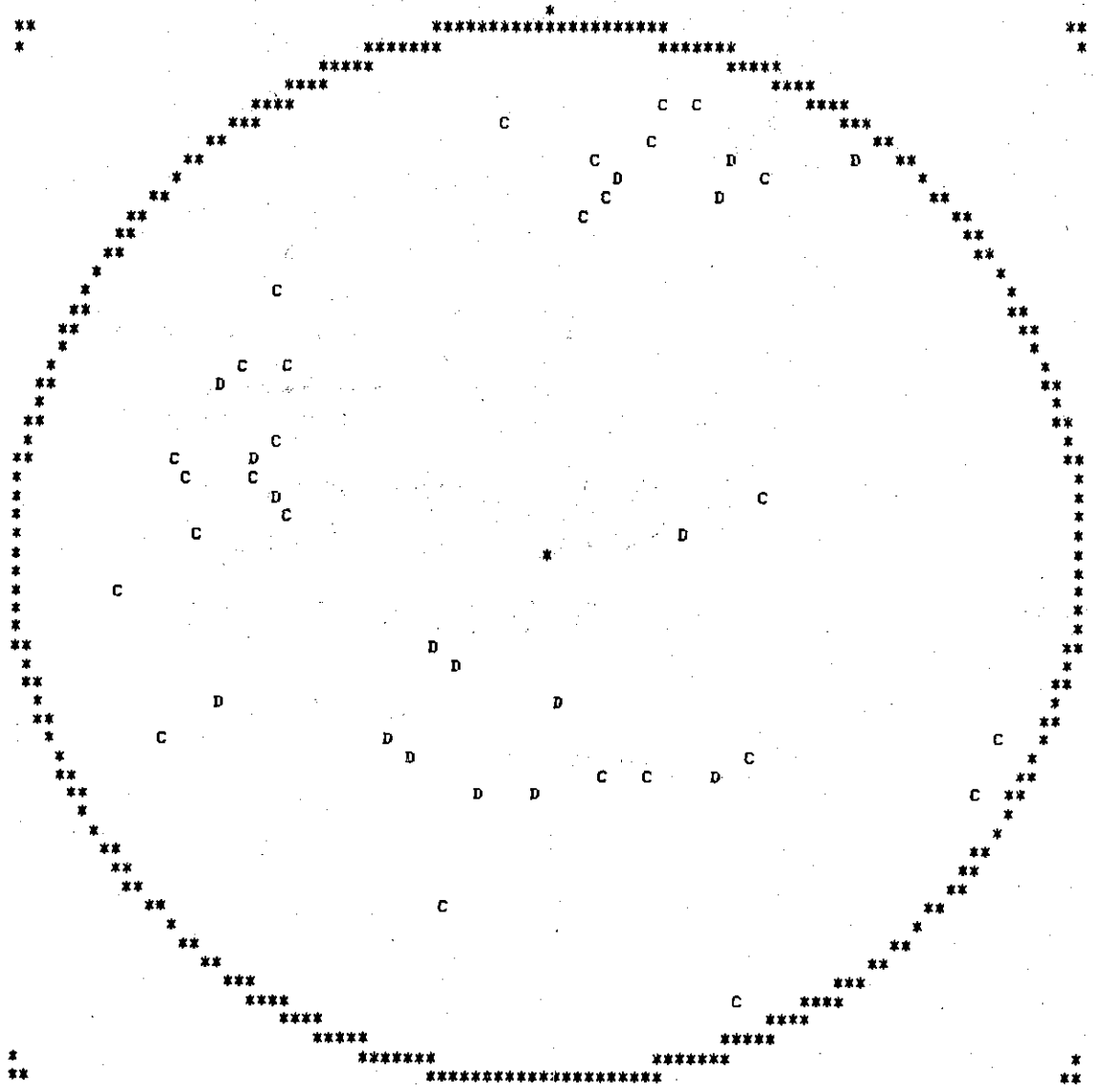


Figure 27. Composite First Motion Plot (Case 2) for the CHRA (after Talwani, 1976).

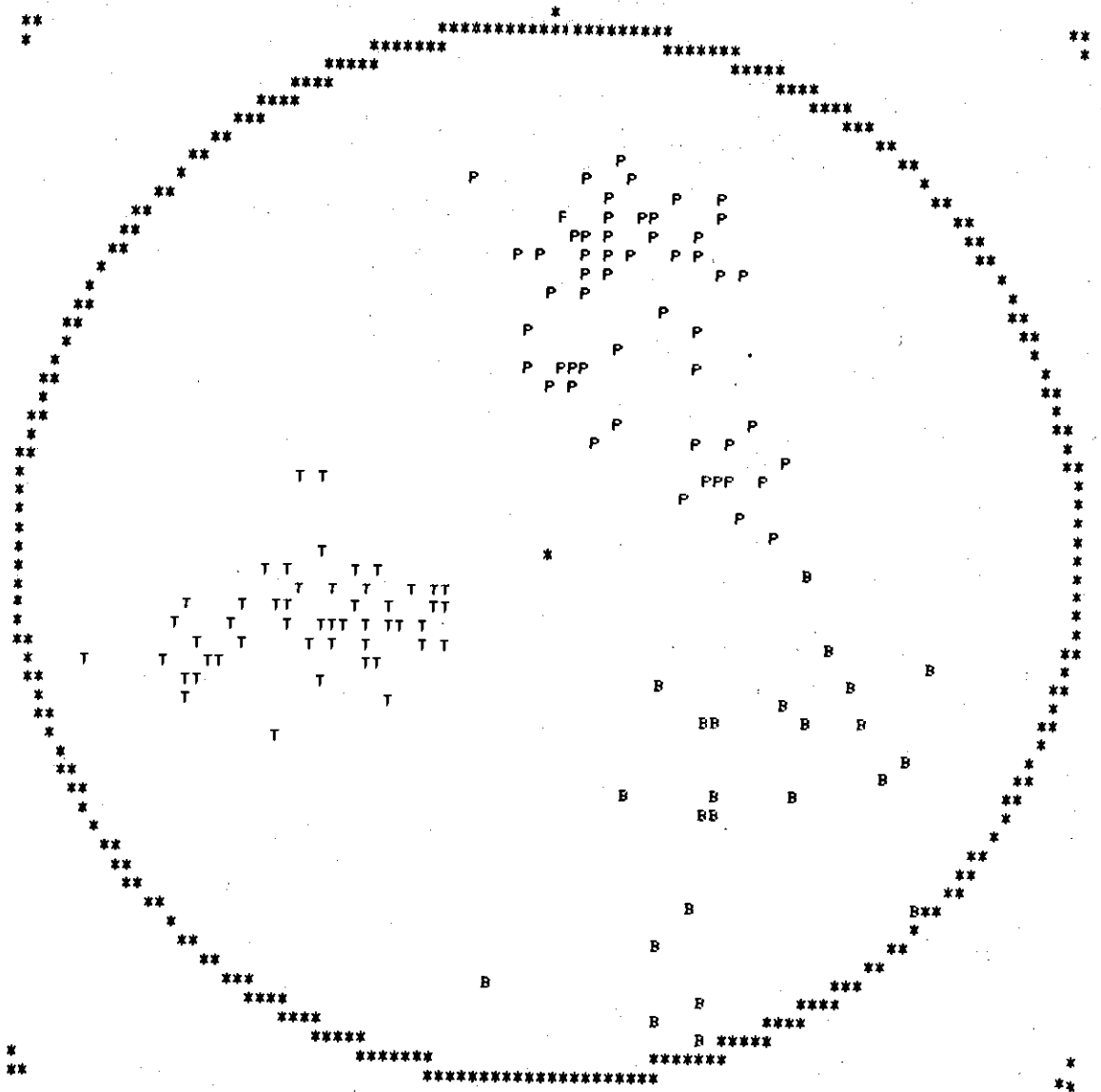


Figure 28. The Domain of Valid Focal Mechanism Solutions for Case 1 for 9 to 13 Errors.

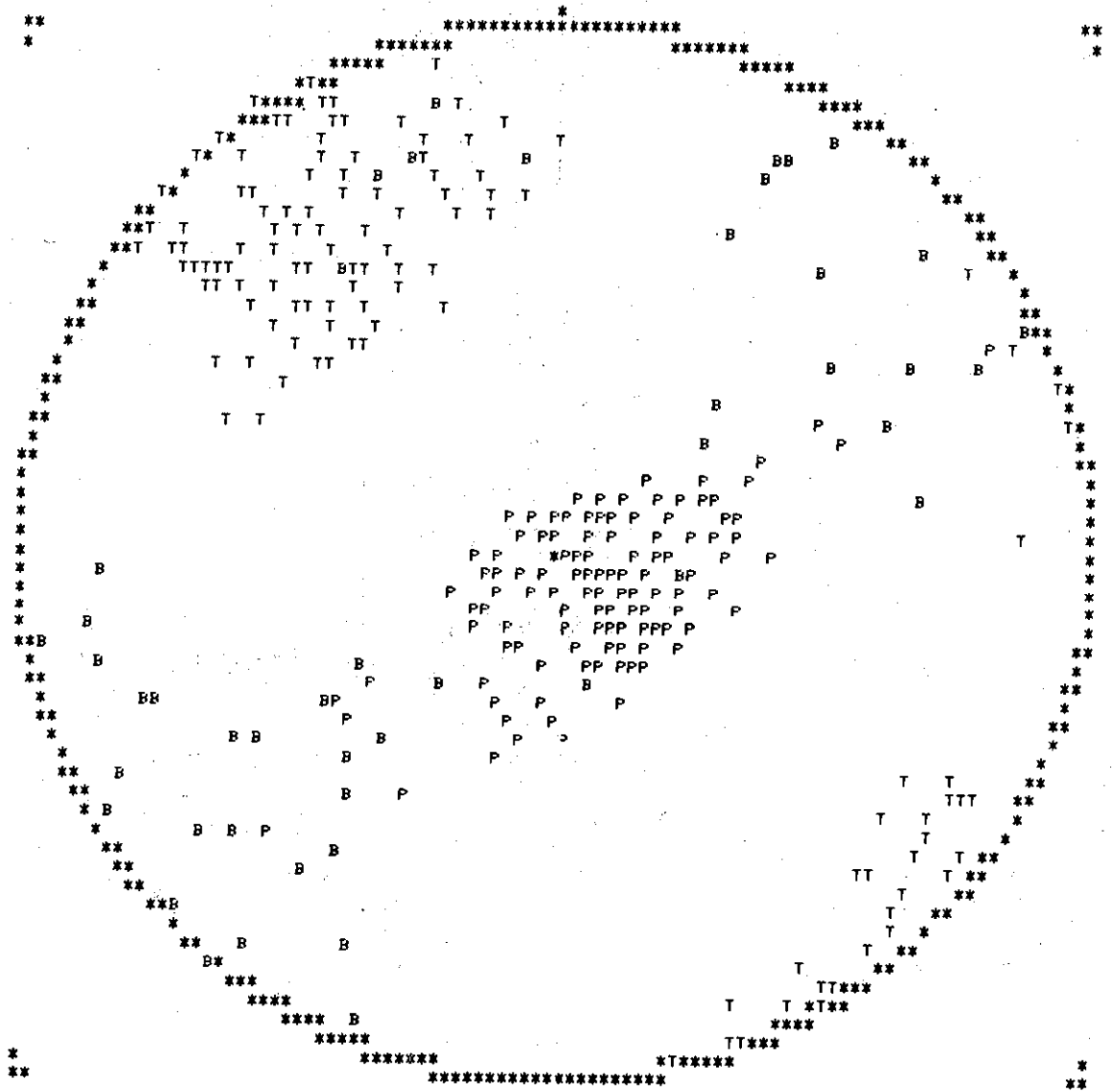


Figure 29. The Domain of Valid Focal Mechanism Solutions for Case 2 for 9 to 13 Errors.

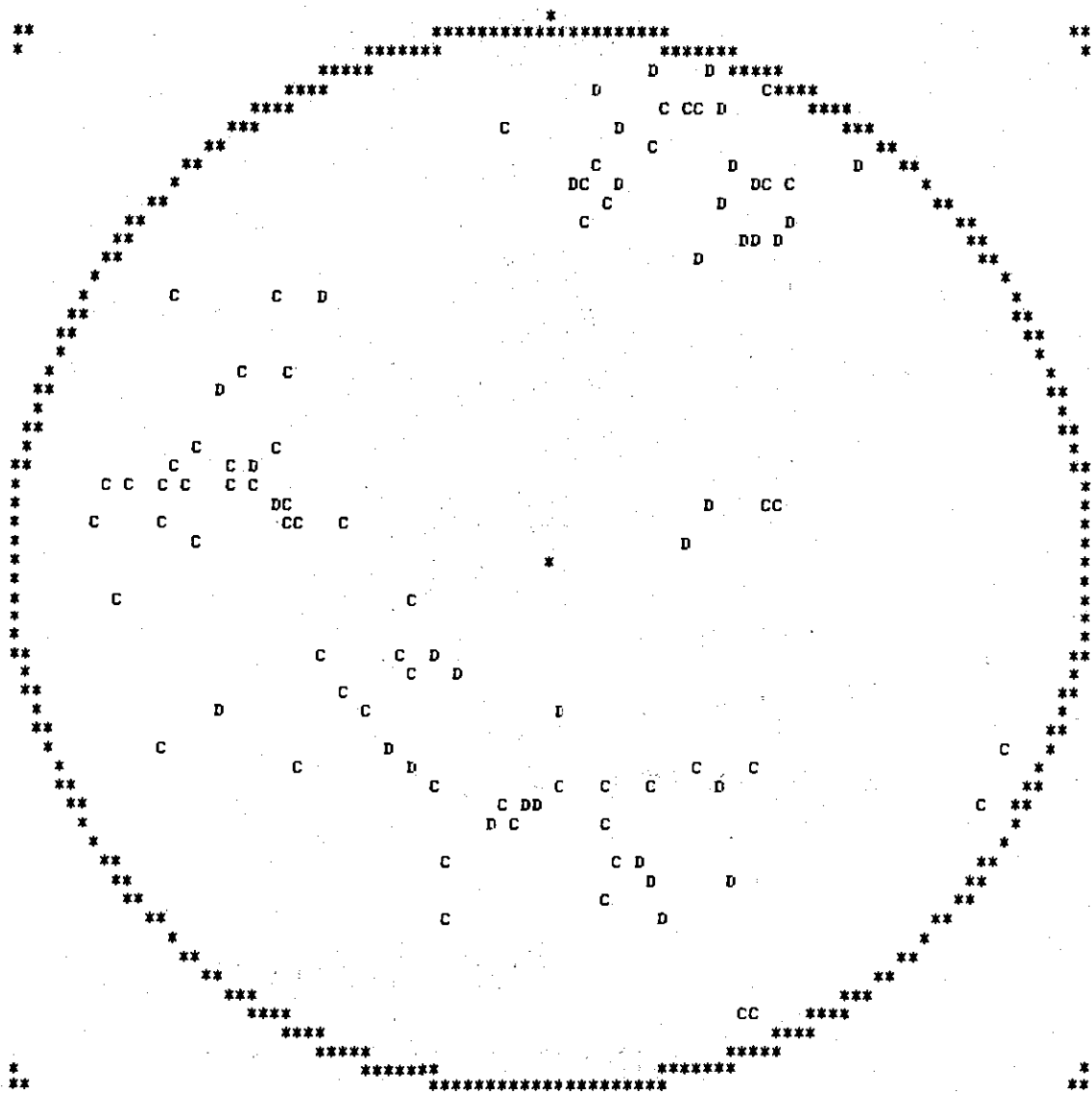


Figure 30. Composite First Motion Plot (Case 1 and Case 2) for the CHRA (after Talwani, 1976).

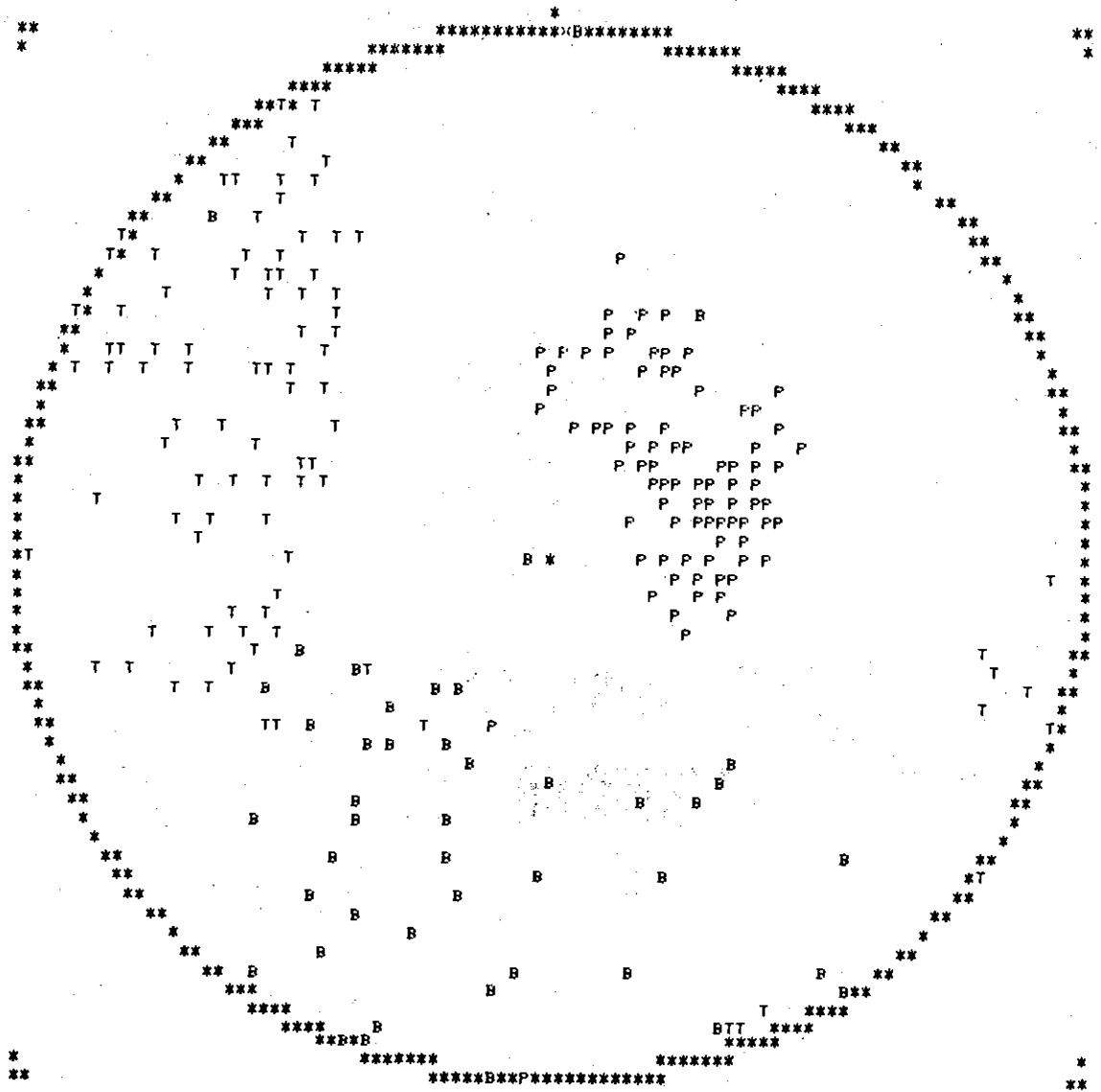


Figure 31. The Domain of Valid Focal Mechanism Solutions for Case 1 and 2 for 31 to 33 Errors.

Based on the number of inconsistent data points the separation does not appear justified. However, the case 1 solutions are similar to the solutions obtained for the April 14, 1977 microearthquake and the case 2 solutions are similar to the solutions obtained for the August 2, 1974 main event. On this basis the separation may be justified. The main event and case 2 solutions give possible fault plane orientations similar to the numerous northwest striking joints observed in the epicentral area of the main shock. The April 14, 1977 microearthquake and case 1 solutions in contrast give possible fault plane orientations similar to the northeast striking joints.

The first motions for the 12 best recorded CHRA microearthquakes, which occurred on March 26, 1977, are given in table 4 and are shown in composite form in figure 32. The focal mechanism solutions were obtained from 36 first motions with a maximum of 10 errors (figure 33). The main result is the apparent similarity of these solutions to the solutions obtained for the August 2, 1974 main shock.

Table 5 contains composite first motion data for two events which occurred on April 14, 1977. Solutions for one of these events have already been shown (see figure 25). Table 6 contains composite first motion data for two events which occurred on March 26, 1977. The first motions for these events were taken from those shown in figure 32. The composite first motion plots are shown in figures 34 and 35. The domains of valid focal mechanism solutions for one error for both composites are shown in figures 36 and 37. The main result here is the definite change from March to April in the maximum and minimum principal stress directions. This suggests at least two possible focal mechanisms which are different.

Table 4. First Motion Data for 12 CHRA Events

Which Occurred on March 26, 1977

Between 02:00 and 21:00 U.T.

No.	Station	Phase	Dist (Km)	Azimuth	Take Off Angle
1	HMR	PC	0.70	90.5	31.0
2	COG	PC	0.93	152.0	38.7
3	CPL	PD	1.88	90.0	58.3
4	HMR	PC	0.36	70.0	20.2
5	GOC	PD	0.69	175.0	35.0
6	CPL	PD	1.52	84.0	57.2
7	HRC	PC	2.80	305.5	70.7
8	HRM	PC	0.18	258.0	12.3
9	GOC	PD	0.96	208.0	49.3
10	CPL	PD	1.00	89.5	50.3
11	HRC	PC	3.16	297.0	75.3
12	HMR	PC	1.04	337.0	82.5
13	GOC	PC	0.70	281.5	79.0
14	CPL	PC	1.28	38.0	83.9
15	HRC	PD	3.88	310.0	88.0
16	HMR	PC	0.29	265.1	65.3
17	GOC	PC	0.87	214.0	81.3
18	CPL	PD	.89	89.0	82.0
19	HRC	PD	3.15	296.5	87.6
20	HMR	PC	0.10	259.0	33.9

No.	Station	Phase	Dist (Km)	Azimuth	Take Off Angle
21	GOC	PD	0.92	205.0	81.1
22	CPL	PD	1.08	90.0	82.5
23	GOC	PD	0.96	209.0	82.1
24	CPL	PD	1.00	90.0	82.4
25	HMR	PC	0.55	85.5	78.8
26	GOC	PC	0.98	165.5	83.6
27	CPL	PD	1.71	93.5	86.3
28	HMR	PC	0.04	168.0	13.9
29	GOC	PD	0.77	198.0	79.3
30	GOC	PC	1.08	206.5	82.5
31	CPL	PD	1.00	105.0	82.0
32	HMR	PC	0.22	133.5	59.0
33	GOC	PD	0.95	187.5	82.2
34	CPL	PD	1.34	93.5	84.4
35	GOC	PC	0.43	244.0	72.5
36	CPL	PD	1.277	59.5	84.0

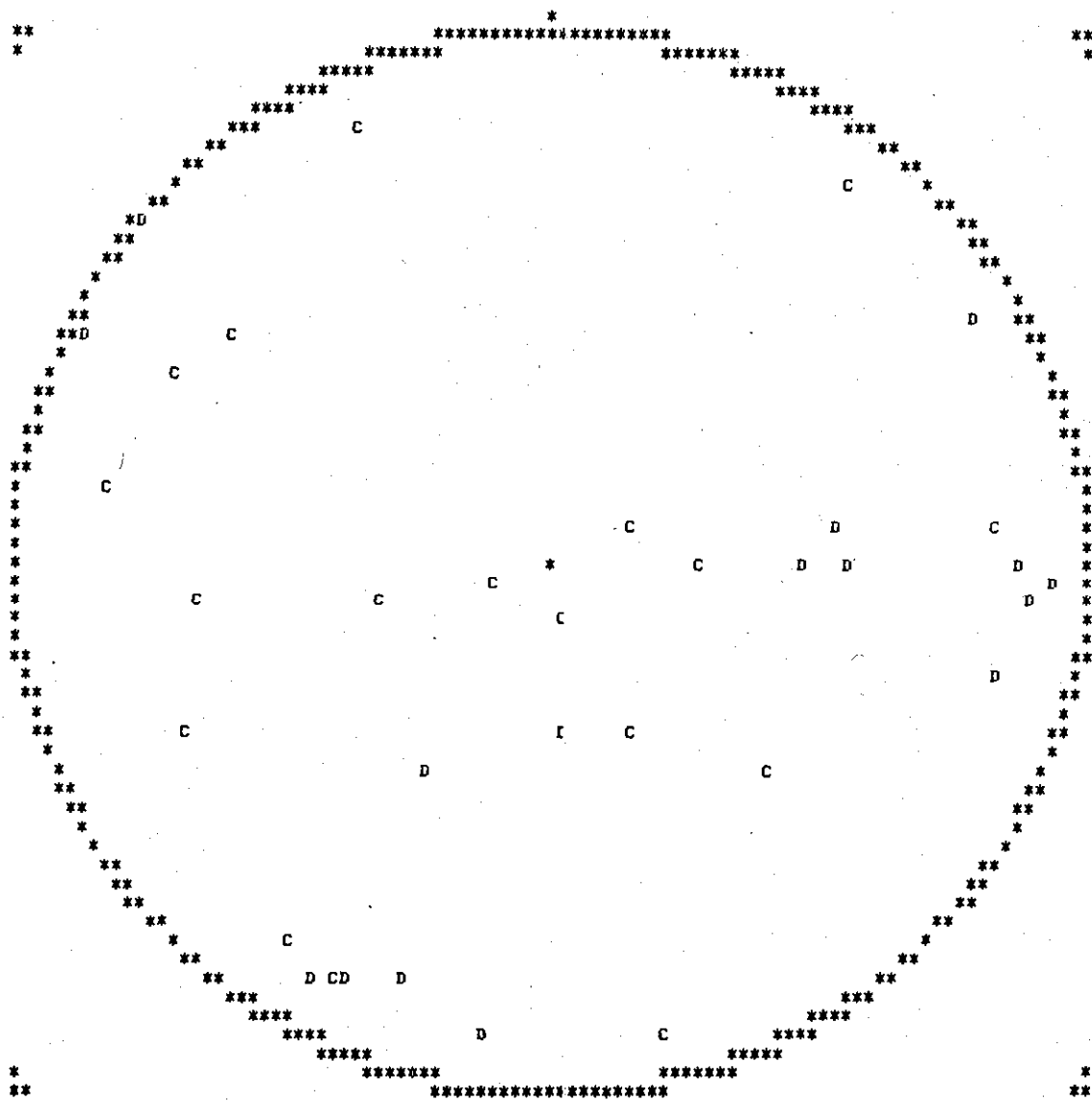


Figure 32. Composite First Motion Plot of 12 CHRA Microearthquakes Which Occurred on March 26, 1977.

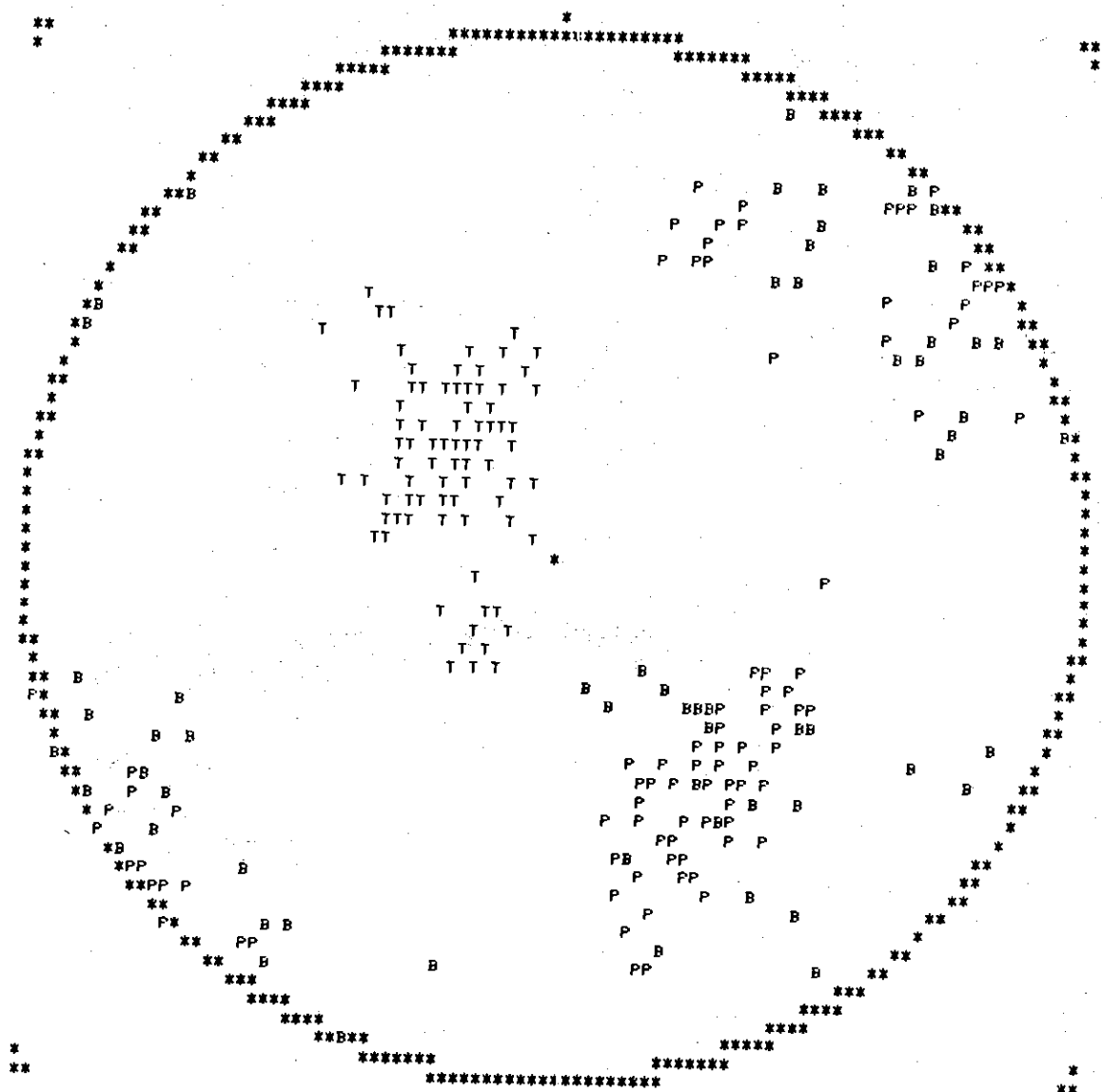


Figure 33. The Domain of Valid Focal Mechanism Solutions for 9 and 10 Errors for 12 CHRA Microearthquakes Which Occurred on March 26, 1977.

Table 5. First Motion Data for Two CHRA Events

Which Occurred on April 14, 1977 at

12:53:32.01 U.T. and 16:33:42.35 U.T.

No.	Station	Phase	Dist (Km)	Azimuth	Take Off Angle
1	BAR	PD	1.20	322.0	20.2
2	GE01	PD	2.34	52.0	35.7
3	DKF	PD	2.09	347.3	32.7
4	CH5	PD	30.80	328.5	84.0
5	CH6	PD	8.97	21.0	70.0
6	RF1	PD	13.40	52.5	76.3
7	MEQ	PD	2.39	72.5	36.3
8	GOC	PC	0.82	157.0	42.6
9	TD3	PC	0.70	210.0	38.1
10	GE01	PD	1.79	57.5	63.6
11	MEQ	PD	1.97	86.0	65.7

Table 6. First Motion Data for Two CHRA Events
 Which Occurred on March 26, 1977 at
 03:49:57.61 U.T. and 05:28:25.81 U.T.

No.	Station	Phase	Dist (Km)	Azimuth	Take Off Angle
1	HMR	PC	0.36	70.0	20.2
2	GOC	PD	0.69	175.0	35.0
3	CPL	PD	1.52	84.0	57.2
4	HRC	PC	2.80	305.5	70.7
5	HMR	PC	1.81	258.0	12.3
6	GOC	PD	0.96	208.0	49.3
7	CPL	PD	1.00	89.5	50.3
8	HRC	PC	3.16	297.0	75.3

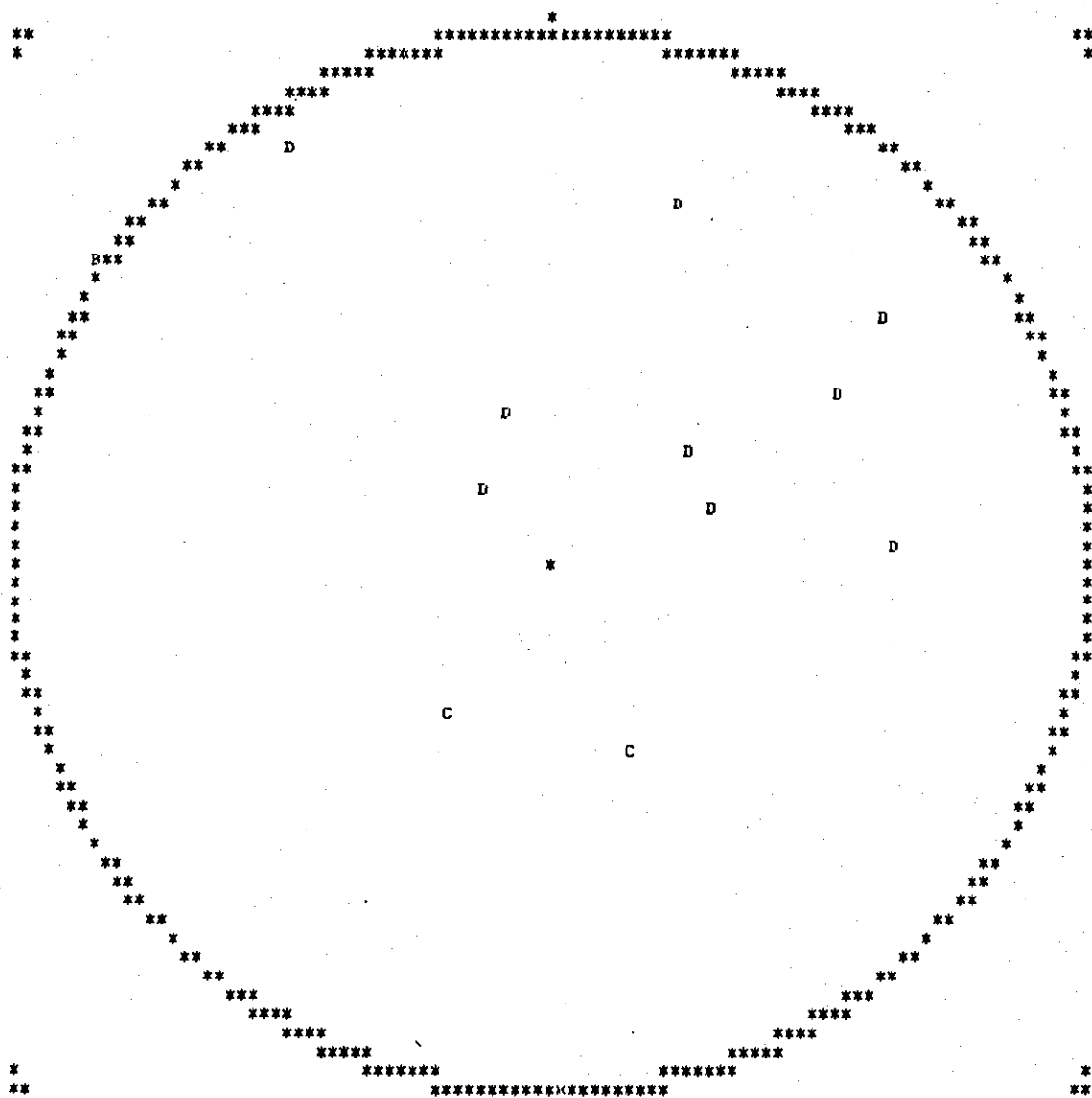


Figure 34. Composite First Motion Plot for Two CHRA
Microearthquakes Which Occurred on April 14, 1977.

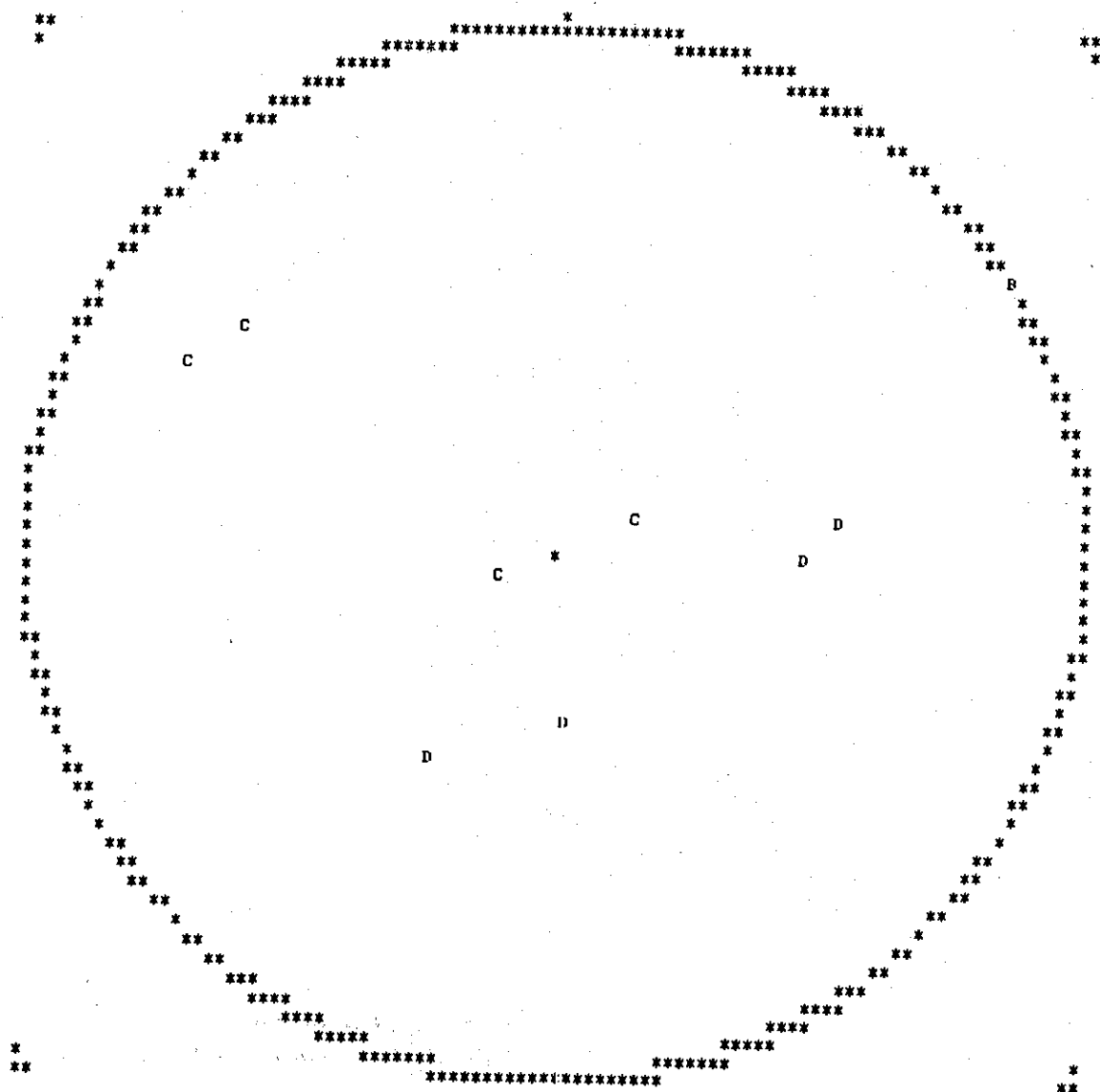


Figure 35. Composite First Motion Plot for Two CHRA
Microearthquakes Which Occurred on March 26, 1977.

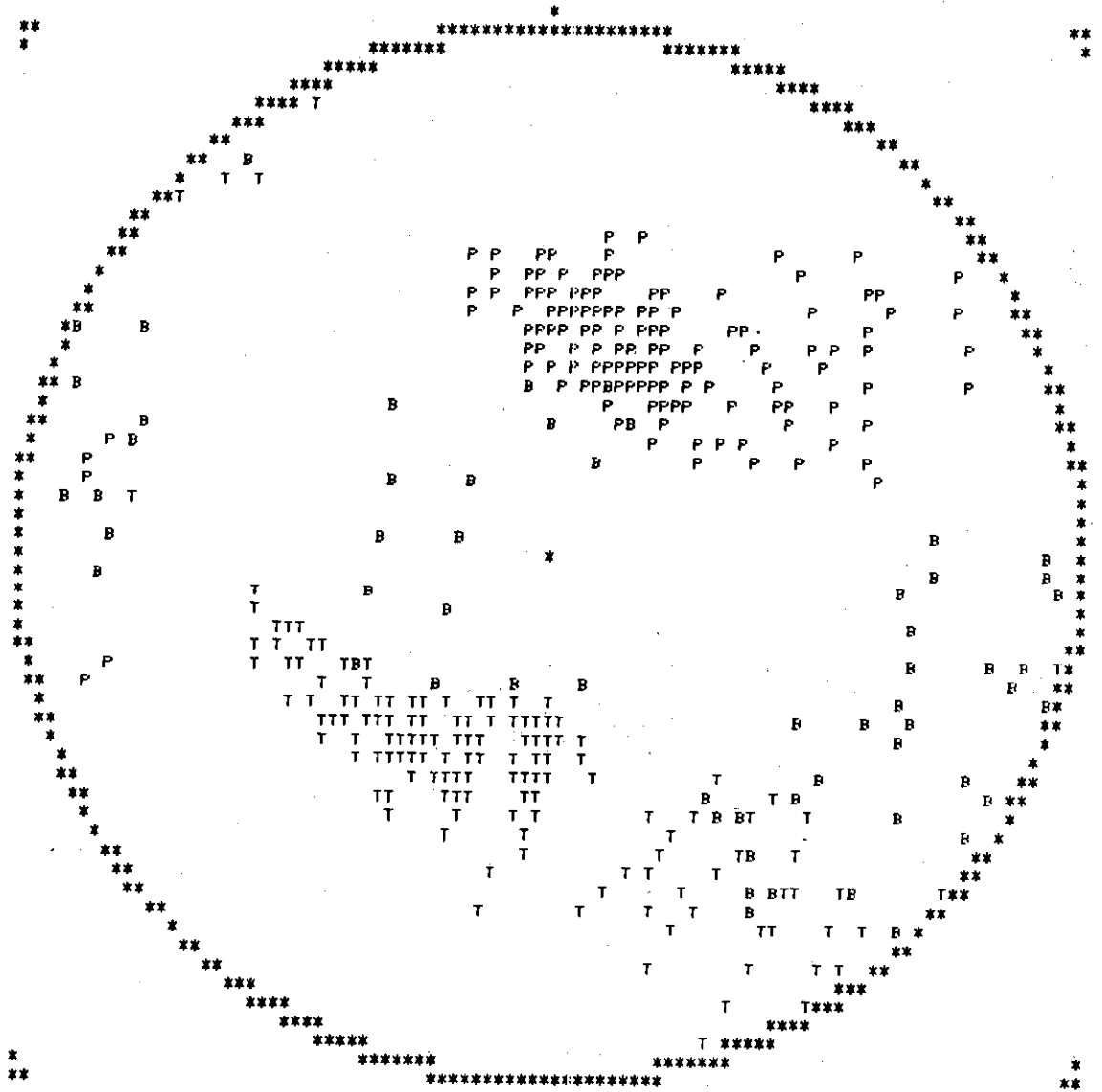


Figure 36. The Domain of Valid Focal Mechanism Solutions for 0 and 1 Errors for Two CHRA Microearthquakes Which Occurred on April 14, 1977.

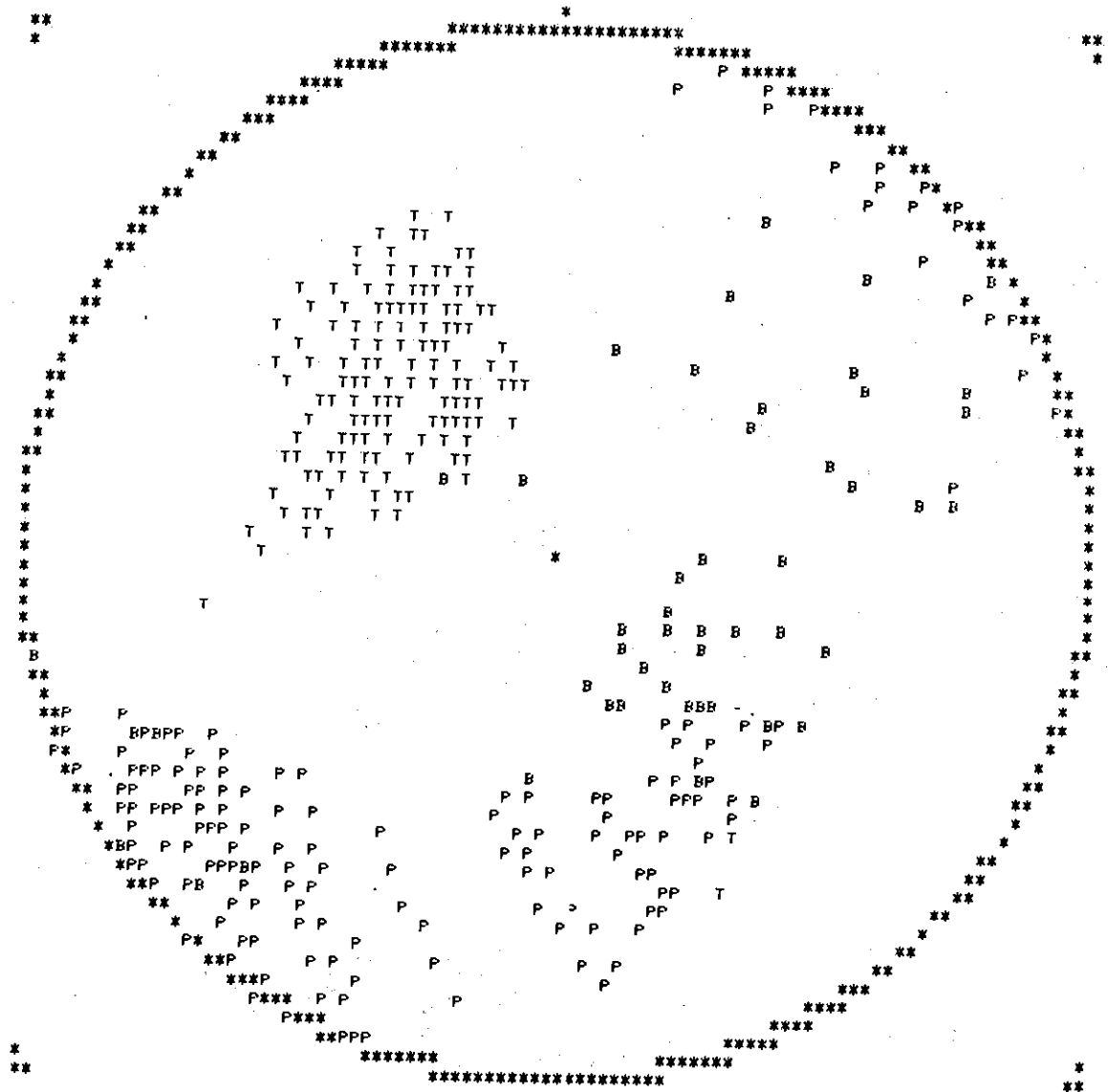


Figure 37. The Domain of Valid Focal Mechanism Solutions for 0 and 1 Errors for Two CHRA Microearthquakes Which Occurred on March 26, 1977.

A stress drop and fault radius has been computed for the August 2, 1974 CHRA earthquake (Bridges, 1975) using several methods. A rupture velocity of 3.5 Km/sec (S wave) was assumed by Bridges (1975) with a spectral corner frequency of 1.4 hertz. From this an effective fault radius of 0.93 Km was obtained and hence a stress drop of about 12 bars. Bridges (1975) noted that a stress drop of this magnitude is abnormally high, since the norm for a similar magnitude event is 0.74 bars. Therefore, the stress drop was recomputed using a rupture velocity equivalent to the compressional wave velocity ($P = 6.0$ Km/sec). From this assumption, Bridges (1975) determined a fault radius of 1.60 Km and a stress drop of 4 bars. This fault radius (1.60 Km) was in agreement with the estimated aftershock zone (1.54 Km), suggesting a rupture velocity of compressional magnitude was valid.

In the same study Bridges (1975) suggested that faulting in the CHRA occurs along two or more planes. The suggestion was based on the scatter of aftershock hypocenters. Talwani (1976), on the basis of composite focal mechanism solutions, has postulated that more than one earthquake mechanism is operative in the CHRA.

A spectral analysis of southeastern United States microearthquakes, presented by Marion (1977), provides more evidence in support of multiple plane faulting in the CHRA main epicentral area. According to Marion's study the CHRA data show sharp, well-defined spectral corners, P and S wave corner frequency ratios (f_p/f_s) greater than or equal to unity, high frequency trends for both P and S wave that decay in amplitude as ω^{-3} , and the absence of intermediate trends. These characteristics are good evidence in favor of the transonic rupture model, which implies slippage along preexisting planes or fractures. The variations observed in the

spectral and the hypocentral data led Marion (1977) to conclude that CHRA microearthquakes occur along multiple planes. The spectra for the CHRA indicate a model which (1) has rupture nucleating at a point (2) results in high frequency content (3) ruptures transonically (i.e. near P wave velocity), and (4) is not confined to one orientation (Marion, 1977).

Stress amplification of corners may explain fracture of brittle rocks in the CHRA (Bridges, 1975) and hence explain the observed high frequency content but cannot explain transonic rupture (Marion, 1977).

The focal mechanism solutions presented here add further constraints on any interpretation concerning seismic activity at the CHRA in that they provide clues to fault plane orientations and acting stress directions. The overall patterns suggested from all focal mechanism solutions, whether composite or not, are those in which 1) the stress directions inferred from focal mechanism solutions are not fixed but rather migrate in time, 2) the possible fault plane orientations in many cases are in good agreement with foliation and joint set directions as determined by the U. S. Army Corps. Engineers (1977), (3) the mechanisms appear to be dominantly on nearly vertical faults with no uniform preference for normal or reverse type movement, and (4) the CHRA earthquake activity occurs along multiple planes rather than on single dominant shear zones.

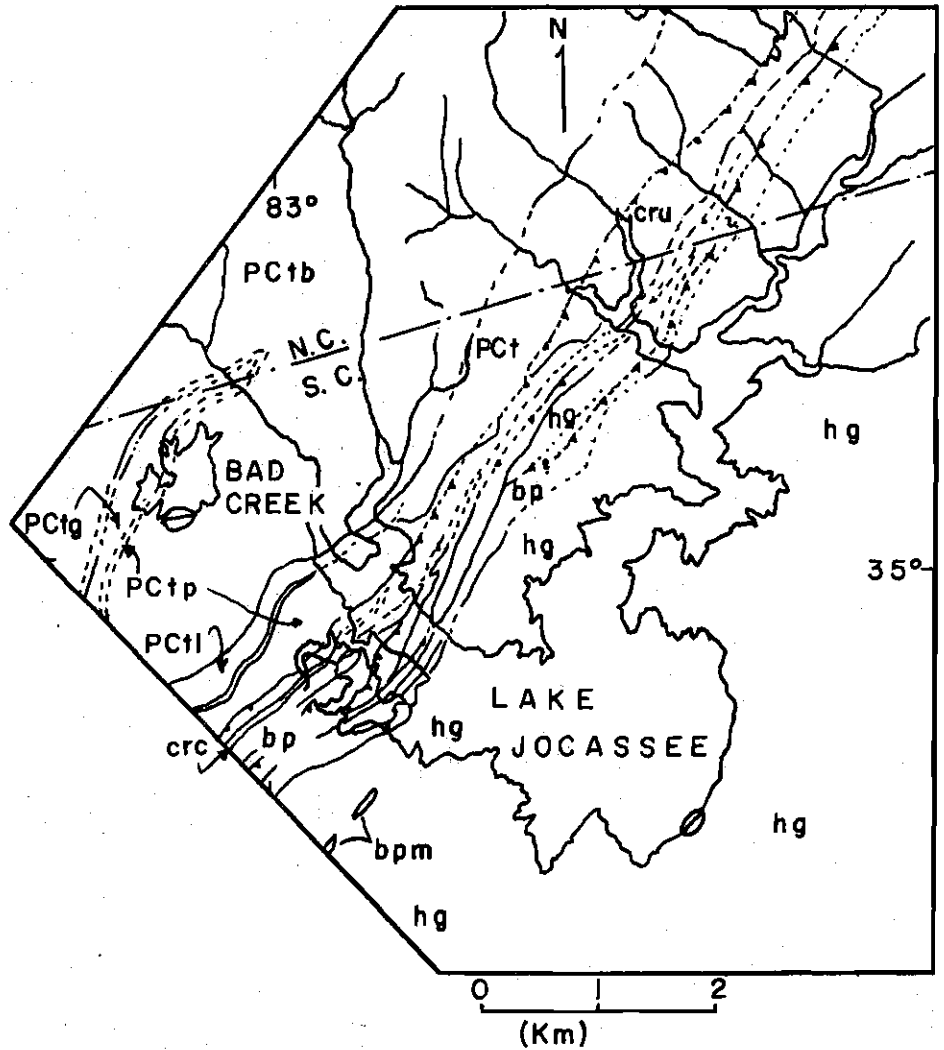
The abnormally high stress drop or suggestion of fresh rock breakage appears dubious since stresses involved in shallow earthquakes and their occurrence along fault planes suggest that the earthquakes occur by failure on weak planes, rather than by brittle fracture of a homogenous material (McKenzie, 1969). The shear stresses associated with shallow earthquakes are at least an order of magnitude too small to produce frac-

ture (Chinnery, 1964, Brune and Allen, 1967, Wyss and Brune, 1968). The transonic rupture model proposed by Marion (1977) requires a well-lubricated dislocation surface. The immediate epicentral area is highly jointed and fractured and, as Marion (1977) noted, such surfaces certainly satisfy the conditions required for transonic slip in which static friction or the normal stress component becomes less than the total stress.

A model for the seismic activity at the CHRA may be proposed by the combination of mechanical processes suggested by Denman (1974) and Talwani (1976), the focal mechanism solutions given here, and the spectral characteristics given by Marion (1977). The model for CHRA seismic activity is one which appears to be the result of an ambient stress field coupled with reservoir impounding in which fluctuations in the water level cause changes in pore pressure at hypocentral depths of 1 to 3 kilometers. The pore pressure changes perturb stress equilibrium conditions and once altered earthquakes with transonic rupture velocities occur along multiple preexisting planes of weakness (not always parallel).

The Jocassee Reservoir Area

The Jocassee Reservoir area (JRA) is located on the Keowee River in northwestern South Carolina near the intersection of the Toxaway and White rivers (figure 38). The JRA is near the northwestern border of the Piedmont Province, and the waters back up across the Brevard Shear Zone and a short distance into the Blue Ridge Province. Lake Jocassee, owned and operated by the Duke Power Company was filled between 1971 and 1974 and has a maximum depth of 107 meters with a maximum capacity of 1.4×10^9 cubic meters.



EXPLANATION

BLUE RIDGE

- PCtg ---- graywacke schist member
- PCt ---- Tallulah Falls Formation (undivided)
- PCtp ---- pelitic schist member
- PCt1 ---- lower member
- unconformity-----
- PCtb ---- Toxaway Gneiss (basement)

CHAUGA BELT

- cru-- Chauga River Formation (undivided)
- hg-- Henderson Gneiss
- bp | pma
- Brevard | amphibolite
- Phyllite | member
- Member |
- crc | bpm
- carbonate | Brevard-Poor
- member | Mountain
- | Transitional
- | Member

Figure 38. Geologic Map of the Jocassee Reservoir Area (after Fogle et al., 1976)

A case history of reservoir induced seismicity has been presented by Fogle et al. (1976). According to Fogle et al. (1976) significant seismic activity began 1.5 years after the lake reached maximum pool. Over 2,000 earthquakes with local magnitudes between -2.0 and +3.2 were recorded by microearthquakes monitors over a period of seven months. The epicenters fell within a crude nine kilometer in diameter circle centered about the lake. Hypocentral depths varied from near surface to about four kilometers below mean sea level (Fogle et al. 1976). In their study the P wave first motions for 65 of the largest events, out of 200 located, were combined to obtain focal mechanism solutions. The published focal mechanism solutions were determined for a variety of small areas in which data from several events were combined in order to obtain a solution for each area. The resulting stress field was interpreted to vary spatially and temporally, but was generalized to be extensional below one kilometer. Also both extensional and compressional distributions were found above one kilometer. According to Fogle et al. (1976) these results are in agreement with a report by Hatcher (1976) which concluded that an extensional stress field is to be expected in the southern Appalachians.

The local geology as shown in figure 38 consists mainly of metamorphic rocks and the overall structural trend in northeast. The dominant structure and rock type are the Brevard Shear Zone and the Henderson Gneiss. The majority of the recorded events at the JRA occurred in the Henderson Gneiss. A more detailed treatment of the geology is given by Fogle et al. (1976).

In this study these 65 events are reanalyzed using the computer adapted method in order to determine the domain of valid focal mechanism

solutions. The first motions for all 65 events are combined to see if a dominant pattern exists, an analysis not included in the above study. Next, only events which occurred below the deeper portion of the reservoir are analyzed. Finally, events which occurred outside the bounds of the lake are analyzed.

The composite plot of all P wave first motions, a total of 177, is shown in figure 39. The domain of valid focal mechanism solutions for 60 inconsistent readings is shown in figure 40. The pressure axes are tightly constrained to the northwest. The tension axes are constrained to southwest trends and the B axes trend east-southeast. The solutions indicate nodal planes which strike east-west and north-south. The east-west planes have almost vertical dips and the north-south planes have shallow dips to the east. Dip-slip type movement is indicated by the solutions for east-west striking planes. Strike-slip movement is indicated for the north-south striking planes. The solutions also indicate northwest and northeast striking planes. The northwest planes have steep dips to the southwest and the indicated movement is normal in which the southwest side has moved down. The northeast planes have dips of about 45 degrees. The sense of movement appears to be left lateral strike-slip. The domain of valid focal mechanism solutions for the minimum of 57 inconsistent P wave first motions was also determined. The domain consisted of only three solutions which occurred in the centers of the pressure, tension, and null axis positions shown in figure 40. The domain of valid focal mechanism solutions was next determined for 65 inconsistent readings. The domain size was much larger, but the pressure, tension, and null axes remained in the same quadrants.

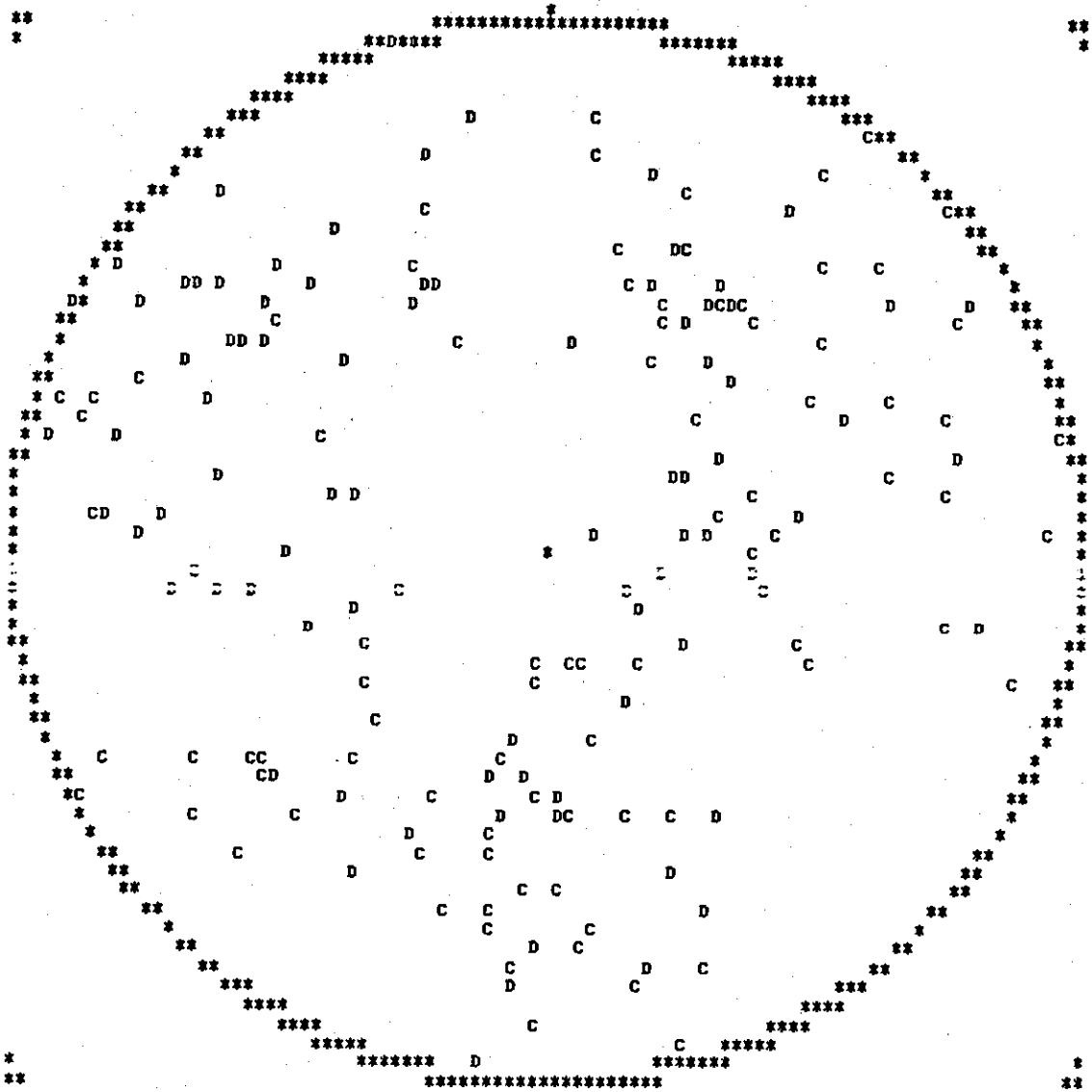


Figure 39. Composite First Motion Plot (177 Data Points) for the Jocassee Reservoir Area (JRA) (Data Courtesy of the Law Engineering Testing Company).

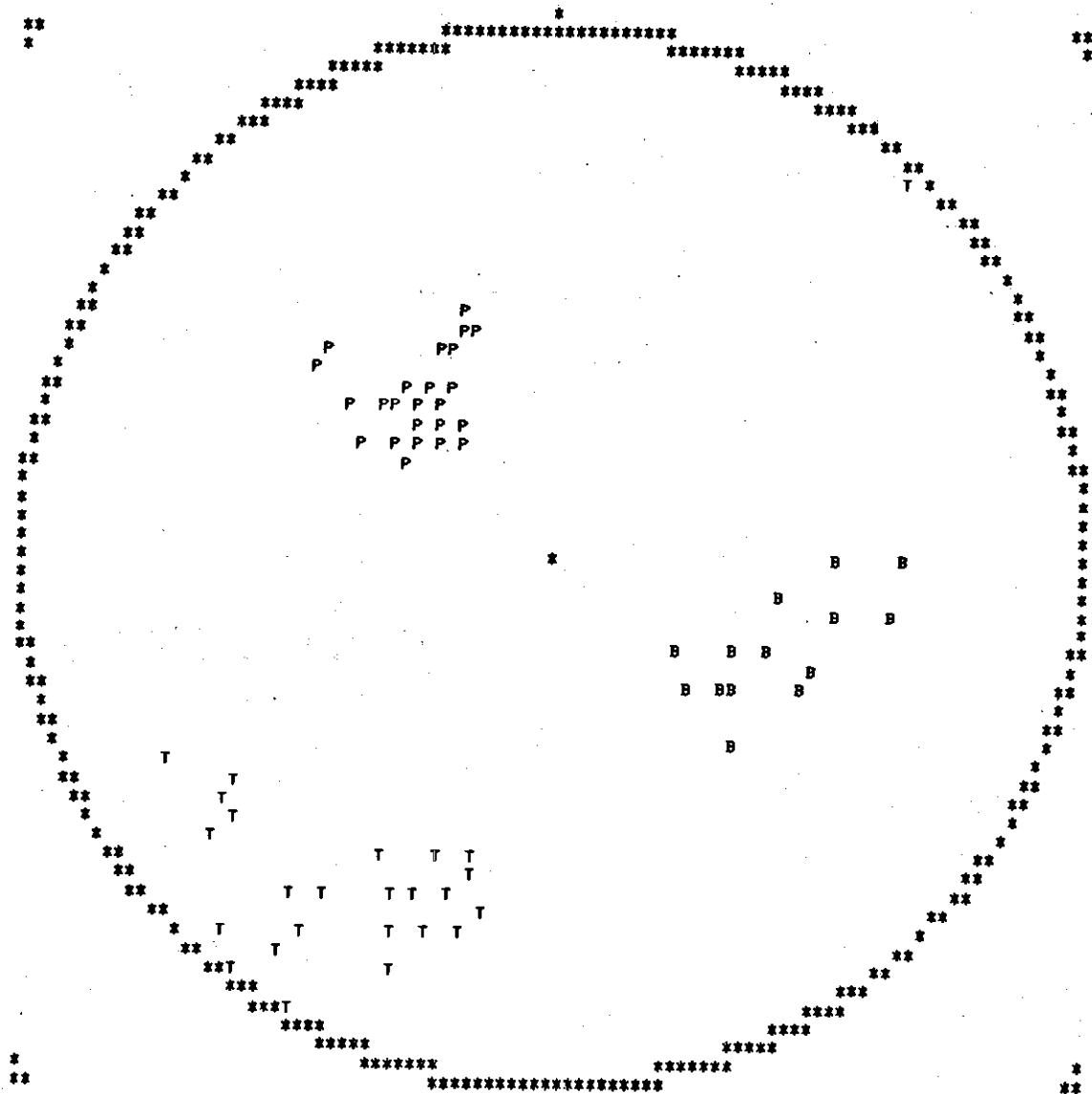


Figure 40. The Domain of Valid Focal Mechanism Solutions for 60 Errors Out of 177 First Motions for the Jocassee Reservoir Area (JRA).

The P wave first motions for events which occurred beneath the deeper portion of the reservoir are shown in composite form in figure 41. A total of 41 first motions were combined in this computation without regard to focal depth. The domain of valid focal mechanism solutions for 13 inconsistent readings is shown in figure 42. The pressure axes are constrained to northern trends with plunges that vary from 40 to 60 degrees. The tension and null axes are less constrained, but the majority are similar to those given in figure 40. The solutions for events which occurred beneath the deeper portion of the reservoir are similar enough to the solutions given for all the composite data that an almost identical interpretation is justified. A much smaller domain was determined for the minimum of 12 inconsistent observations. Solutions in this domain were confined to only east-west striking nodal planes. Dip-slip type movements on the vertical east-west planes are the preferred fault planes. The domain of valid focal mechanism solutions were also found for 15 inconsistent readings. The domain was as expected much larger, but the PTB axes remained in the same quadrants.

The P wave first motions for earthquakes which occurred outside the bounds of the reservoir are combined in figure 43. The domain of valid focal mechanism solutions for 16 inconsistent first motions is shown in figure 44. The solutions are similar, with a few exceptions, to the solutions obtained from the composite of all the data. The solutions are similar enough such that the interpretation is about the same. The domain of valid focal mechanism solutions, determined for the minimum of 14 inconsistent readings, indicated only two solutions were valid. The two solutions occurred in the center of the larger domain.

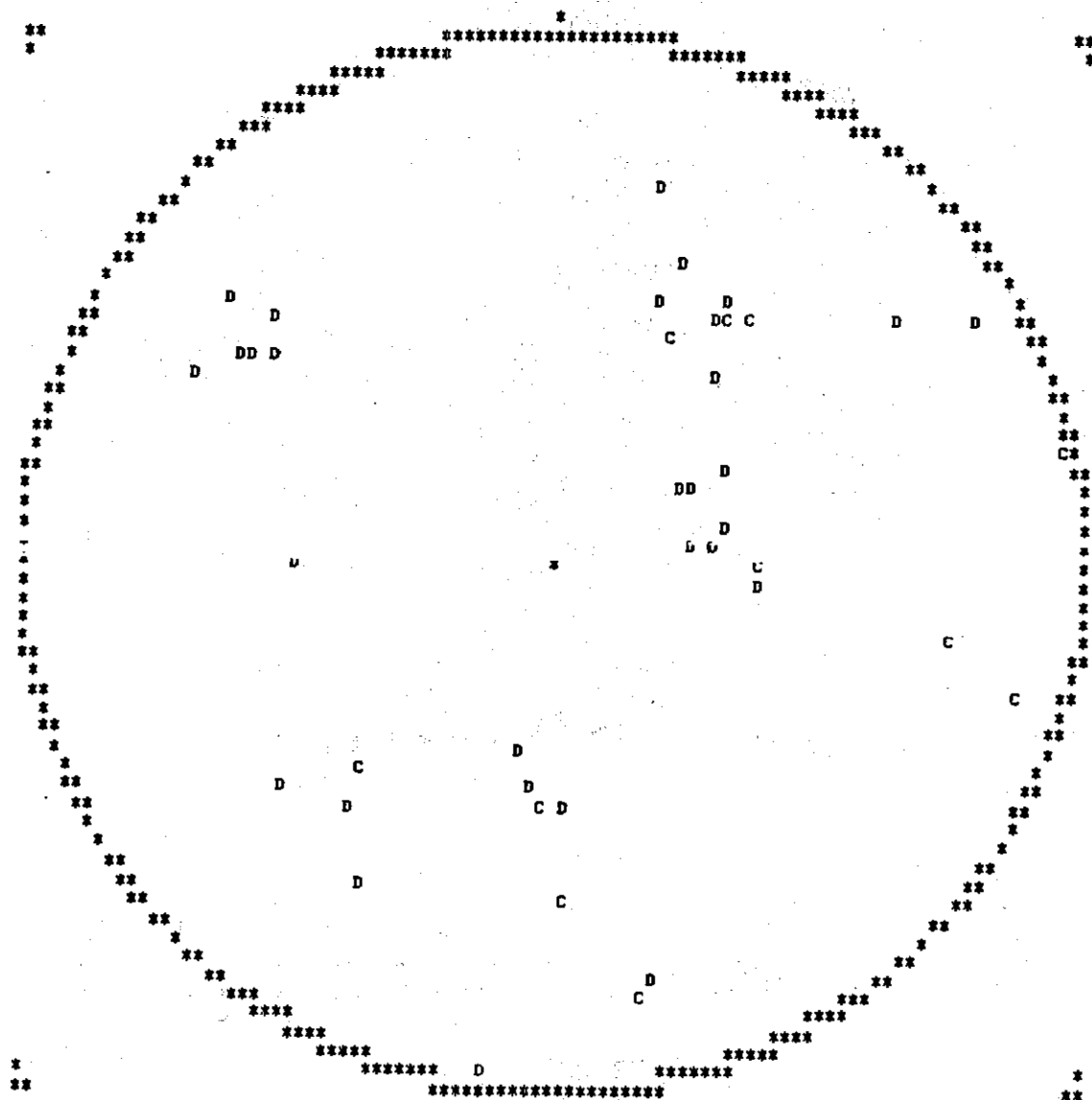


Figure 41. Composite First Motion Plot for Events Which Occurred Beneath the Deep Portion of the Jocassee Reservoir (42 Data Points) (Data Courtesy of the Law Engineering Testing Company).

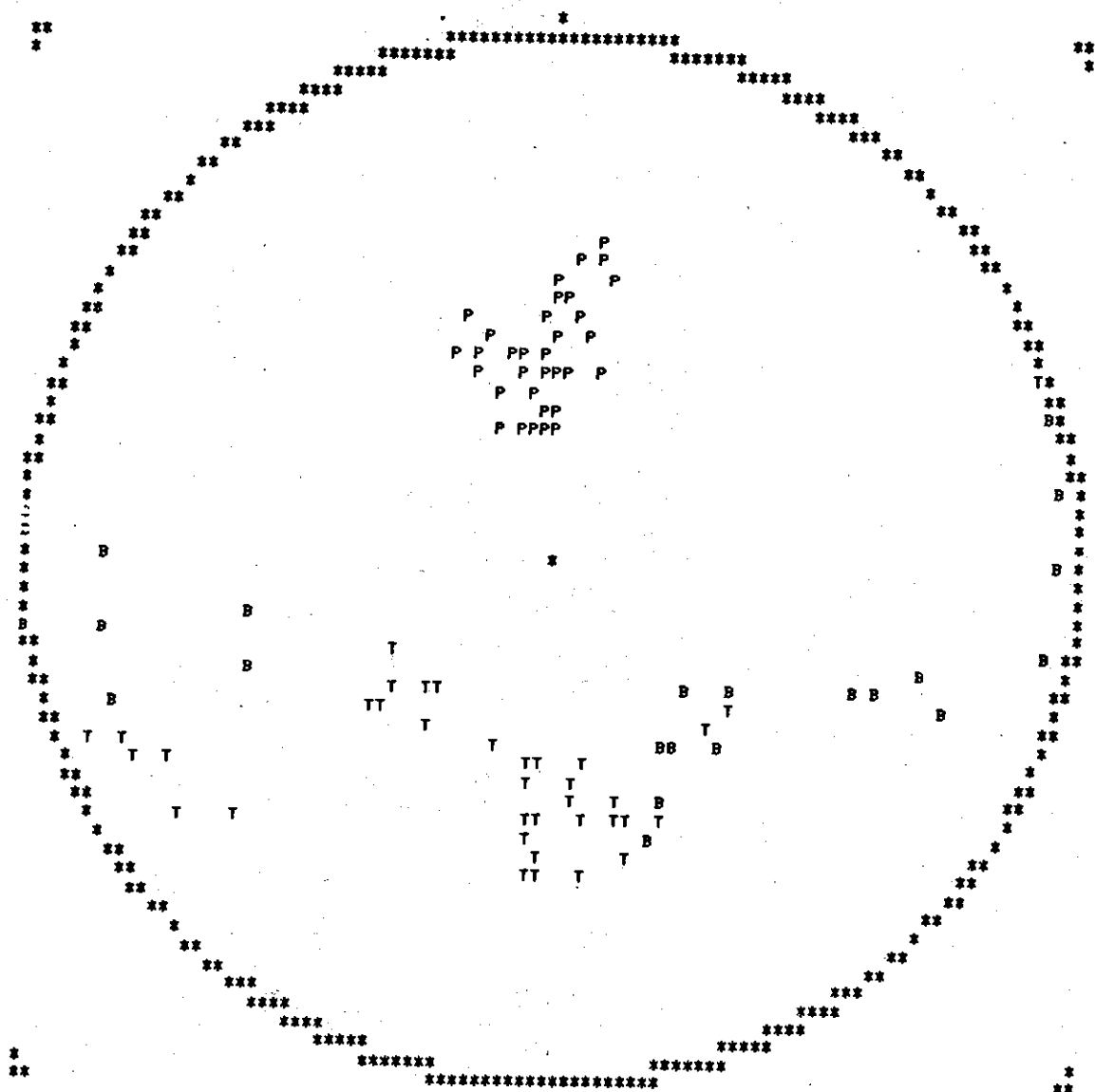


Figure 42. The Domain of Valid Focal Mechanism Solutions for 13 Errors Out of 42 First Motions for the Deep Portion of the Jocassee Reservoir.

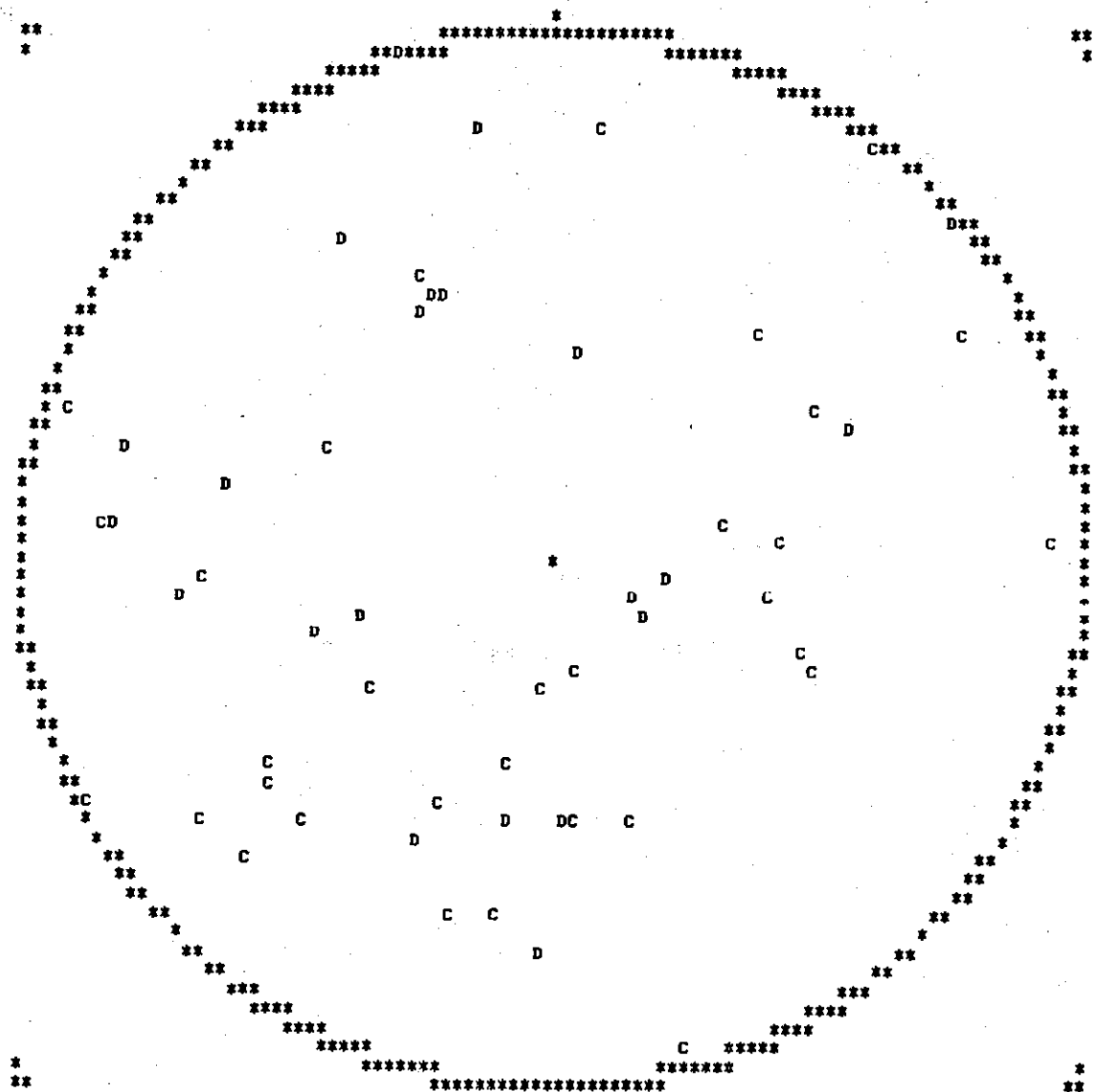


Figure 43. Composite First Motion Plot for Events Which Occurred Outside the Bounds of the Jocassee Reservoir (55 Data Points) (Data Courtesy of the Law Engineering Testing Company.).

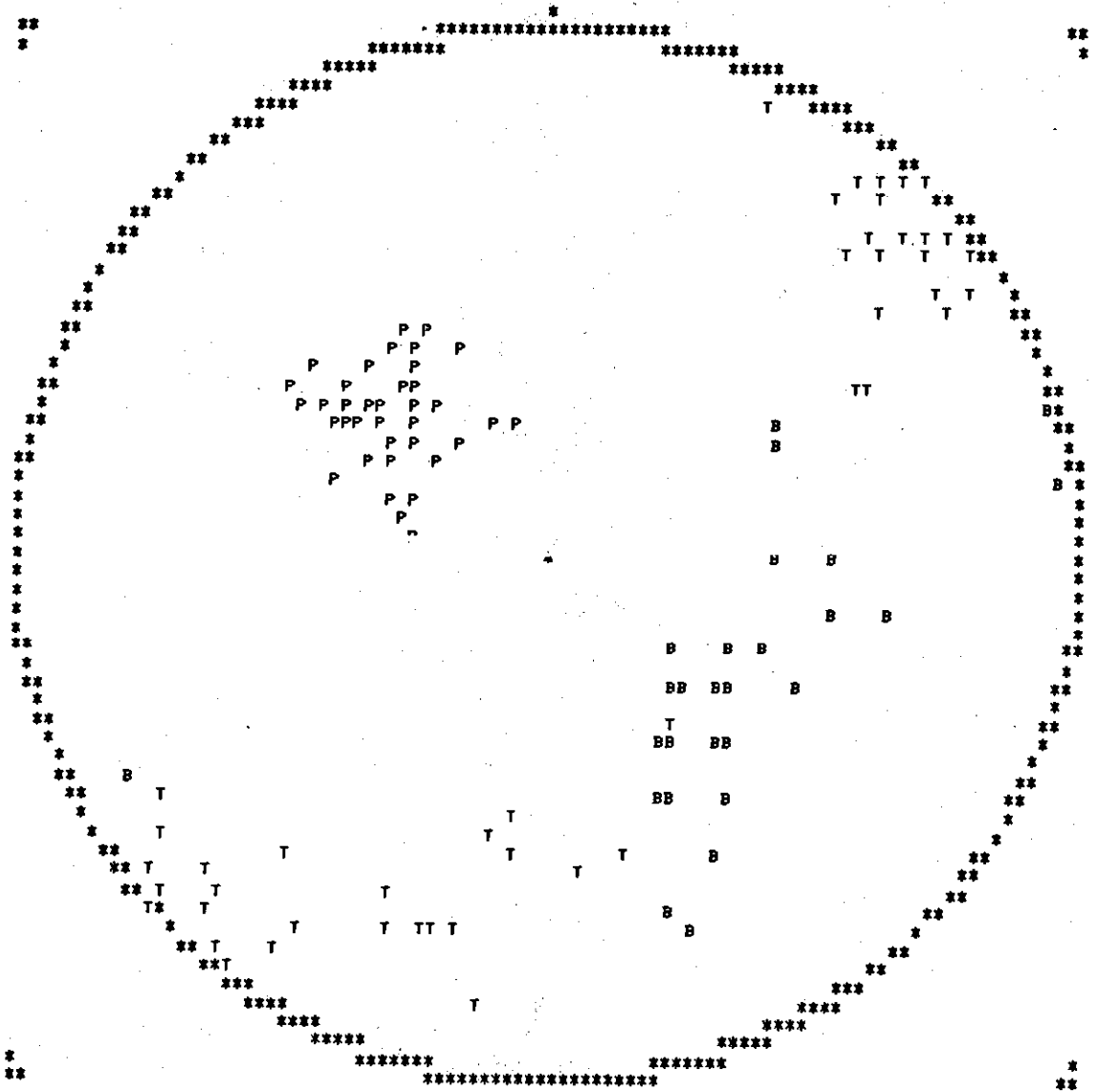


Figure 44. The Domain of Valid Focal Mechanism Solutions for 16 Errors Out of 55 First Motions for Events Which Occurred Outside the Bounds of the Jocassee Reservoir.

Reevaluation of the composite JRA focal mechanism data indicates that similar focal mechanism solutions exist for the two separate areas analyzed. The solutions in general support nearly vertical east-west, northwest and northeast striking fault planes. In all cases the pressure axes are confined to small zones in the north-northwest quadrant. The majority of the pressure axes have vertical components which are greater than the horizontal components. This may suggest a tensional stress field.

Marion (1977) noted the similarity in spectral characteristics between the JRA and the CHRA. The JRA spectra showed f_p/f_s ratios only greater than unity indicating a prevailing transonic rupture velocity for the microearthquakes. This result suggests that the microearthquakes at the JRA are occurring along preexisting planes of weakness.

Detailed geologic mapping in the JRA revealed the presence of several faults and a major joint set (N45E and N45W) which has near vertical dips at the surface. None of the observed faults have been suggested as being active (Fogle et al., 1976). On the basis of over 300 joint measurements, Amick and Talwani (1977) concluded that the joints are steeply dipping and outside the epicentral area trend northeast and southwest. They found joints within the epicentral area had a predominant northwest trend. The joints at the JRA do satisfy the conditions required for transonic rupture. The joints can also explain the scatter of hypocenters. The preferred focal mechanism solutions are those which give nodal planes which strike northeast and northwest and have nearly vertical dips. This preference satisfies the observed geologic structure and spectral characteristics of Jocassee Reservoir area microearthquakes.

The Bowman South Carolina Area

The Bowman, South Carolina epicentral area (BSCA) is located in Orangeburg County in the Coastal Plain Province (figure 1). The geology consists of clastics and marine sequences underlain by dense rocks of basaltic composition.

The seismic activity in South Carolina has been interpreted by Bollinger (1972) as one which forms a northwest-southeast seismic zone extending from Charleston to the Appalachians. This proposed seismic belt is perpendicular to the regional structure, but parallels numerous Mesozoic diabase dikes and other lineaments of Mesozoic age and younger. According to Bollinger (1972), a total of 438 earthquakes have occurred in South Carolina between the years of 1754 and 1971, of which 402 were located in the Charleston-Summerville area.

McKee (1974) has completed a geophysical study of microearthquake activity in the Bowman area. Detailed gravity data in the Bowman area suggest a nearly linear high density basement structure of basaltic composition trending northeast-southwest, underlies much of the Bowman microearthquake epicentral area (McKee, 1974). Apparent irregularities in the gravity contours defining the linear anomaly strike northwest-southeast, and from detailed profiles and modeling the northwest-southeast perturbation may be approximated as a fault at a depth of ≤ 0.32 Km (McKee, 1974).

The Bowman, South Carolina earthquake of May 28, 1974 at 05:01:36.2 U.T. was a relatively small event, $M_{LSE} \sim 2.5$, and hence the number of first

motions was limited (Table 7). The event occurred approximately 90 Km northwest of Charleston, South Carolina at $33^{\circ}22'55''N$ and $82^{\circ}42'05''W$. Although the number of observations is important, the azimuthal distribution is the most important parameter as indicated by some of the previously cited solutions and by the first motion plot for this event, shown in figure 45. This particular set of first motions is remarkably well constrained. The take off angles given in table 7 may appear somewhat peculiar, but a detailed geophysical study of the Bowman area (McKee, 1974), which included a close in microearthquake, gravity, and velocity study, indicated hypocenters occurring at the boundary between a low velocity (5.8 Km/sec) material to the northwest and a high velocity (6.6 Km/sec) material to the southeast. Therefore, the computed take off angles are strongly dependent on azimuth. The domain of valid focal mechanism solutions was determined for zero errors (figure 46). The solutions indicate fault planes striking $N35^{\circ}W \pm 10^{\circ}$ with the maximum principal and minimum principal stress directions located respectively in the northeast and southwest quadrants. The solutions indicate probable dip-slip (normal) faulting, where the east side has moved up, and the less likely horizontal thrust. The domain of valid focal mechanism solutions was also obtained by allowing one inconsistent first motion. The solutions showed more variation, as expected, but the northwest vertical orientation was preserved. The northwest fault plane interpretation is compatible with the hypothesis that the northeast side is being uplifted (Hsaio, 1977).

First motions were also obtained for the BSCA earthquake of November 22, 1976 at 00:31:02.0 U.T. (table 8). The depth was assumed to be from 1 to 3 Km. The plotted first motion, which were all compressional,

Table 7. First Motion Data for the Bowman, South
Carolina Earthquake of May 28, 1974

No.	Station	Phase	Dist (Km)	Azimuth	Take Off Angle
1	PBS	PD	47.0	122.0	80.0
2	NHS	PD	94.0	112.5	80.0
3	HBF	PC	59.0	151.0	80.0
4	SMA	PD	44.0	52.0	80.0
5	SGS	PD	27.0	142.0	80.0
6	VSC	PC	65.0	211.0	61.0
7	OSC	PC	21.0	322.5	61.0
8	JSC	PD	110.0	330.0	58.0

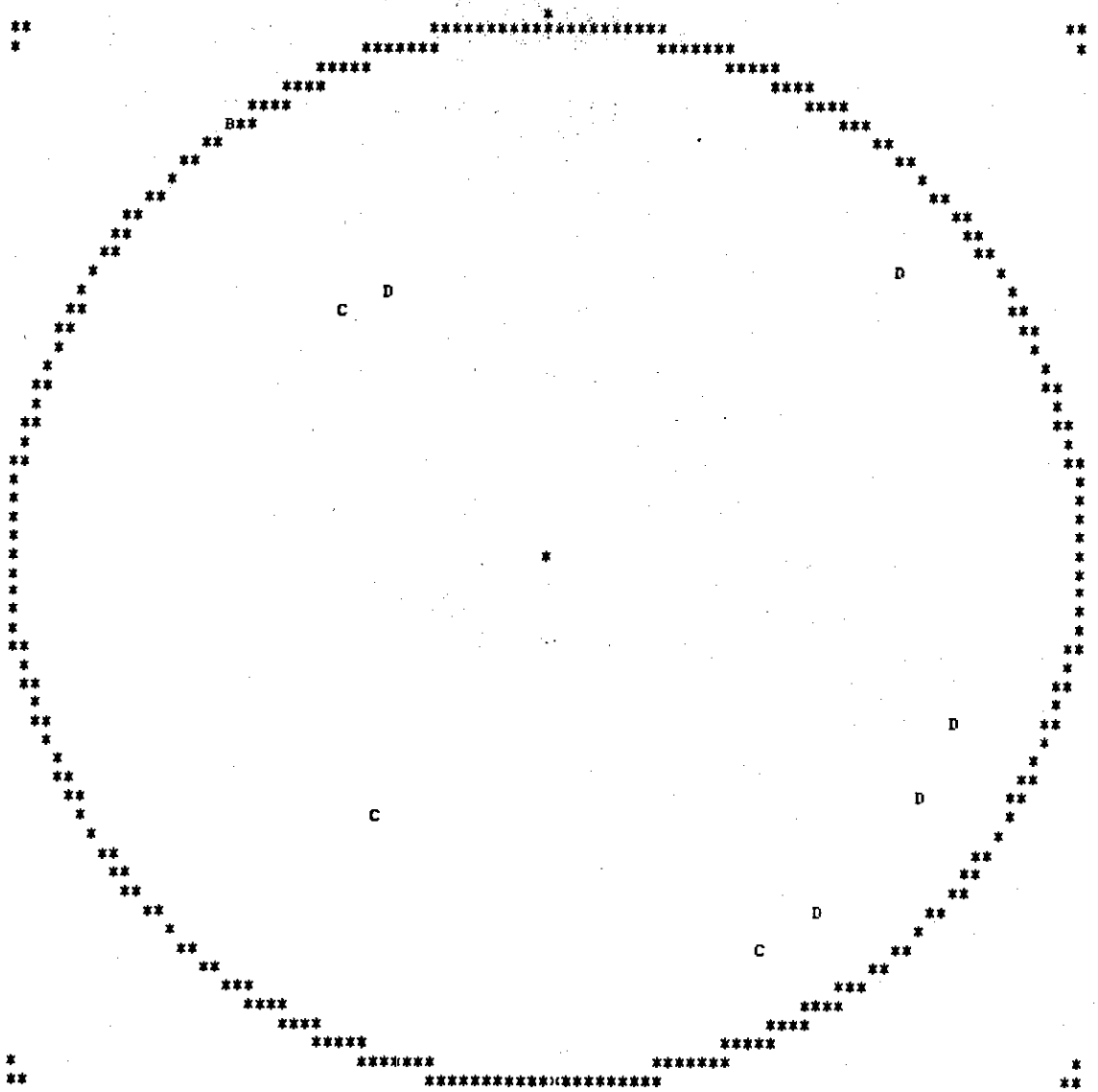


Figure 45. First Motion Plot for the Bowman, South Carolina Area (BSCA) Earthquake of May 28, 1974.

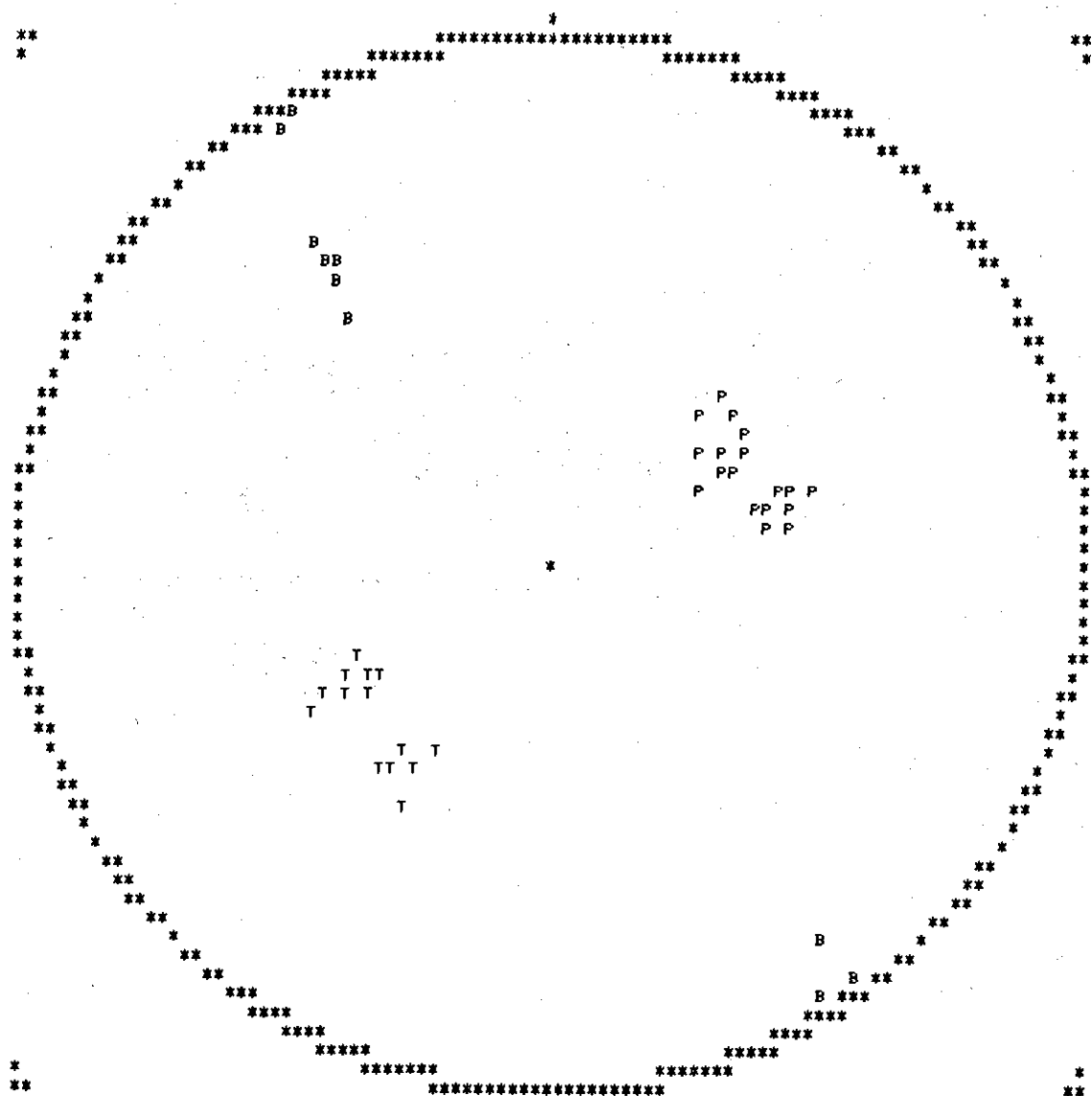


Figure 46. The Domain of Valid Focal Mechanism Solutions for Zero Errors for the BSCA Earthquake of May 28, 1974.

Table 8. First Motion Data for the Bowman South
Carolina Earthquake of November 22, 1976

No.	Station	Phase	Dist (Km)	Azimuth	Take Off Angle
1	OSC	PC	21.0	322.0	61.0
2	SGS	PC	27.0	142.0	80.0
3	HBF	PC	59.0	151.0	80.0
4	VSC	PC	65.0	211.0	61.0
5	SRPN	PC	84.0	265.0	61.0
6	SRPW	PC	98.0	256.0	61.0
7	JSC	PC	110.0	330.0	58.0
8	PRM	PC	173.0	297.0	61.0

are shown in figure 47. The domain of valid focal mechanism solutions for zero errors is shown in figure 48. The wide variation in solutions indicates poorly constrained data. The location of the pressure axes is similar to those obtained for the May 28, 1974 BSCA earthquake, but a definitive fault plane orientation appears tentative.

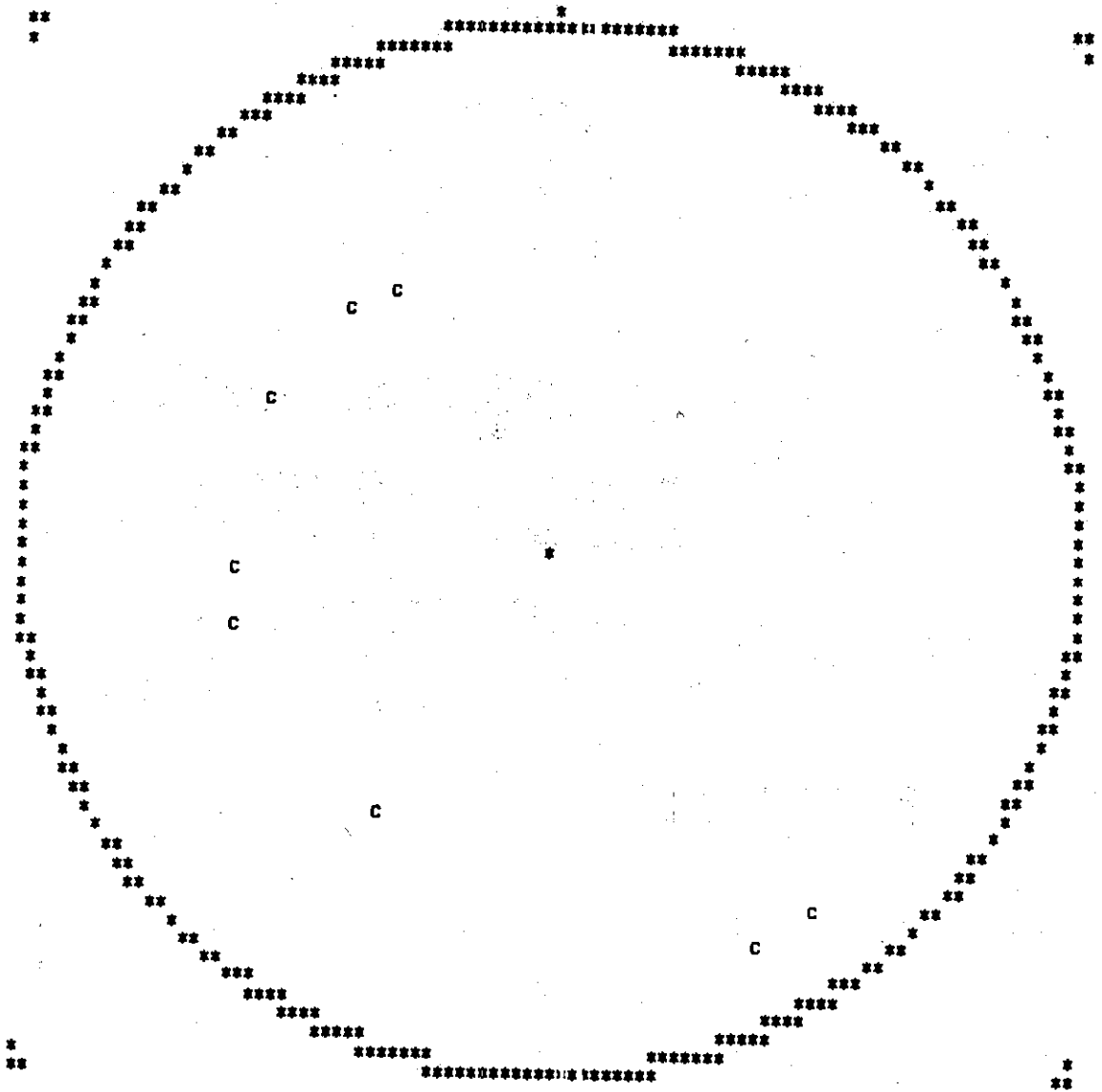


Figure 47. First Motion Plot for the Bowman, South Carolina Area (BSCA) Earthquake of November 22, 1976.

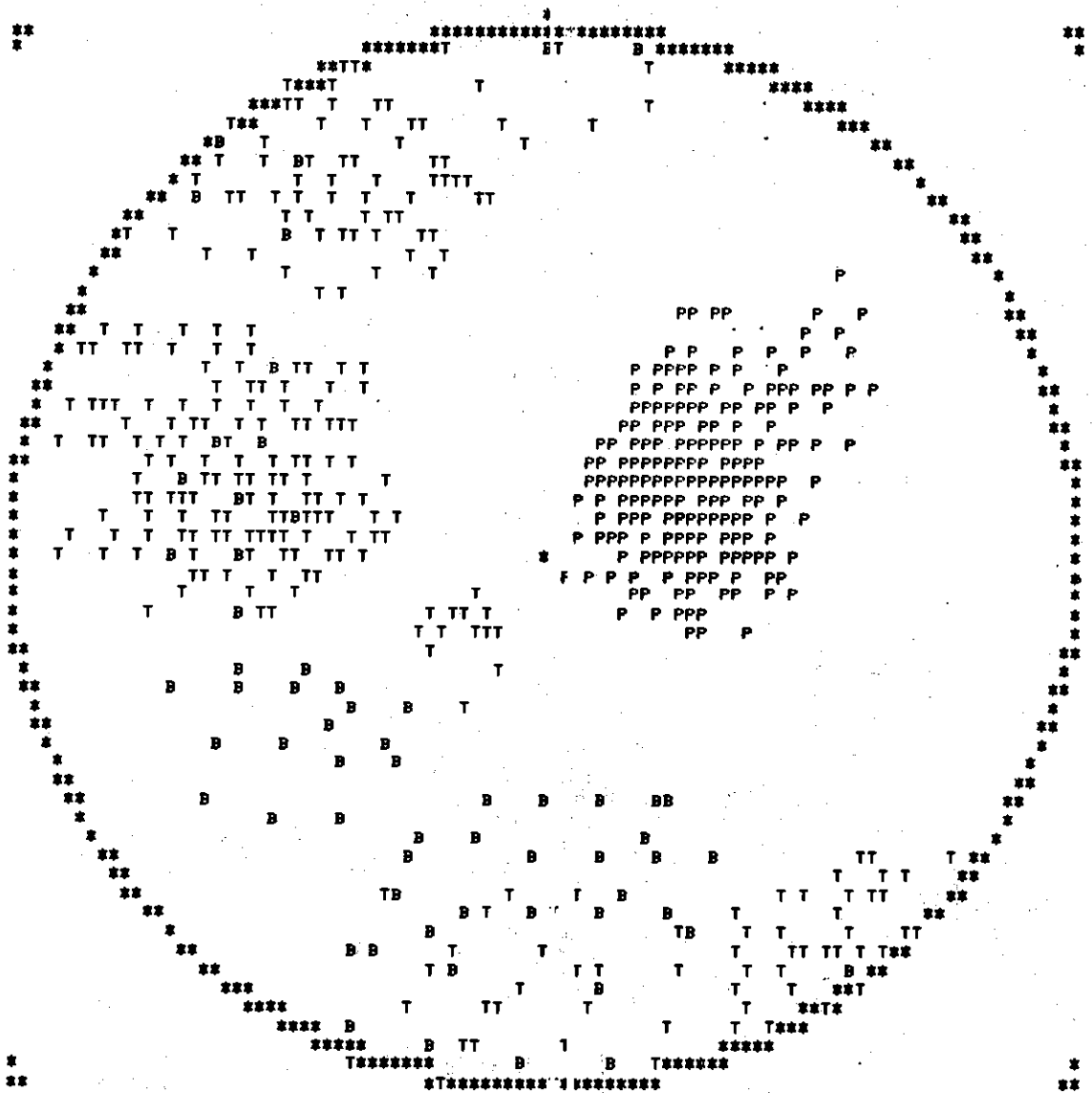


Figure 48. The Domain of Valid Focal Mechanism Solutions for Zero Errors for the Bowman, South Carolina Area (BSCA) Earthquake of November 22, 1976.

The Charleston-Summerville Area

The Charleston-Summerville, South Carolina area (CSSCA), figure 1, has left its mark in recorded history, having had several damaging earthquakes and the one lethal August 31, 1886 earthquake. Although many earthquakes have been reported since 1886, the mechanism has not yet been determined. As Champion (1975) points out, the probable reason no mechanism has been found is that the structure is hidden below 0.76 kilometers of Post-Paleozoic sedimentary and extrusive rock, and is therefore unknown.

Using only intensity data, Taber (1914) attempted to explain the seismic activity in the Charleston-Summerville area as being the result of an unobserved northeast-southwest trending basement fault located 8 Km southeast of Summerville (Long and Champion, 1977).

Wollard, et al. (1957), and Pooley et al. (1960) using well data interpreted by Cooke (1936) and later by Mansfield (1936), proposed that the seismicity might be related to a topographic feature of the basement surface, termed the Yamacraw Ridge, and the basement valley to the north, rather than to a Triassic basin (Long and Champion, 1977). Bollinger (1973) suggested that the activity may be related to regional uplift and ancient Appalachian structures. Oliver and Isacks (1972) and Fletcher et al. (1974) have expressed the opinion that the seismicity in the Charleston-Summerville area is related to the landward extension of a major transform fault associated with the early opening of the Atlantic Ocean.

Recently, perhaps the most detailed gravimetric study of any area in the southeast United States was carried out by Champion (1975) for the

Charleston-Summerville area. From this study and prior data, Long and Champion (1977) have proposed two large scale structures which possibly relate to the mechanism of the 1886 Charleston earthquake. The long, narrow northeast band shown in figure 49 represents the first structure and may be interpreted as a basement fault striking, $N45^{\circ}E$ at the edge of a Triassic basin. This interpreted structure essentially agrees with Taber's (1914) fault proposition, but is displaced 6.0 Km to the northwest. The second structure or feature proposed by Long and Champion is the apparent linear positive anomaly extending east from the positive high (figure 49), and is suggestive of a ridge or dike-like structure of high density material in a depth range of 1.0 to 6.0 kilometers.

In brief, these two large scale features allow two independent explanations for seismic activity in the CSSCA, 1) the earthquakes result from an active northeast striking basement fault, 2) the earthquakes result from fracturing of material associated with the eastward protruding anomaly by the mechanism of stress amplification (Long and Champion, 1977). From this study Long and Champion (1977) conclude that the stress amplification mechanism is better satisfied by historical intensity and recent epicenter data.

Table 9 contains the first motion data for the Summerville, South Carolina earthquake of April 28, 1975. The take off angles were computed using the structural interpretation presented by Long and Champion (1977). The plotted first motions demonstrate inadequate station distribution and indicate one obvious inconsistent observation (figure 50). The domain of valid focal mechanism solutions was determined for one error (figure 51). Both northwest and northeast fault plane orientations appear

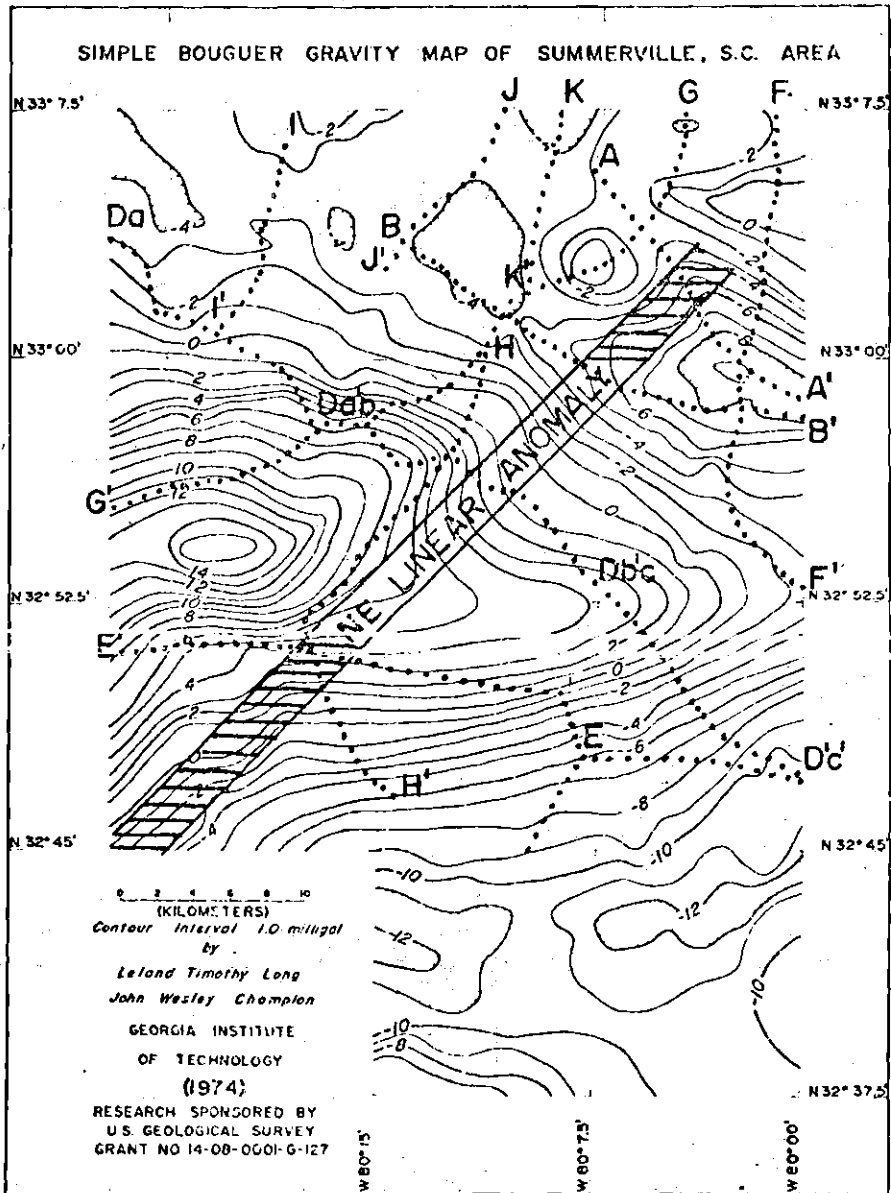


Figure 49. Simple Bouguer Gravity Map of the Summerville, South Carolina Area (after Champion, 1975).

Table 9. First Motion Data for the Charleston-Summerville
South Carolina Area Earthquake of April 28, 1975

No.	Station	Phase	Dist (Km)	Azimuth	Take Off Angle
1	NHS	PD	41.0	84.5	61.0
2	PBS	PC	16.0	334.0	61.0
3	HBF	PC	20.0	238.0	61.0
4	SMA	PD	69.0	351.0	61.0
5	SGS	PC	35.0	303.0	61.0
6	OSC	PC	82.0	315.0	61.0
7	LHS	PD	171.0	342.0	61.0
8	JSC	PD	170.0	325.0	61.0
9	VSC	PC	82.0	259.0	61.0

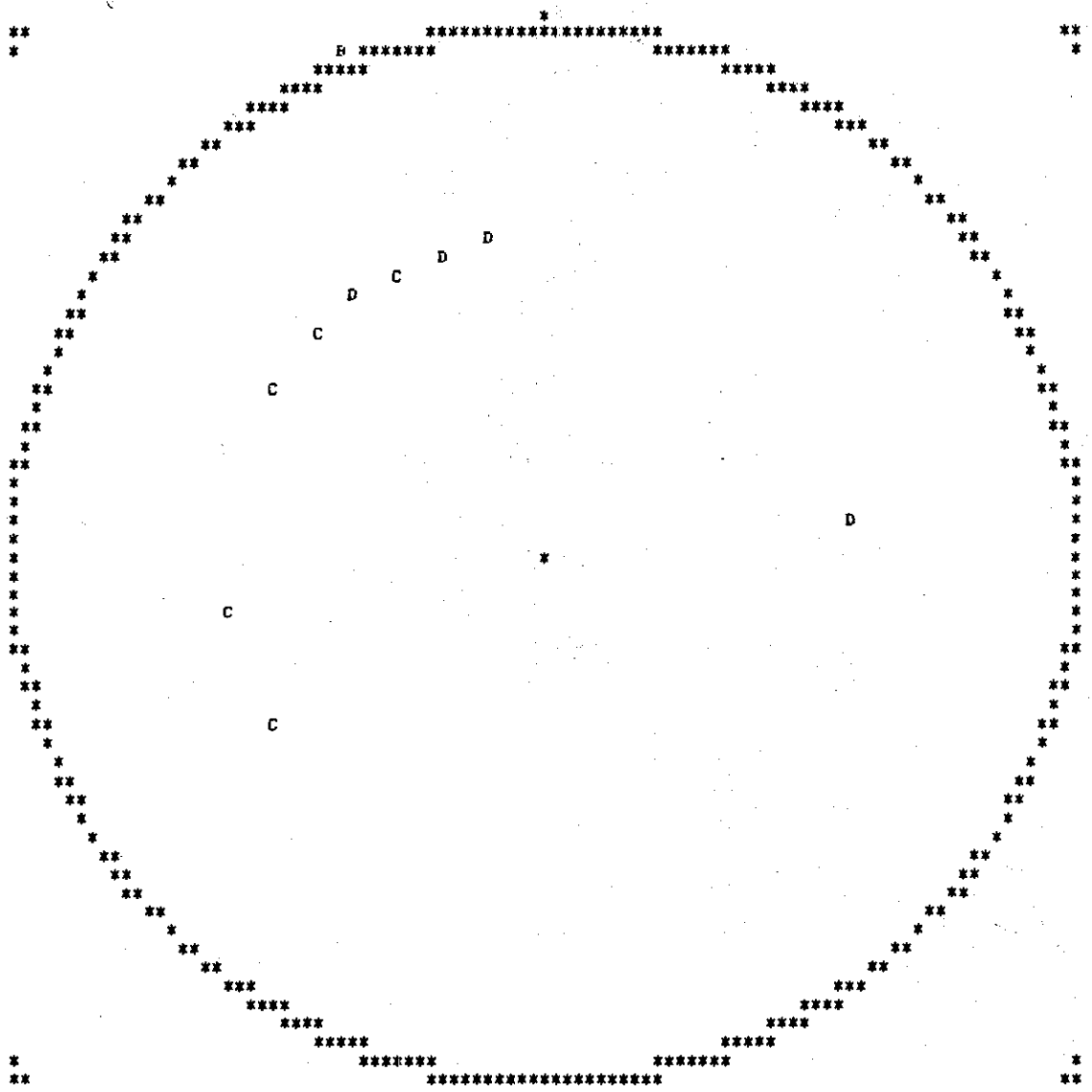


Figure 50. First Motion Plot for the Charleston--Summerville, South Carolina Area (CSSCA) Earthquake of April 28, 1975.

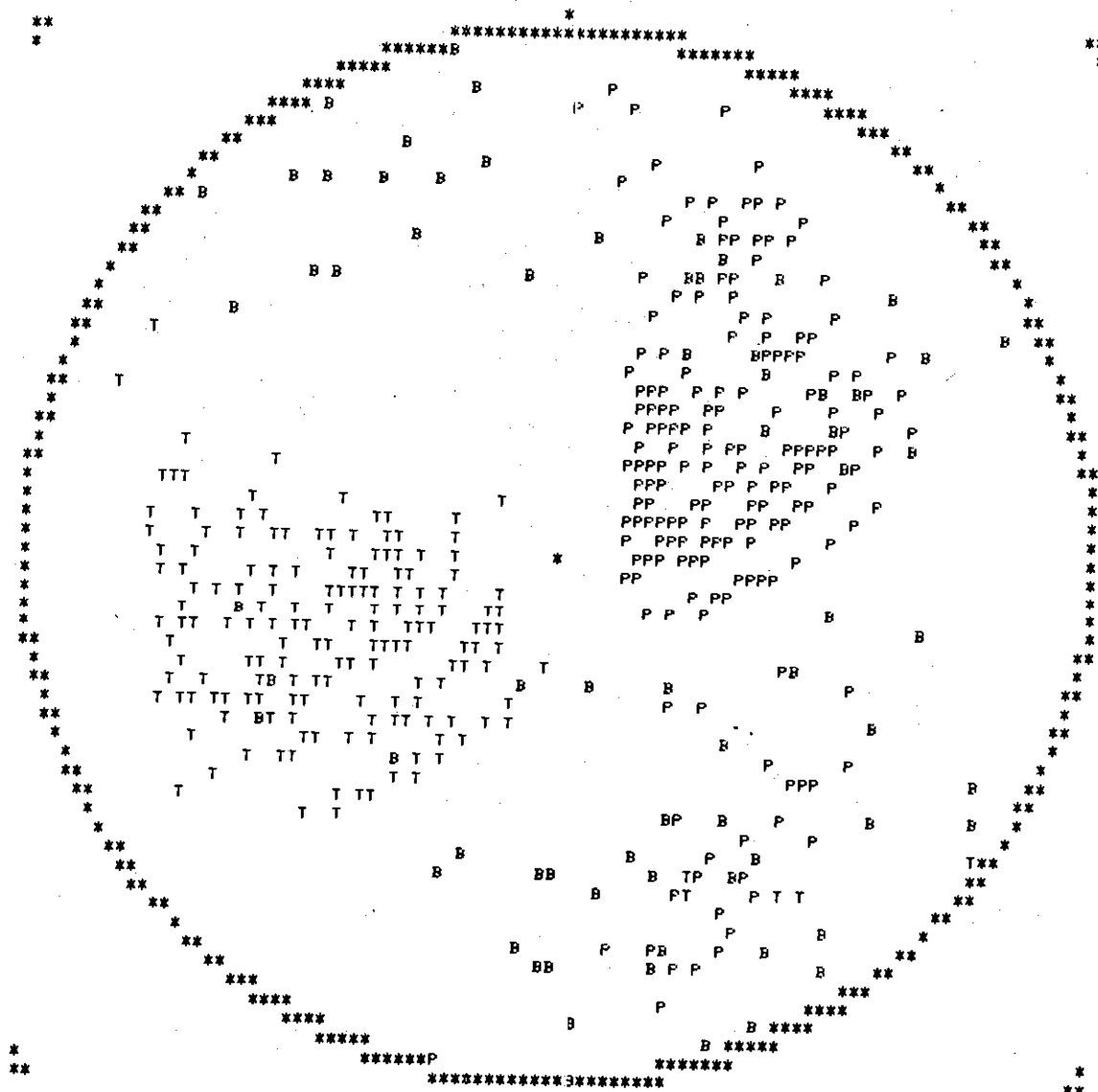


Figure 51. The Domain of Valid Focal Mechanism Solutions for One Error for the CSSCA Earthquake of April 28, 1975.

valid.

The pressure and tension axis positions for the April 28, 1975 Summerville event, although larger in area, show a marked similarity to those obtained for the Bowman earthquake of May 28, 1974. A northeast striking fault cannot be ruled out, but the majority of the solutions favor northwest striking fault plane orientations.

Recently Caver et al. (1977) published first motion data for earthquakes which occurred in the Charleston-Summerville area. The first motions and locations for events which occurred near the Summerville area were composited in order to obtain focal mechanism solutions. The angles of incidence were determined for a fixed depth of 2 Km below the surface. The composite first motions for all first motion readings given by Carver et al. (1977) are plotted in figure 52. The domain of valid focal mechanism solutions was determined for 11 errors out of a total of 34 first motions, but the solutions were found to be strongly dependent on one first motion (figure 53). Hence, the domain of valid mechanism solutions was determined for an additional error (figure 54). Since the domains of PTB axes are so wide and varied, no one predominant focal mechanism is apparent. The fact that composited first motion data from the same area yielded no predominant PTB axis trend may indicate that the data distribution is poor, that the take off angles or structure are poorly defined or that more than one focal mechanism occurs in this area.

The first motion plot shown in figure 55 represents the first motion data for the November 22, 1974 main event and aftershock which occurred in the Summerville area at 05:25:55.61 U.T. and 06:22:44.28 U.T. respectively. The domain of valid focal mechanism solutions was deter-

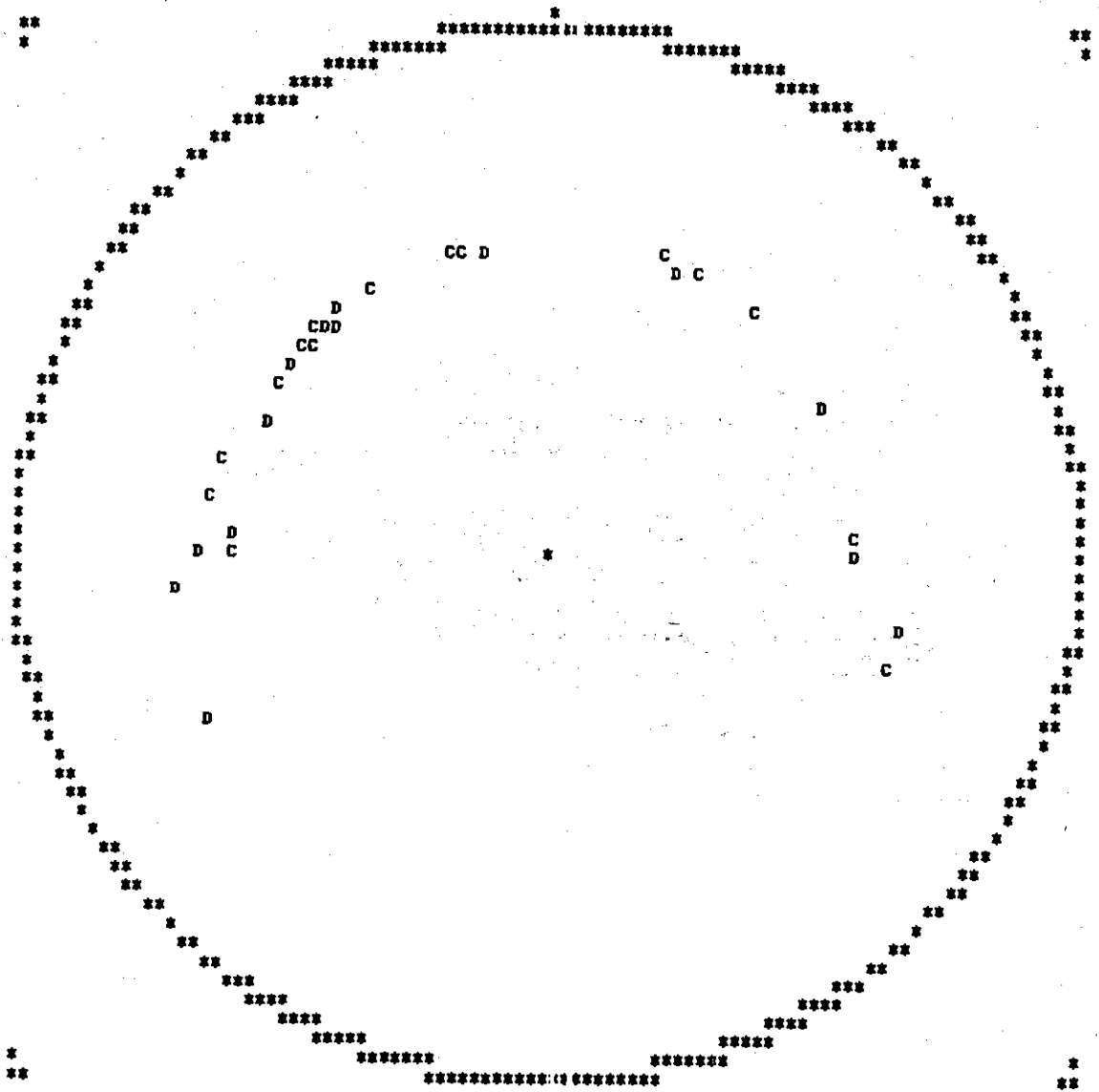


Figure 52. Composite First Motion Plot for the Charleston--Summerville, South Carolina Area (CSSCA), First Motion Data Excluding Angles of Incidence (after Carver et al., 1977).

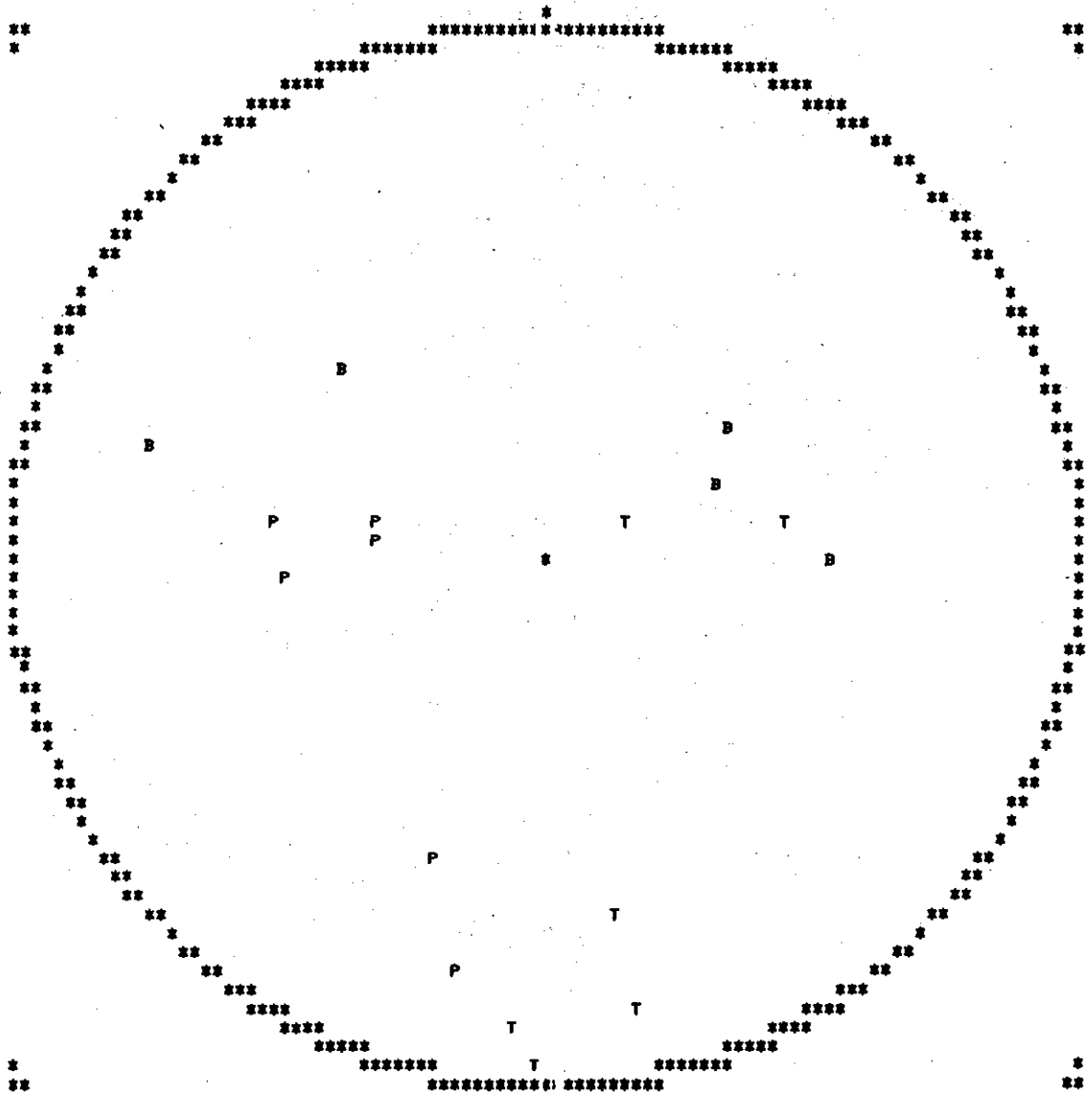


Figure 53. The Domain of Valid Focal Mechanism Solutions for 11 Errors from Composite First Motions for the Charleston--Summerville, South Carolina Area (CSSCA).

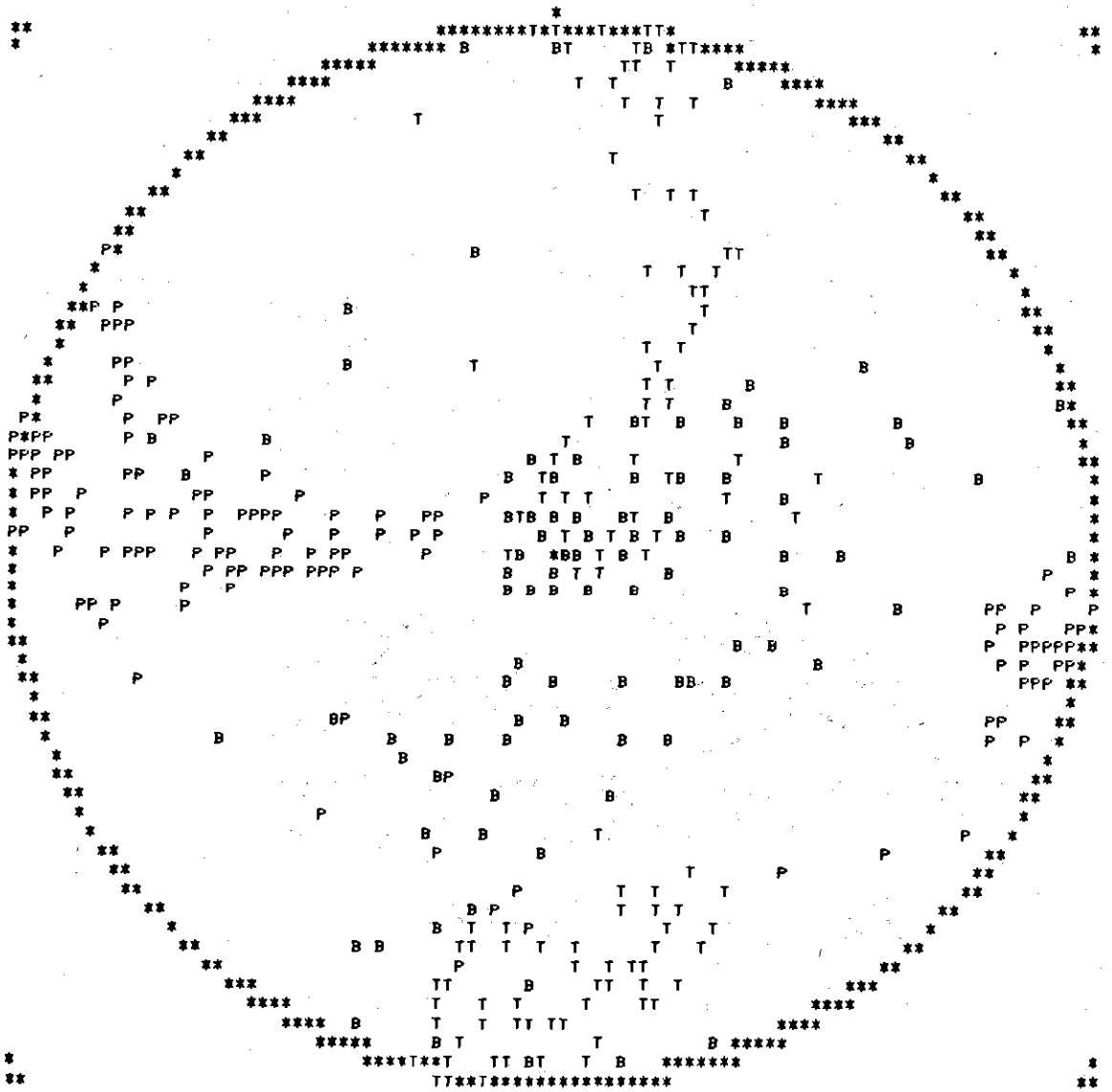


Figure 54. The Domain of Valid Focal Mechanism Solutions for 12 Errors from Composite First Motions for the Charleston--Summerville, South Carolina Area (CSSCA).

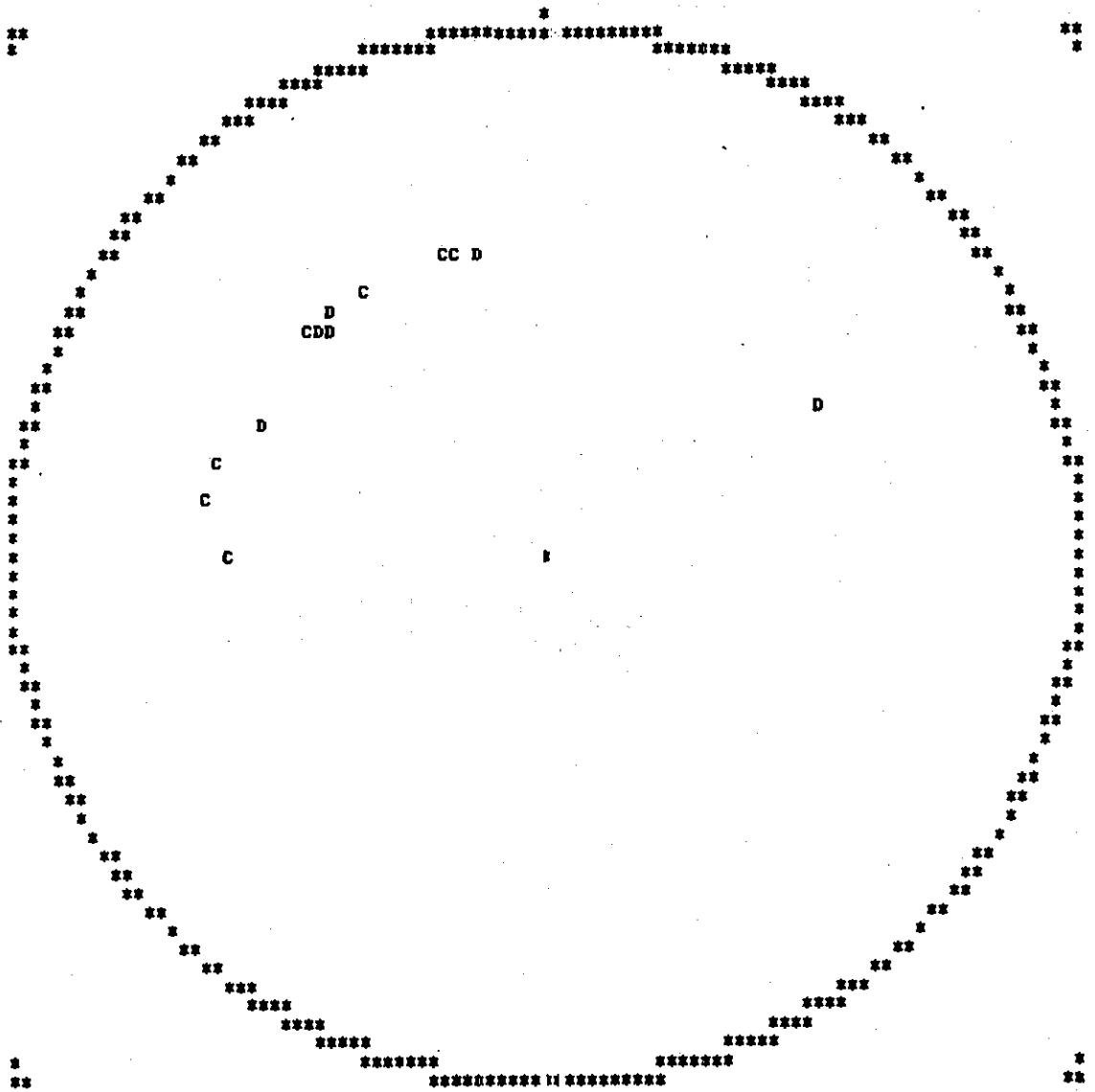


Figure 55. Composite First Motion Plot for the November 22, 1974 Charleston--Summerville, South Carolina Area (CSSCA) Earthquake and Aftershock.

mined for a minimum of four inconsistent readings (figure 56) out of a total of 15 first motions. Even though only a few solutions were found for four errors, the PTB axes show considerable scatter. The domain size becomes quite large and varied when only one additional error is allowed (figure 57). The solutions show some similarity to the solutions determined for the April 28, 1975 CSSCA earthquake. However, a predominant northwest fault plane orientation still appears tentative. The possibility that the November 22, 1974 event and its aftershock had different focal mechanisms cannot be ruled out.

The Reidsville Georgia Area

The only recent earthquake known to have occurred in the Georgia portion of the Atlantic Coastal Plain was the Reidsville, Georgia earthquake of December 27, 1976. The main shock, magnitude $m_b = 3.6$ (U.S.G.S.) occurred at 06:58:11.49 U.T. and was located at 32.046°N and 82.31°W , with an assumed depth of 2 to 3 Km (figure 58). The Reidsville, Georgia area (RGA) earthquake was assigned a maximum intensity of V (MM) as determined from interviews and questionnaires sent out the following day. The intensity map (figure 58) suggests an elongated felt configuration oriented northeast-southwest. Historically, only five earthquakes are known to have occurred in the south Georgia Coastal Plain and none has been reported near the Reidsville, Georgia area.

Basement geology is obscured by surface Miocene to Pliocene terrace deposits, which are underlain by Mesozoic and Cenozoic limestones and sands, silts and clays. The basement rocks are probably gneiss or granitic with possible mafic flows intermixed.

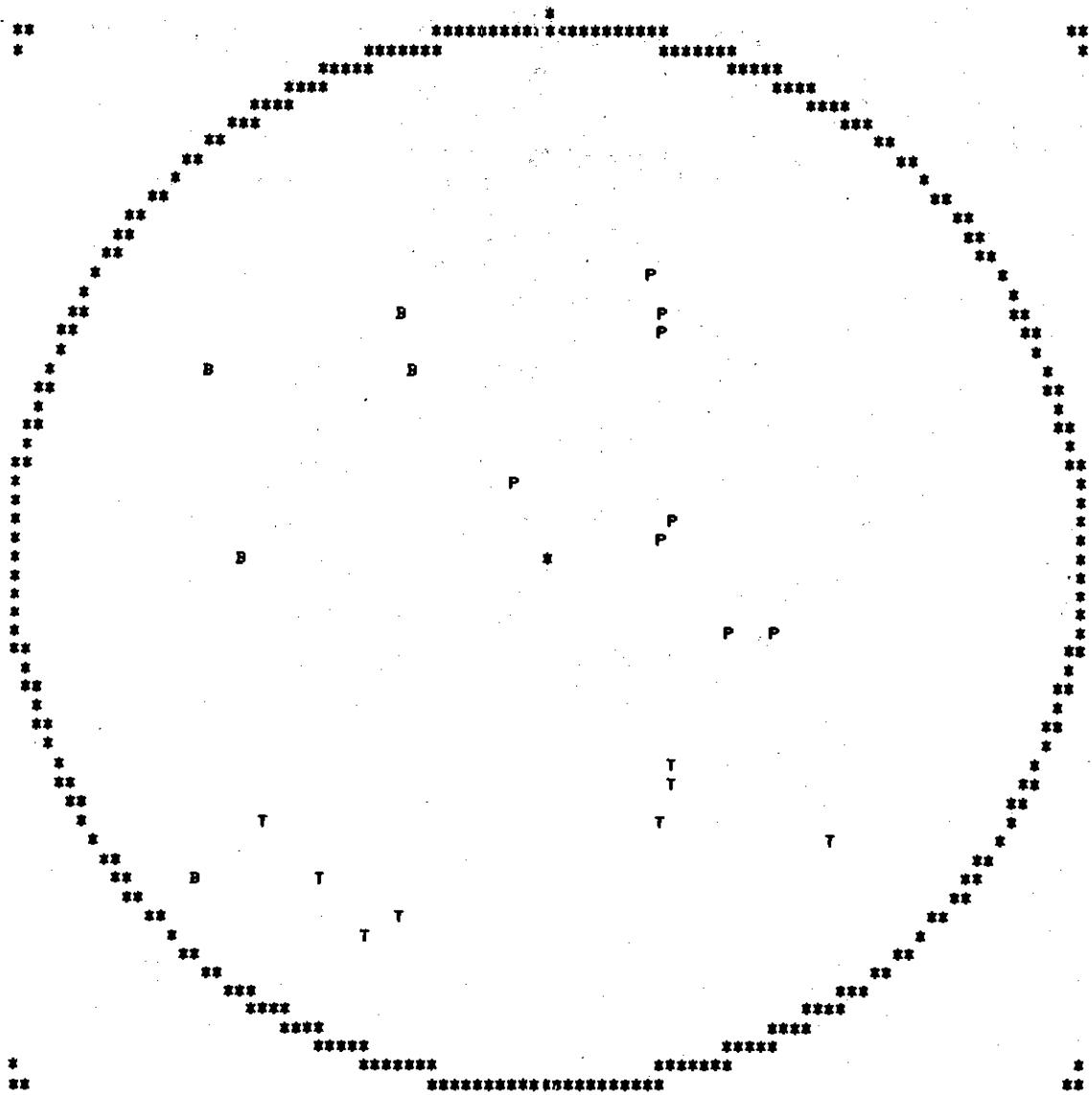


Figure 56. The Domain of Valid Focal Mechanism Solutions for Four Errors for the November 22, 1974 Charleston--Summerville, South Carolina Area (CSSCA) Earthquake and Aftershock.

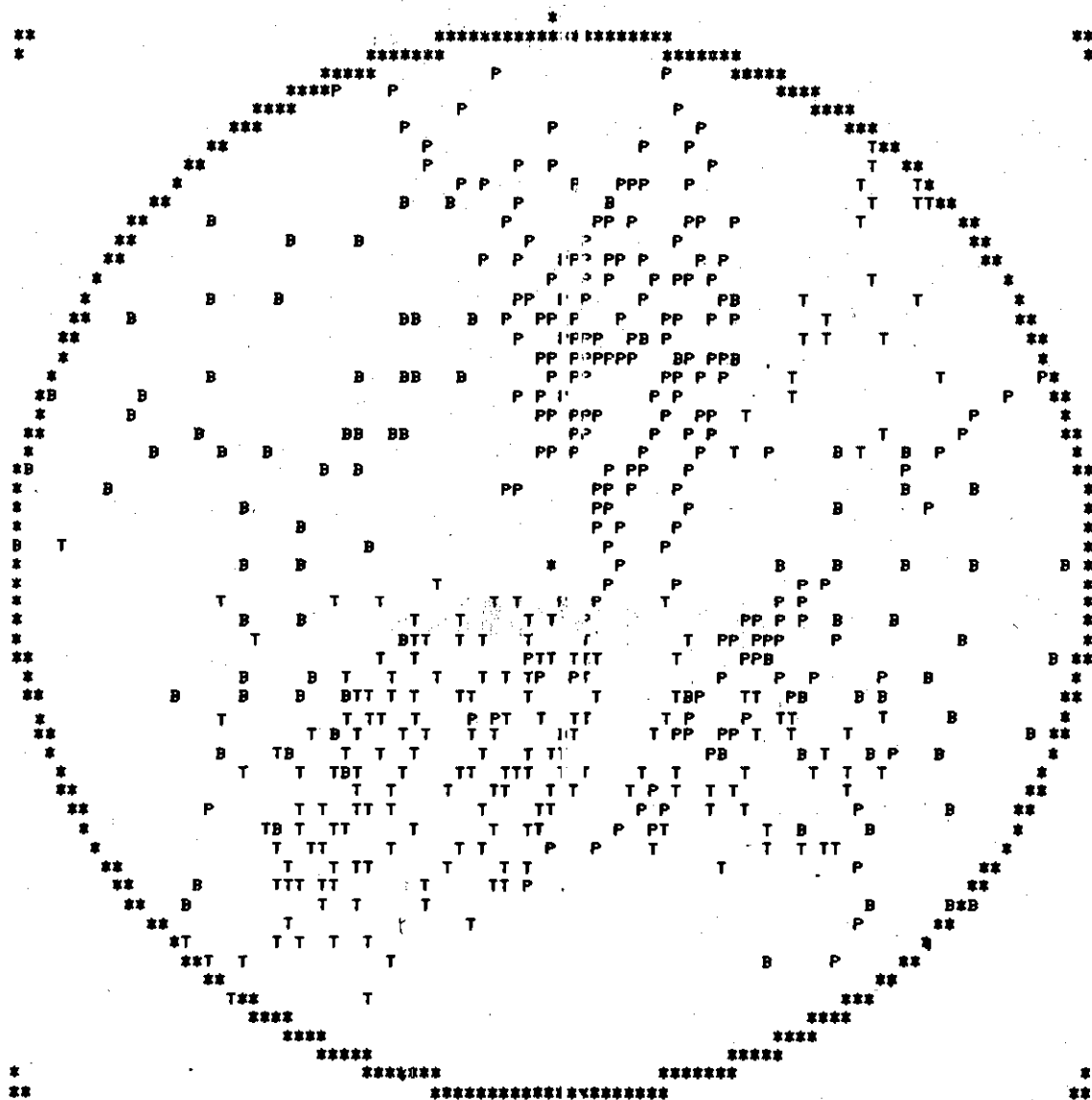


Figure 57. The Domain of Valid Focal Mechanism Solutions for Five Errors for the November 22, 1974 Charleston--Summerville, South Carolina Area (CSSCA) Earthquake and Aftershock.

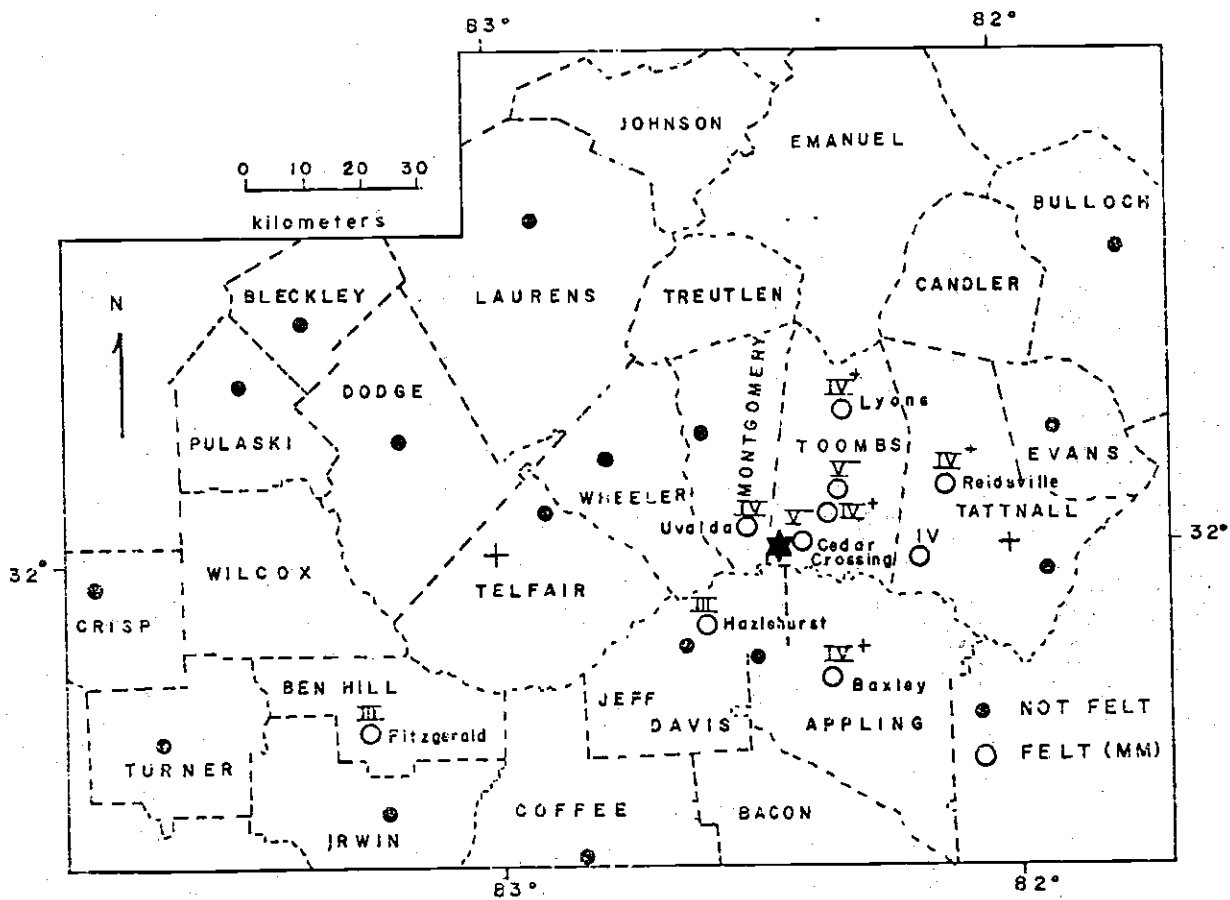


Figure 58. Intensity Data Map and Epicenter Location (STAR) for the December 27, 1976 Reidsville, Georgia Area Earthquake.

The first motion data for the Reidsville, Georgia earthquake are given in table 10. The first motion plot, figure 59, indicates inadequate station distribution to the south. The domain of valid focal mechanism solutions, based on one error, is given in figure 60. The solutions indicate fault planes which strike $N40^{\circ}E \pm 10^{\circ}$ and $N15^{\circ}W \pm 10^{\circ}$ and dip respectively $90^{\circ} \pm 10^{\circ}$ and $30^{\circ} \pm 10^{\circ}$. The northeast fault plane shows reverse to normal movement in which the southeast side has moved up. Solutions for the northwest striking planes indicate left lateral strike-slip motion. The solutions for two errors (figure 61) indicate the previous solutions are strongly dependent on one data point. The domain of valid focal mechanism solutions for two errors is larger but it preserves the characteristics found for one less error.

The Barnwell South Carolina Area

The Barnwell, South Carolina area (BASCA) is located in the Coastal Plain Province about 65 Km southeast of Augusta, Georgia and about 75 Km southwest of the BSCA.

On June 5, 1977 at 00:42:29.4 an earthquake of magnitude $M_{LSE} \sim 3.0$ occurred between Barnwell, South Carolina and Allendale, South Carolina. The event, located from regional seismic arrivals, occurred at $33.12^{\circ}N$ and $81.44^{\circ}W$ with an estimated depth of 2 to 5 Km. The Police and Fire departments of Allendale and Barnwell, South Carolina were contacted the same day, but none of the local inhabitants reported feeling the event.

The first motion data are given in table 11. The angles of incidence were determined from southeastern travel time curves. The plotted first motions show two obvious inconsistent readings in the eastern qua-

Table 10. First Motion Data for the Reidsville, Georgia
Earthquake of December 27, 1976

No.	Station	Phase	Dist (Km)	Azimuth	Take Off Angle
1	ATL	PNC	244.0	310.0	48.0
2	VSC	PNC	148.0	53.0	50.0
3	OSC	PNC	213.0	41.0	48.0
4	SRP1	PND	150.0	26.5	51.0
5	SRP2	PND	132.0	26.0	52.0
6	PBS	PND	226.0	58.0	48.0
7	HBF	PND	204.0	63.0	48.0
8	CH5	PNC	185.0	1.0	48.0
9	JSC	PNC	260.0	22.0	48.0
10	MTT	PNC	197.0	19.0	48.0
11	CH6	PNC	205.0	355.0	48.0
12	AMG	PNC	181.0	270.0	48.0
13	PRM	PNC	234.0	0.0	48.0
14	SRP3	PNC	143.0	29.0	50.0

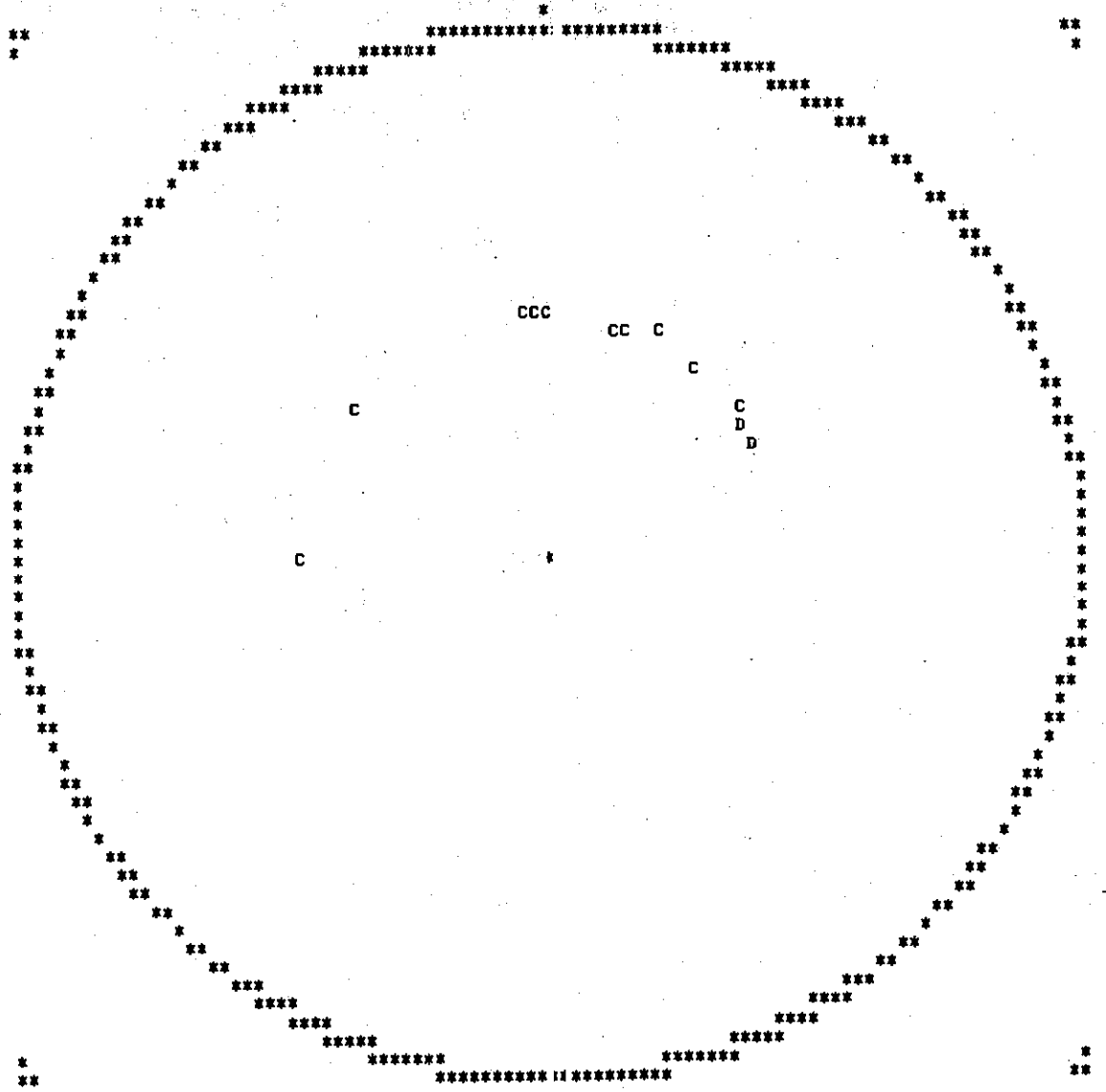


Figure 59. First Motion Plot for the Reidsville, Georgia Area (RGA) Earthquake of December 27, 1976.

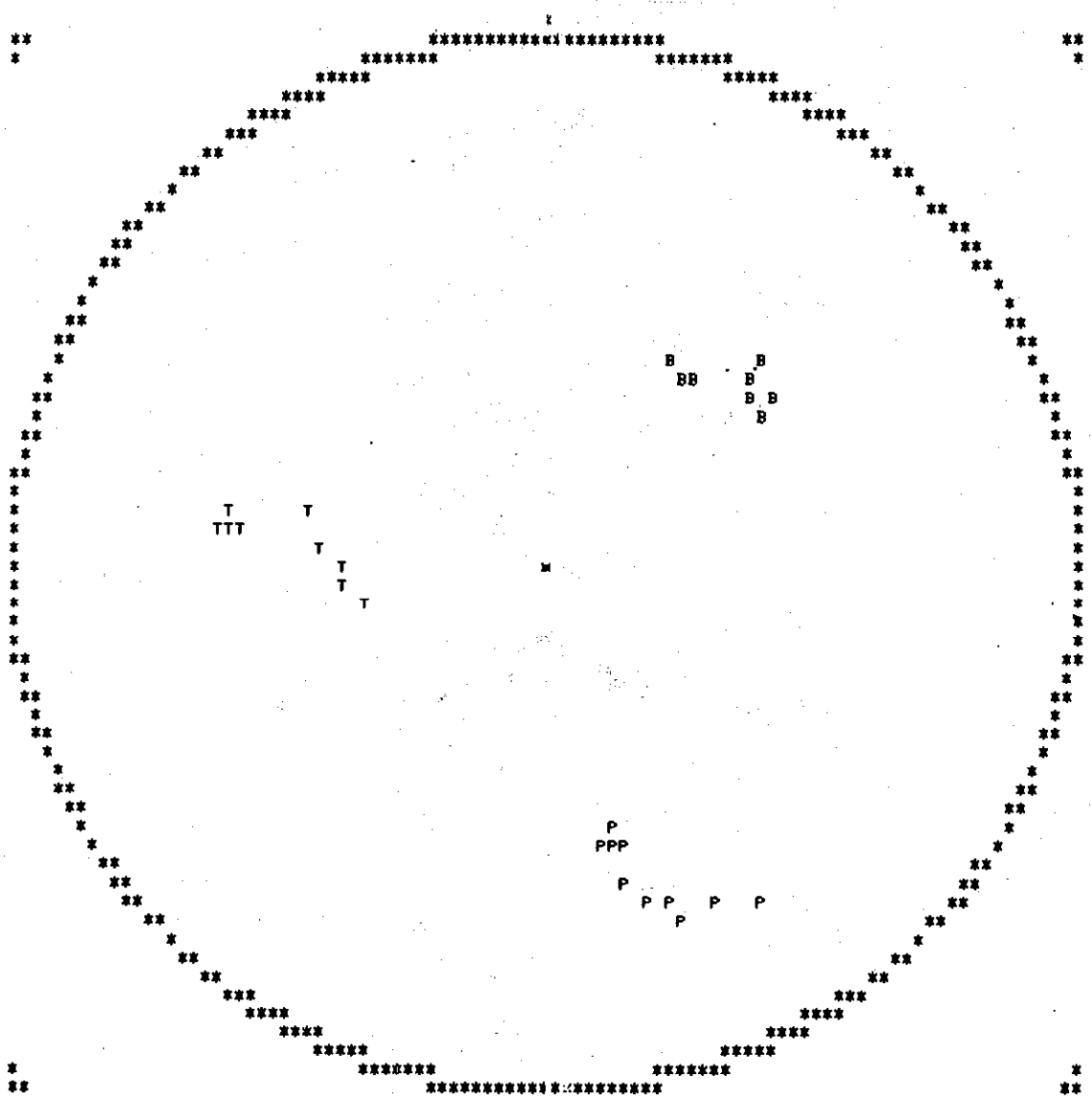


Figure 60. Domain of Valid Focal Mechanism Solutions for One Error for the Reidsville, Georgia Area (RGA) Earthquake of December 27, 1976.

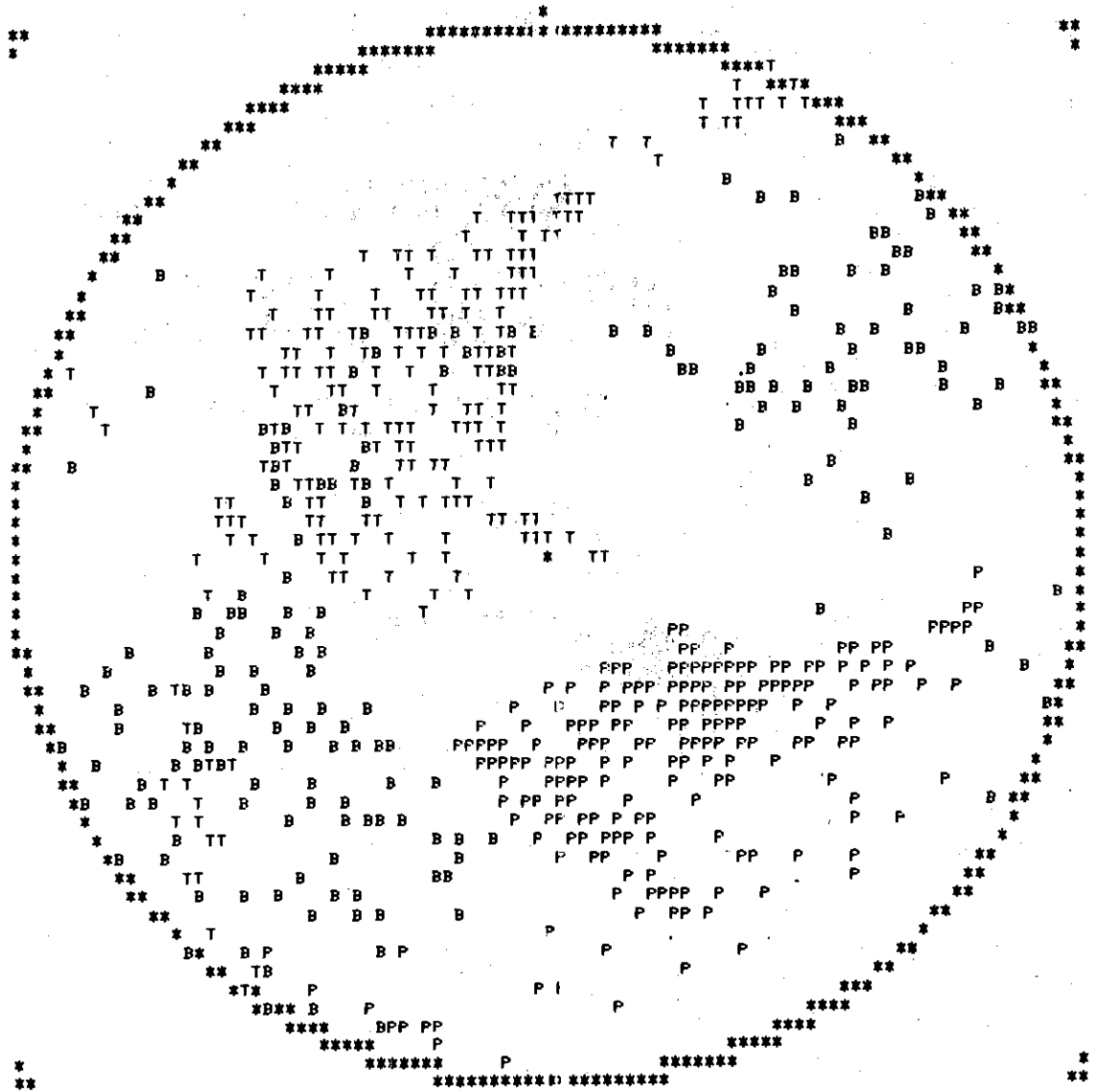


Figure 61. Domain of Valid Focal Mechanism Solutions for Two Errors for the Reidsville, Georgia Area (RGA) Earthquake of December 27, 1976.

Table 11. First Motion Data for the Barnwell, South
Carolina Area Earthquake of June 5, 1977

No.	Station	Phase	Dist (Km)	Azimuth	Take Off Angle
1	NHS	P*C	149.0	98.0	67.0
2	HBF	PD	100.0	103.0	75.0
3	SGS	PD	86.0	85.0	75.0
4	PRM	P*C	138.0	323.0	67.0
5	JSC	PD	126.0	7.0	75.0
6	PBS	PC	110.0	82.0	75.0
7	SRPN	PD	29.0	329.0	75.0
8	SRPD	PD	26.0	279.0	75.0
9	SRPW	PD	17.0	302.0	75.0
10	SVS	PC	113.0	98.0	75.0
11	CCS	PC	116.0	106.0	75.0
12	REG	PND	179.0	282.0	50.0

drant (figure 62). The domain of valid focal mechanism solutions, determined for a minimum of two errors, is shown in figure 63. The PTB axes are tightly constrained and indicate fault planes striking northwest with thrusting on southwest and northeast dipping planes. Although the domains are tightly constrained, they are seen to be dependent on the one compressional motion in the northwest portion of the focal sphere (see figure 62), since the two inconsistent first motion in the eastern portion cancel four of the readings.

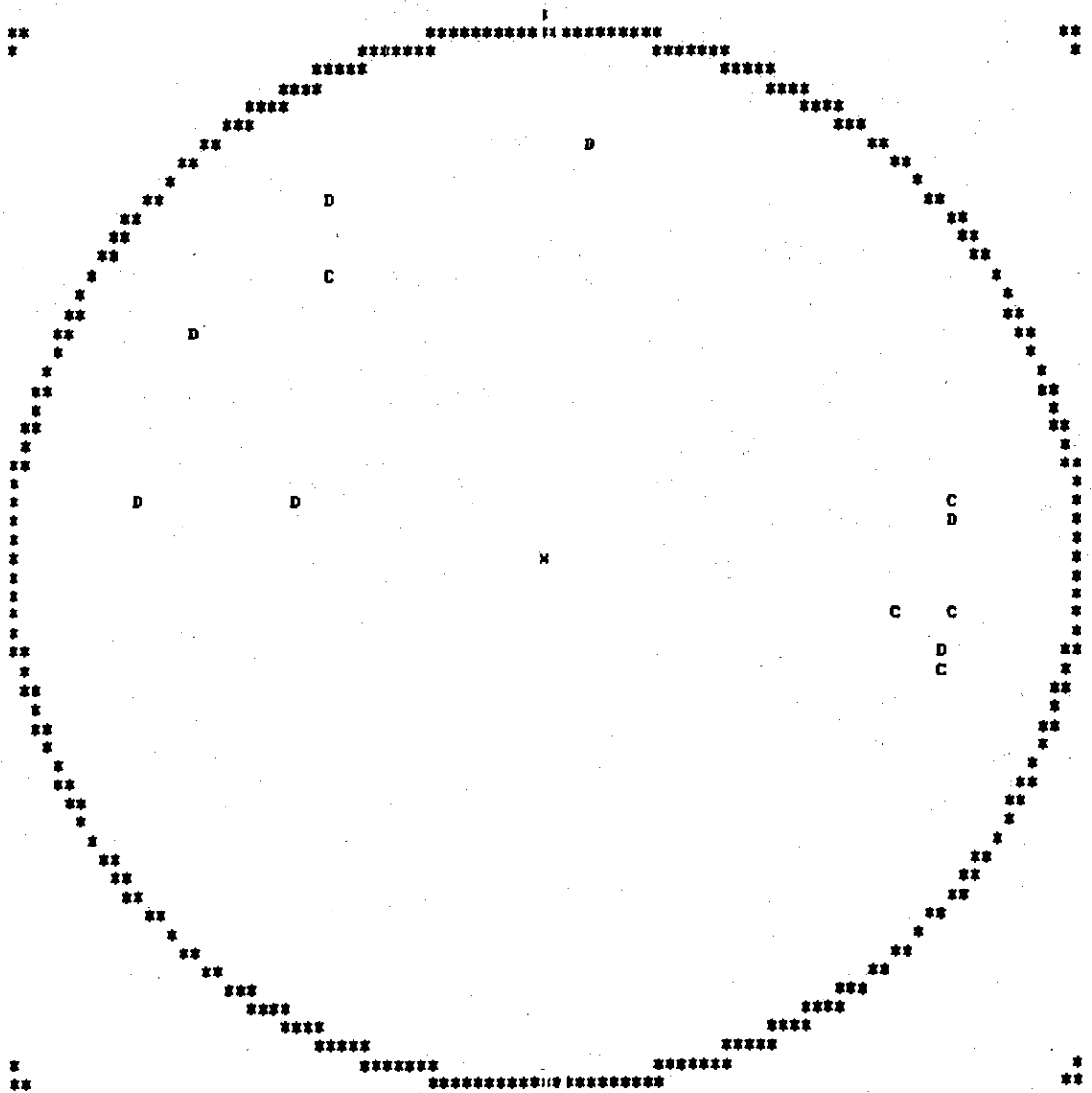


Figure 62. First Motion Plot for the Barnwell, South Carolina Area (BASCA) Earthquake of June 5, 1977.

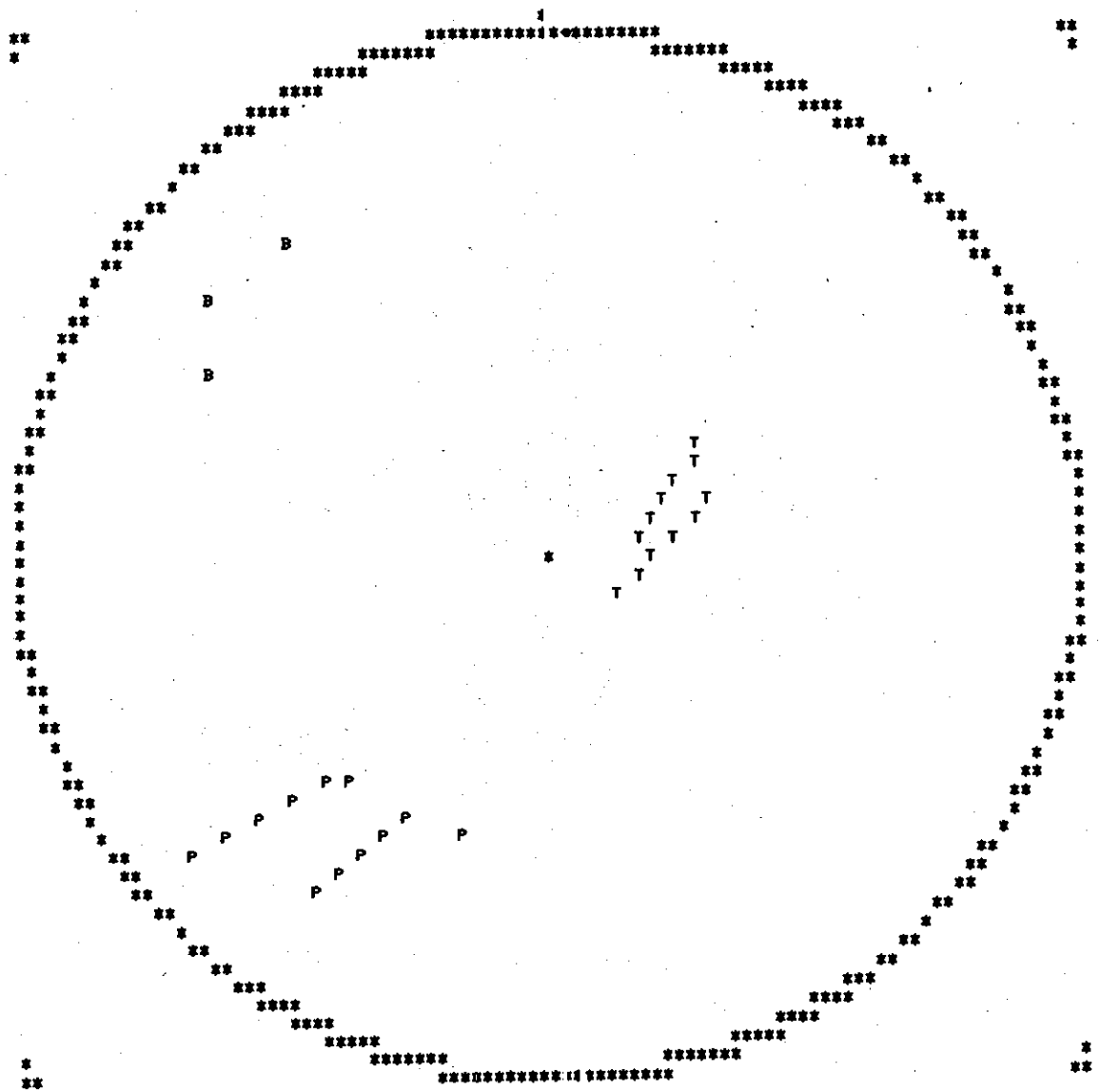


Figure 63. Domain of Valid Focal Mechanism Solutions for One Error for the Barnwell, South Carolina Area (BASCA) Earthquake of June 5, 1977.

CHAPTER V

OVERALL DISCUSSION

The discussion that follows compares the results obtained from focal mechanism solutions for the southeastern United States with results obtained from areas in other parts of the world.

Mendiuren (1969) has demonstrated, using P wave first motion and the combination of P and S wave data, that focal mechanisms for northern Argentina have approximately the same average characteristics. Stauder (1962a) has also shown that, near Kamchatka, focal mechanisms repeat themselves from earthquake to earthquake. In such regions of intermediate to deep earthquakes associated with subduction zones, the above results are not surprising since dominant directed forces of large magnitude exist.

Sbar and Sykes (1973), from a combination of focal mechanism solutions, in-situ stress measurements and geologic observations, have proposed that much of eastern North America is presently experiencing horizontal compressive stresses greater than those expected from the effects of lithostatic loading alone. According to Sbar and Sykes each of the above methods for evaluating stress gave nearly identical directions for the principal stresses and therefore they concluded that the maximum compressive stress trends east to northeast over an area extending from west of the Appalachians to the middle of the continent, and from southern Illinois to southern Ontario. Their work supports the hypothesis that the compressive stress observed within the North American plate may be generated by the same mechanism that drives the movements of large lithospheric plates.

The stress pattern in the Appalachian Mountain System appears to be different and possibly a more complex stress distribution exists as compared to the adjacent region to the west. From in-situ (strain relief) stress measurements made in Piedmont granite and gneiss near Atlanta, Georgia, Hooker and Johnson (1969) suggested that the maximum principal stress direction may be aligned with the trend of the Appalachian Mountains. Sbar and Sykes (1973) point out that this may be the case for New England and the Middle Atlantic States, but the southern data do not support this hypothesis. The measurements in the Georgia Piedmont may reflect the stress conditions at the time of crystallization (remnant stress) rather than a contemporary pattern (Sbar and Sykes, 1973). Sbar and Sykes (1973) were unable to fit the distribution of observed stresses in this region to a simple model with available data and they concluded that the stress distribution in the Appalachian system may be modified by remnant stress, uplift, or edge effects related to continental margins. According to Sbar and Sykes (1973) the central United States is presently experiencing a predominantly horizontal compressive stress which trends east-northeast. Street et al. (1974) point out that the central United States earthquake activity, as related to the stress model proposed by Sbar and Sykes (1973) should be a consequence of high angle thrust faulting with planes striking in a north-south direction. However, from a detailed study of focal mechanism solutions of moderate size earthquakes which occurred over a period of thirteen years within the area of Missouri, Kentucky, Tennessee, Illinois, Mississippi and Arkansas, Street et al. (1974) have concluded that such a simple regional stress model is not applicable. This result was obtained from the analysis of 38 focal mechanism solutions obtained

by two independent methods, one using the first P wave motion and the other using the amplitude spectrum of surface wave motion. Most of the nodal planes were determined by a visual fit with an estimated error of 10° to 20° (Street et al. 1974). Their results indicated, with a few exceptions, that the strikes of the nodal planes could be grouped into two trends. The most prominent trend is a nearly north-south strike for events which occurred northward from Memphis, Tennessee through latitude 38.5°N . The second trend consists of nodal planes which strike east-west for events southeast of Missouri. The remaining data apparently did not fall in either trend. Street et al. (1974) concluded that the compressive stress distribution on a localized scale within the interior of a continental plate may be modified or influenced significantly by local features. For the central United States they proposed such features as the Mississippi Embayment, the Ozark Uplift and possibly the Quachita Front.

The focal mechanism solutions for southeastern intraplate earthquakes do not imply a single dominant stress direction (see figure 64). In this respect the interpretation for the southeast is consistent with the results from the central United States. The lack of a single dominant stress direction in the southeast is inferred from the orientations of the pressure and tension axes and not from nodal plane orientations. Apparently individual and local stress perturbations allow accumulation of enough stress to produce the low level shallow seismic activity. The focal mechanism solutions presented for the southeast perhaps can be explained by a combination of factors including; vertical movement of the crust induced by isostatic readjustment, stress amplification in structural irregularities, and near surface conditions such as pore pressure changes

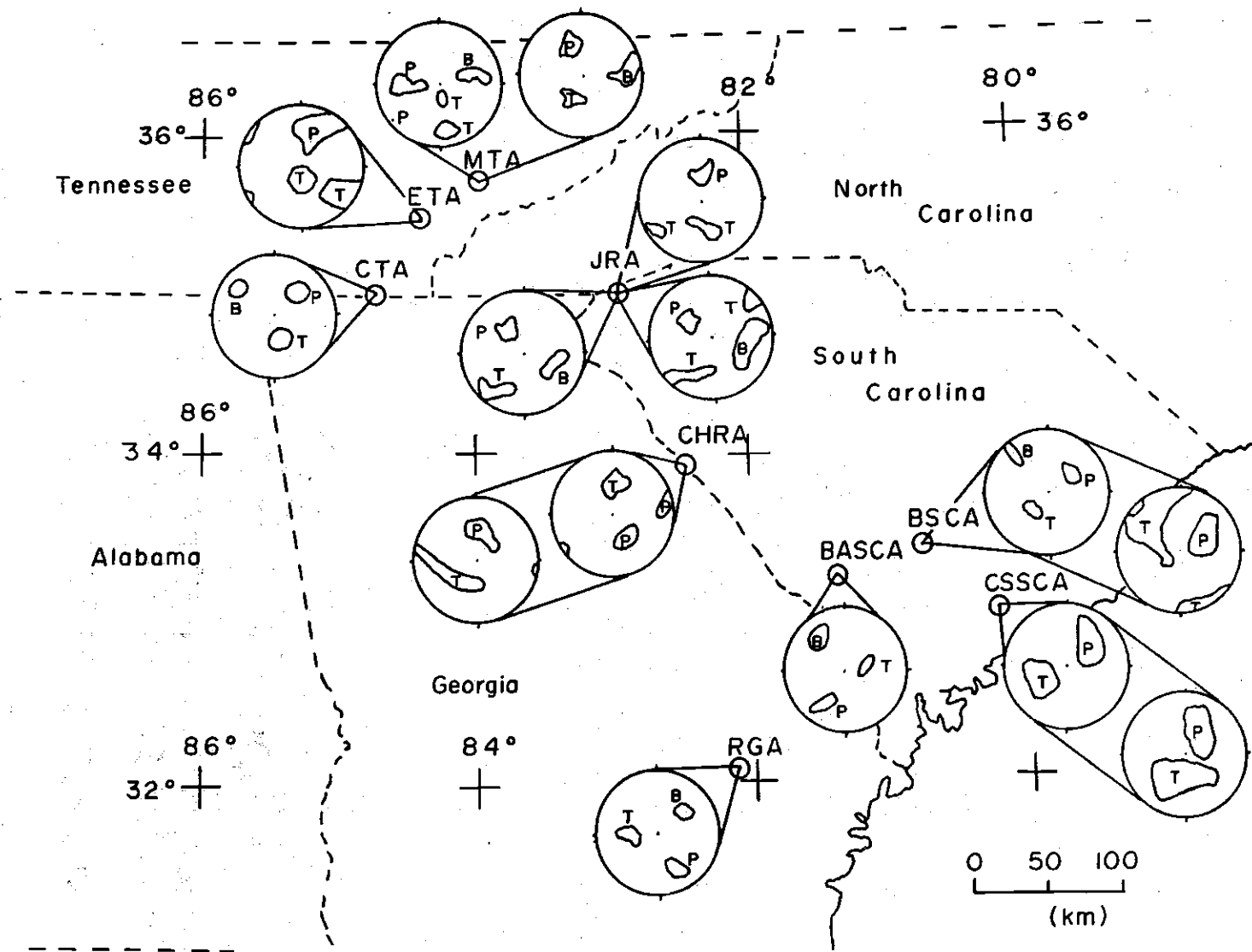


Figure 64. Regional Map of Southeastern United States Showing the Domain of Valid Focal Mechanism Solutions for Nine Epicentral Areas.

and loading induced by reservoir impounding. The focal mechanism solutions for the Valley and Ridge Province do in general support east to northeast compression. Also the CHRA and JRA could be compatible with east to northeast compression, but these data could be explained by other mechanisms.

In a study of tectonic stress and motion direction for southern Europe and western Asia, Scheidegger (1964) found that some focal mechanism solutions were consistent with the plate boundary mechanism, but many were not. More recently Tandon and Srivastava (1975) found, using focal mechanism solutions from 12 recent earthquakes which occurred along the northern boundary of the Indian plate, that some of the solutions were inconsistent with the plate theory asserted for this region. It is therefore not unreasonable that an area void of plate boundaries exhibits patterns similar to those presented for the southeast when compared to attempts to characterize stress directions involving plate boundaries in other areas.

CHAPTER VI

CONCLUSIONS

Based on the analysis technique, previous research, and interpretation of new data the following may be concluded:

1. Given a finite number of P wave first motions from a single earthquake there exists a domain of valid focal mechanism solutions which satisfy the requirements set forth by the theory of the double couple without moment earthquake source. The computer adapted analysis technique allows direct, rapid and objective evaluation of fault plane solutions by finding the domain of valid focal mechanism solutions in terms of the orthogonal pressure, tension and null axes.
2. In general, the focal mechanism solutions indicate that southeastern intraplate seismic activity does not appear to be the result of a single dominant stress direction. If a dominant stress direction exists, it is not verified by the focal mechanism solutions.
3. The interpretation of multiple planes, transonic rupture on existing planes perhaps controlled by joints and the low level to tensional stress environment are conclusions supported by both spectral data and focal mechanism solutions in the CHRA and JRA.
4. Even though the data are limited no one dominant mechanism

appears to be characteristic of provincial subdivisions with the possible exception of the BSCA and CSSCA.

5. Focal mechanism solutions for the CHRA indicate multiple plane orientations, many of which correspond to dominant joint orientations.
6. Focal mechanism solutions for the Valley and Ridge Province support the hypothesis that ancestral Appalachian structures are aseismic.
7. Analysis has shown that for the area studied the pressure or tension axes form a discrete zone while the B axes form a less discrete zone.
8. Focal mechanism solutions for the BSCA were found to be compatible with the stress amplification model.
9. The possibility that a northwest vertical plane mechanism may exist for the BSCA and CSSCA cannot be ruled out at this time, but more data are needed to confirm such a proposition.
10. In general, near vertical fault plane orientations are shown as possible solutions. This may suggest a tensional stress environment for the southeast.

CHAPTER VII

RECOMMENDATIONS

1. Focal mechanism data should continue to be collected and analyzed to further elucidate the contemporary stress pattern associated with southeastern seismic activity.
2. Displacement spectra and focal mechanism solutions should be related in order to better define the source mechanisms associated with southeastern earthquakes.
3. Attempts should be made to utilize S wave polarization data in conjunction with P wave data in order to constrain focal mechanism solutions in the southeast.
4. Composite focal mechanism data can give ambiguous results. Single event focal mechanism solutions should be obtained for the JRA in order to determine more definitely that earthquakes at the JRA result from slippage along joint planes.
5. Fault planes at the CHRA may be defined with greater precision utilizing data from the recently installed three component seismometer in the epicentral area. Also, first motions may be read from portable microearthquake recorders with greater reliability if the maximum rotation rate is used and if higher frequencies are eliminated from the record by setting the band pass filters for low frequency response (1 to 5 Hz).

6. A routine check on the polarity of the seismometers (portable or not) should be made, since repairs do often reverse the polarity.

APPENDIX I**COMPUTER PROGRAM****Input Statement****Flowchart of Main Program****Program Listing**

INPUT STATEMENTS

LAB: 50 character description or title of earthquake

INDEX: Index = 1 Plot first motions on lower hemisphere Wulff net
 ≠ 1 No Plot

N: Number of first motions, up to 200 allowed

AZM: Azimuth of observation station from epicenter measured in degrees
 positive clockwise from north.

DIP: Angle of incidence measured in degrees from vertical upward (0° to
 180°).

RANDOM: = 1.0 compressional first motion
 = -1.0 dilatational first motion

NERR: Number of inconsistent first motions
 NERR = 1000 Program is terminated

IWANT: IWANT=999 single grid is used (see note below)
 ≠ 999 focal sphere is systematically searched

GANG: Spacing of B axes in 5 x 5 grid, 10° recommended when IWANT ≠ 999

* NOTE

INPUT READ WHEN IWANT = 999

NERR: Number of inconsistent first motions

TAUZ: Azimuth of B axis measured in degrees clockwise from north

PHIZ: Dip of B axis measured in degrees from horizontal downward to
 vertical

GANG: Grid interval; detailed results for small interval.

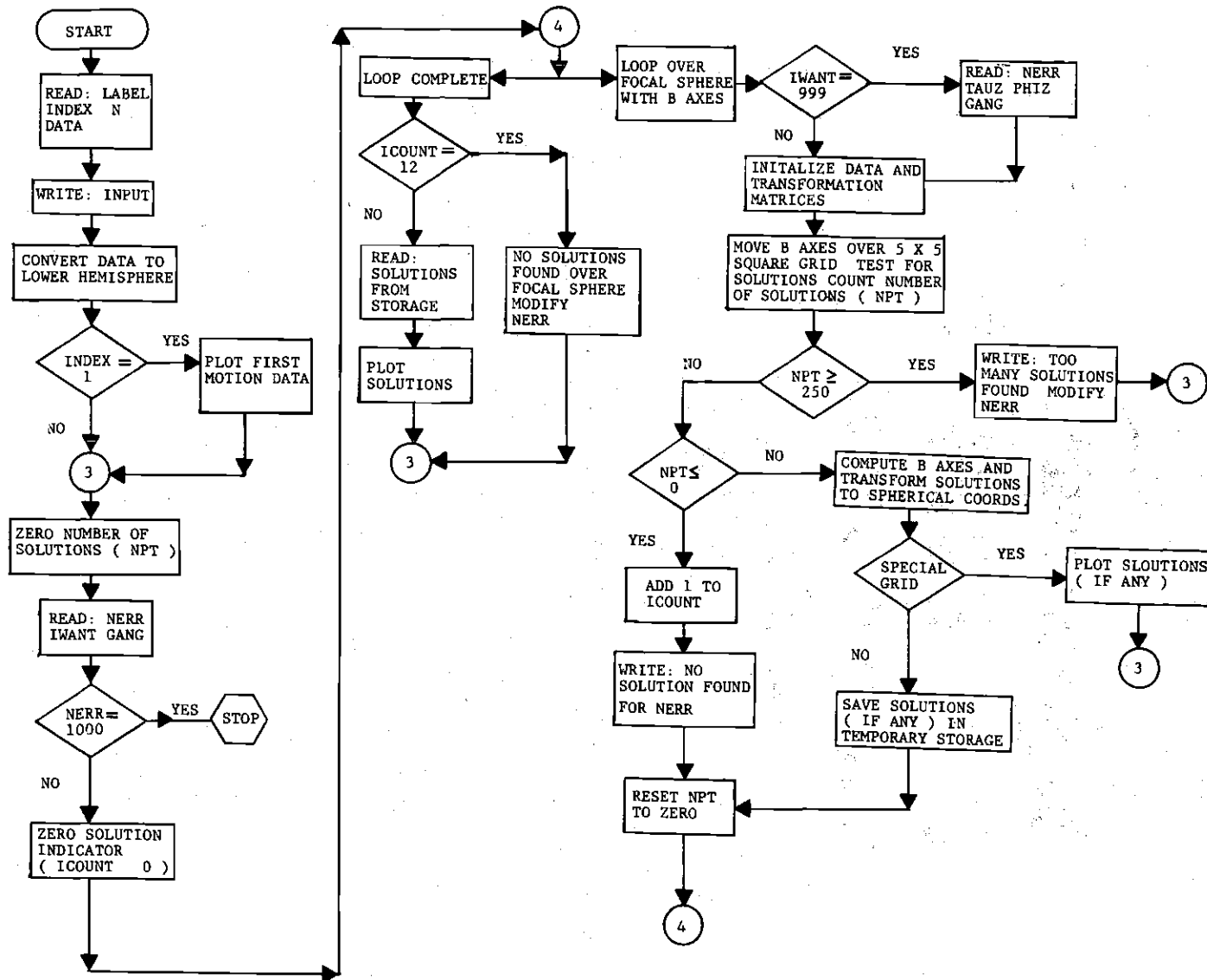


Figure 65. Flowchart of Main Program.

C THIS PROGRAM, WRITTEN IN FORTRAN IV FOR A
 C CONTROL DATA CORPORATION CYBER (74), IS AN
 C ITERATIVE TECHNIQUE WHICH DETERMINES THE
 C DOMAIN OF VALID FOCAL MECHANISM SOLUTIONS
 C FOR A GIVEN EARTHQUAKE USING P WAVE FIRST
 C MOTIONS. THE SOLUTIONS ARE GIVEN
 C IN TERMS OF THE PRESSURE (P), TENSION (T), AND
 C NULL AXIS (B) DIRECTIONS. THE ENTIRE FOCAL
 C SPHERE IS SEARCHED USING A 5 X 5 GRID OF B
 C AXES. THE RESULTS ARE WRITTEN OUT ON AN
 C AUXILLARY TAPE FOR FURTHER ANALYSIS OR
 C PLOTTING ON THE LOWER HEMISPHERE OF A
 C WULFF NET PROJECTION. ONCE THE DOMAIN
 C IS FOUND A SPECIAL GRID OF B AXES MAY
 C BE USED TO INVESTIGATE THE DOMAIN SIZE AND
 C SHAPE IN GREATER DETAIL.

C
 C
 C

```

PROGRAM MAIN(IN,INPUT,IR,OUTPUT,TAPE5=INPUT,
1TAPE6=OUTPUT,TAPE1=IN,TAPE7=IR)
  DIMENSION AZC(2000),ROEC(2000),X(3,2000),C(3,3),
  CA(3,3),B(3,3),SENSE(2000),PT(3,2000),LAB(5),
  1 AZM(200),DIP(200),RANDOM(200),D(3,3)
  REWIND 7
  SRAD=0.01745329252
C SRAD IS THE CONVERSION FACTOR FROM DEGREES TO RADIANS.
  READ(1,910) LAB(1),LAB(2),LAB(3),LAB(4),LAB(5)
C LAB STANDS FOR THE TITLE OR IDENTIFICATION
C OF THE EARTHQUAKE.
  910 FORMAT(5A10)
  WRITE(6,910) (LAB(I),I=1,5)
  READ(1,*) INDEX,N
C INDEX IS A DEVICE WHICH ALLOWS AN OPTION TO
C PLOT THE ORIGINAL INPUT (INDEX = 1) OR NOT
C (INDEX NOT = 1).
C N REPRESENTS THE NUMBER OF P WAVE FIRST MOTIONS.
  WRITE(6,903) INDEX,N
  903 FORMAT(/," INDEX=",I5," ; NUMBER OF DATA POINTS=",I5)
  ENDFILE6
  WRITE(6,957)
  957 FORMAT(//,"AZIMUTH-----TOA-----1ST MOTION--)")
  DO 20 I=1,N
  READ(1,*) AZM(I),DIP(I),RANDOM(I)
C AZM IS THE AZIMUTH OF THE OBSERVATION STATION
C AND IS MEASURED IN DEGREES FROM THE EPICENTER.
C DIP IS THE CORRESPONDING TAKE OFF ANGLE AND IS
C MEASURED IN DEGREES FROM THE VERTICAL UPWARD.
C RANDOM IS AN INDEX WHICH CATALOGUES THE DIRECTION
C OF FIRST MOTION AND THE SYMBOLS FOR THE

```

```

C PTB AXES EG,
C   COMPRESSION = 1.0
C   DILATATION  = -1.0
C   B AXIS      = 7
C   P AXIS      = 8
C   T AXIS      = 9
      WRITE(6,956) AZM(I),DIP(I),RANDOM(I)
956  FORMAT(2X,F7.3,7X,F7.3,8X,F5.2)
      IF(DIP(I).GE.0.0.AND.DIP(I).LE.90.0)GO TO 111
112  AZM(I)=AZM(I)+180
      DIP(I)=180-DIP(I)
111  IF(AZM(I).GT.360.0)AZM(I)=AZM(I)-360.0
      DIP(I)=DIP(I)*SRAD
20   AZM(I)=AZM(I)*SRAD
      IF(INDEX.EQ.1) CALL PLOT(AZM,DIP,RANDOM,N)
3   NPT=0
C NPT REPRESENTS THE NUMBER OF PRESSURE
C AND TENSION AXES.
      READ(5,*) NERR,IWANT,GANG
C NERR IS THE NUMBER OF INCONSISTENT FIRST
C MOTIONS AND IF NERR = 1000 THE PROGRAM
C IS TERMINATED.
C IWANT IS A DEVICE WHICH ALLOWS AN OPTION
C TO SEARCH THE ENTIRE FOCAL SPHERE
C (IWANT NOT = 999) OR EXAMINE A PARTICULAR
C AREA OF THE FOCAL SPHERE (IWANT = 999).
C GANG IS THE INTERVAL BETWEEN B AXES
C IN THE 5 X 5 GRID.
C WHEN THE FOCAL SPHERE IS TO BE SEARCHED
C 10 DEGREES IS RECOMMENDED FOR GANG.
      IF(NERR.EQ.1000) GO TO 42
      ICOUNT=0
C ICOUNT KEEPS A RUNNING SUM OF THE NUMBER
C ITERATIONS IN WHICH NO SOLUTION WAS FOUND.
C IF ICOUNT IS GREATER THAN OR EQUAL TO 12
C NO SOLUTION EXISTS OVER THE ENTIRE
C FOCAL SPHERE INDICATING NERR MUST BE MODIFIED.
      DO 600 IDIP=22,65,43
      PHIZ=IDIP
      ISTEP=(1+IDIP/63)*45
      DO 500 IAZ=45,360,ISTEP
C THE GRID COORDINATES ARE DETERMINED
C BY THE ABOVE LOOPS FOR SEARCHING OVER
C THE FOCAL SPHERE.
      TAUZ=IAZ
      IF(IWANT.EQ.999)READ(5,*)NERR,TAUZ,PHIZ,GANG
C A SPECIAL GRID MAY BE USED AT THIS POINT,
C SUBJECT TO THE VALUE OF IWANT, TO INVESTIGATE
C A PARTICULAR AREA OF THE FOCAL SPHERE.
C WITH THE SPECIAL GRID THE NUMBER OF INCONSISTENT
C OBSERVATIONS (NERR) ARE READ IN AGAIN ALONG WITH THE

```

```

C B AXIS COORDINATES, TAUZ AND PHIZ, AND THE NEW
C GRID INTERVAL.
C TAUZ IS THE AZIMUTH IN DEGREES OF THE B AXIS AND IS
C MEASURED CLOCKWISE FROM NORTH.
C PHIZ IS THE DIP OF THE B AXIS AND IS
C MEASURED FROM THE HORIZONTAL DOWN TO
C VERTICAL IN DEGREES.
    TAUZ1=TAUZ
    PHI1=PHIZ
  10 DO 40 I=1,N
    ROSIN=SIN(DIP(I))
    X(1,I)=COS(AZM(I))*ROSIN
    X(2,I)=SIN(AZM(I))*ROSIN
    X(3,I)=COS(DIP(I))
  40 SENSE(I)=RANDOM(I)
C THE FIRST MOTIONS IN SPHERICAL COORDINATES
C ARE TRANSFORMED INTO VECTOR FORM IN A RIGHT-
C HANDED RECTANGULAR SYSTEM, WHERE
C   NORTH = +X
C   EAST  = +Y
C   DOWN  = +Z
    CALL AB(A,TAUZ,PHIZ)
C THE FIRST TRANSFORMATION MATRIX IS COMPUTED
C USING DIRECTION COSINES.
    CALL AB(B,-TAUZ,90.0)
C A SECOND TRANSFORMATION MATRIX IS COMPUTED
C TO CORRECT FOR UNWANTED ROTATION.
    CALL BA(B,A)
C THE CORRECTION IS ACCOMPLISHED BY MATRIX
C MULTIPLICATION.
    PHI2=90.0-SQRT(8.0)*GANG
    TAUZ=-45.0
    CALL AB(B,TAUZ,PHI2)
    CALL BA(B,A)
    CALL AB(B,-TAUZ,90.0)
    CALL BA(B,A)
    CALL AX(A,X,N)
C THE FIRST GRID POSITION IS COMPUTED AND
C CORRECTED FOR ROTATION.
C THE FIRST MOTIONS ARE TRANSFORMED WITH
C RESPECT TO THE FIRST GRID POSITION
C OR FIRST COORDINATE SYSTEM.
    PHI2=90.0-GANG
    TAUZ=90.0
    CALL AB(B,TAUZ,PHI2)
    CALL AB(C,-TAUZ,90.0)
    CALL BA(C,B)
C THE TRANSFORMATION MATRICES ARE NEXT
C COMPUTED FOR THE REMAINING 4 GRID POSITIONS
C ALONG THE Y AXIS AND CORRECTED FOR ROTATION.
    TAU2=-104.0

```

```

    PHI2=90.0-SQRT(17.0)*GANG
    CALL AB(C,TAU2,PHI2)
    CALL AB(D,-TAU2,90.0)
    CALL BA(D,C)
C THE TRANSFORMATION MATRIX WHICH MOVES THE
C GRID POSITION TO THE NEXT LINE IS FOUND
C AND CORRECTED FOR ROTATION.
C THE PROCEDURE IS REPEATED UNTIL THE 25 TH
C GRID POSITION IS FOUND.
    41 DO 60 M1=1,5
        CALL TEST(X,N,SENSE,NPT,PT,NERR,A)
C EACH OF THE 25 GRID POSITIONS AND FIRST
C MOTIONS ARE TESTED FOR POSSIBLE SOLUTIONS.
C IF THE NUMBER OF P AND T AXES (NPT) IS
C GREATER THAN OR EQUAL TO 250 THEN TOO MANY
C SOLUTIONS EXIST INDICATING THE DATA INPUT
C IS POORLY DEFINED AND CONTROL IS TRANSFERED
C BACK TO 3 TO READ A NEW NERR,IWANT,GANG.
        DO 61 N1=1,4
            IF(NPT.GE.250) GO TO 101
            CALL AX(B,X,N)
            CALL BA(B,A)
        61 CALL TEST(X,N,SENSE,NPT,PT,NERR,A)
            CALL AX(C,X,N)
        60 CALL BA(C,A)
            IF(NPT.LE.0) GO TO 100
C IF THE NUMBER OF P AND T AXES IS LESS THAN
C OR EQUAL TO ZERO ICOUNT IS INCREMENTED BY
C ONE AND THE MESSAGE " NO SOLUTION FOUND FOR
C NERR = 0,1,2,..." IS WRITTEN OUT AND CONTROL
C IS TRANSFERED BACK TO 3.
            NPT1=NPT/2
            WRITE(6,110) TAUZ1,PHI1,GANG,NERR,NPT1
C IF SOLUTIONS ARE FOUND A MESSAGE CONTAINING
C THE AZIMUTH AND DIP OF THE CORRESPONDING GRID
C POSITION, ANGLE INCREMENT, NUMBER OF ERRORS,
C AND NUMBER OF SOLUTIONS IS WRITTEN OUT.
110  FORMAT(" B AXIS AT   ",F8.1," AZIMUTH,DIPPING AT: ",F8.1,
           1 " ANGLE INC.: ",F8.1," NO. OF ERRORS: ",I3,2X,
           2 "NO. OF SOLUTIONS: ",I3)
        24 CALL PLOT(PT,NPT,SENSE,AZC,ROEC)
C THE SOLUTIONS FOUND ARE THEN PREPARED FOR
C PLOTTING.
            IF(IWANT.EQ.999.AND.NPT.GE.1.AND.NPT.LT.250)
C IF THE SPECIAL GRID WAS USED THE SOLUTIONS
C ARE PLOTTED, IF NOT THE SOLUTIONS ARE
C WRITTEN ON TAPE 7 UNTIL THE FOCAL SPHERE
C HAS BEEN TESTED FOR POSSIBLE SOLUTIONS.
            1CALL PLOT(AZC,ROEC,SENSE,NPT)
            IF(IWANT.EQ.999) GO TO 3
            WRITE(7,801) (AZC(I),ROEC(I),SENSE(I),I=1,NPT)

```

```

801 FORMAT(3(3X,F12.5))
    GO TO 46
101 WRITE(6,34) NERR
    34 FORMAT(10X,"TOO MANY SOLUTIONS FOR ",I3," ERRORS")
    GO TO 888
100 ICOUNT=ICOUNT+1
    WRITE(6,33) NERR
    33 FORMAT(10X,"NO SOLUTION FOUND FOR ",I4," ERRORS")
    46 NPT=0
500 CONTINUE
600 CONTINUE
    IF(ICOUNT.GE.12) GO TO 888
    IF(IWANT.EQ.999) GO TO 3
700 LM=1
    REWIND 7
901 READ(7,801) (AZC(LM),ROEC(LM),SENSE(LM),I=1,NPT)
C AFTER THE FOCAL SPHERE HAS BEEN SEARCHED
C THE SOLUTIONS ARE READ FROM TAPE 7 AND PLOTTED.
C CONTROL IS THEN RETURNED TO 3 FOR FURTHER
C ANALYSIS OF THE SAME EARTHQUAKE DATA.
    IF(EOF(7)) 902,905
905 LM=LM+1
    GO TO 901
902 LM=LM-1
    CALL PLOT(AZC,ROEC,SENSE,LM)
888 CONTINUE
    REWIND 7
    GO TO 3
42 STOP
END

```

C
C

```

SUBROUTINE AB(A,TZ,PZ)

```

C
C

```

C THIS SUBROUTINE SETS UP THE NEW RIGHT-
C HANDED COORDINATE SYSTEM, WHERE THE
C B AXIS OR NULL DIRECTION CORRESPONDS
C TO THE Z AXIS AND COMPUTES THE TRANSFORMATION
C MATRIX USING DIRECTION COSINES AS DESCRIBED BY
C HERRMANN (1975)

```

```

    DIMENSION A(3,3)
    TAUZ=TZ*0.01745329252
    PHIZ=PZ*0.01745329252
    TAUX=TAUZ-180.0*0.01745329252
    TAUY=TAUZ-90.0*0.01745329252
    PHIX=90.0*0.01745329252-PHIZ
    PHIY=0.0
    A(1,1)=COS(TAUX)*COS(PHIX)
    A(1,2)=SIN(TAUX)*COS(PHIX)
    A(1,3)=SIN(PHIX)

```

```

A(2,1)=COS(TAU Y)*COS(PHI Y)
A(2,2)=SIN(TAU Y)*COS(PHI Y)
A(2,3)=SIN(PHI Y)
A(3,1)=COS(TAU Z)*COS(PHI Z)
A(3,2)=SIN(TAU Z)*COS(PHI Z)
A(3,3)=SIN(PHI Z)
RETURN
END

```

C
C

```

SUBROUTINE PLOT(AZC,ROEC,SENSE,N)

```

C
C

C THIS SUBROUTINE IS A SOMEWHAT MODIFIED VERSION,
C TAKEN FROM WARNER (1969), OF A TERMINAL OUTPUT
C PLOT FOR PROJECTIONS MADE ON A WULFF NET

```

DIMENSION JM(75),IM(75),AZC(N),ROEC(N),
CCTPC(57,95),SENSE(N),DUMMY(30)

```

```

DATA (JM(I),I=1,74)/95,1,48,48,48,47,46,45,44,43,
C42,41,40,39,38,38,37,36,35,34,33,32,32,31,30,29,28,28,27,
C26,25,25,24,23,22,22,21,20,19,18,17,16,15,14,13,12,11,
C11,10,10,9,8,7,7,6,6,5,5,4,4,3,3,3,2,2,2,1,1,1,1,1,1,
C2,1/

```

```

DATA (IM(I),I=1,74)/29,29,29,57,1,1,1,1,1,1,1,1,1,1,
C1,1,2,2,2,2,2,2,2,3,3,3,3,3,4,4,4,4,5,5,5,5,6,6,6,
C7,7,8,8,9,10,10,11,11,12,12,13,13,14,15,16,16,17,
C17,18,19,20,20,21,22,22,23,24,24,25,26,27,28,1,1,
C2/

```

```

DATA (DUMMY(I),I=1,9)/1H ,1H-,1H*,1HZ,1HC,1HD,1HB,1HP,1HT/

```

```

DO 60 I=1,57

```

```

DO 60 J=1,95

```

60 CTPC(I,J)=0.0

```

XN=N

```

```

DO 107 I=1,N

```

```

RAD=TAN(ROEC(I)/2.0)

```

```

X=RAD*SIN(AZC(I))*142.5+142.5

```

```

Y=RAD*COS(AZC(I))*142.5+142.5

```

C THE DATA ARE CONVERTED TO PROJECTION FORM

```

K=58.0-Y*0.2

```

```

M=X*0.333333+.5

```

```

IF(K.LT.1)K=1

```

```

IF(M.LT.1)M=1

```

```

CTPC(K,M)=5.

```

```

IF(SENSE(I).LT.0.0)CTPC(K,M)=6.

```

```

IF(SENSE(I).EQ.8)CTPC(K,M)=8

```

```

IF(SENSE(I).EQ.9)CTPC(K,M)=9

```

```

IF(SENSE(I).EQ.7)CTPC(K,M)=7

```

C THE ELEMENTS PLOTTED FOLLOW THE NOTATION BELOW

C
C
C
C

```

C = COMPRESSION

```

```

D = DILATATION

```

```

P = PRESSURE AXIS

```



```

C      T = TENSION AXIS
C      B = B AXIS OR NULL DIRECTION
107  CONTINUE
      XXXX=-999.9
      DO 150 I=1,5
        K=IM(I)
        M=JM(I)
        IF(CTPC(K,M).LE.0.0)CTPC(K,M)=XXXX
150  CONTINUE
      DO 151 I=6,74
        I1=IM(I)
        I2=58-I1
        J1=JM(I)
        J2=96-J1
        IF(CTPC(I1,J1).LE.0.0)CTPC(I1,J1)=XXXX
        IF(CTPC(I1,J2).LE.0.0)CTPC(I1,J2)=XXXX
        IF(CTPC(I2,J2).LE.0.0)CTPC(I2,J2)=XXXX
        IF(CTPC(I2,J1).LE.0.0)CTPC(I2,J1)=XXXX
151  CONTINUE
      DO 812 I=1,57
        DO 812 J=1,95
          IF(CTPC(I,J).LE.-999.9) GO TO 814
          IF(CTPC(I,J).LE.0.0) GO TO 810
          IF(CTPC(I,J).EQ.5.)CTPC(I,J)=DUMMY(5)
          IF(CTPC(I,J).EQ.6.)CTPC(I,J)=DUMMY(6)
          IF(CTPC(I,J).EQ.7.)CTPC(I,J)=DUMMY(7)
          IF(CTPC(I,J).EQ.8.)CTPC(I,J)=DUMMY(8)
          IF(CTPC(I,J).EQ.9.)CTPC(I,J)=DUMMY(9)
          GO TO 812
814  CTPC(I,J)=DUMMY(3)
          GO TO 812
810  CTPC(I,J)=DUMMY(1)
812  CONTINUE
      WRITE(6,110)
110  FORMAT(1H1,51X,1H*)
      DO 111 I=1,57
        WRITE(6,112) (CTPC(I,J),J=1,95)
112  FORMAT(5X,95A1)
      DO 111 J=1,95
        CTPC(I,J)=0.0
111  CONTINUE
      RETURN
      END

```

C
C

```

SUBROUTINE P PLOT(PT,N,SENSE,AZC,ROEC)

```

C
C

C THIS ROUTINE PREPARES THE INCOMING DATA
C (IN VECTOR FORM) FOR PLOTTING

```

      DIMENSION PT(3,2000),SENSE(2000),AZC(2000),ROEC(2000)

```

```

      TWOPHI=4*1.570796327
      SRAD=0.01745329252
      PHI=2*1.570796327
      ISG=1
      IPT=8
      DO 40 I=1,N
      IPT=IPT+ISG
      ISG=-ISG
40  SENSE(I)=IPT
      M=N-1
      DO 50 K=1,M,2
      L=((K+1)/2)+N
      SENSE(L)=7
C  SINCE THE P AND T AXES ARE ORTHOGONAL
C  IN THEORY AND ARE PROBABLY FAIRLY CLOSE NUMERICALLY
C  THE B AXIS MAY BE COMPUTED BY TAKING THE CROSS
C  PRODUCT OF THE T AND P AXES
      PT(1,L)=-PT(2,K)*PT(3,K+1)+PT(3,K)*PT(2,K+1)
      PT(2,L)=-PT(3,K)*PT(1,K+1)+PT(1,K)*PT(3,K+1)
50  PT(3,L)=-PT(1,K)*PT(2,K+1)+PT(2,K)*PT(1,K+1)
      N=N+N/2
      DO 60 I=1,N
      AZC(I)=ATAN2(PT(2,I),PT(1,I))
      IF(AZC(I).LT.0.0) GO TO 1
      IF(AZC(I).GT.TWOPHI) GO TO 2
      GO TO 3
1  AZC(I)=AZC(I)+TWOPHI
      GO TO 3
2  AZC(I)=AZC(I)-TWOPHI
3  IF(PT(3,I).LT.0.0) GO TO 4
      GO TO 5
4  ROEC(I)=PHI-ACOS(PT(3,I))
      AZC(I)=AZC(I)+PHI
      GO TO 6
5  ROEC(I)=ACOS(PT(3,I))
6  IF(AZC(I).GT.TWOPHI) AZC(I)=AZC(I)-TWOPHI
C  THE PTB SET IS CONVERTED BACK INTO SPHERICAL
C  FORM AND CORRECTED FOR THE LOWER HEMISPHERE
60  CONTINUE
      RETURN
      END
C
C
      SUBROUTINE AX(A,X,N)
C
C
C  SUBROUTINE AX TRANSFORMS THE FIRST MOTION DATA
C  IN VECTOR FORM TO THE NEW SYSTEM BY MULTIPLYING
C  THE TRANSFORMATION MATRIX TIMES THE COLUMN
C  VECTOR (FIRST MOTIONS)
      DIMENSION A(3,3),X(3,2000),XX(3)

```

```

      DO 40 I=1,N
      DO 10 J=1,3
10    XX(J)=X(J,I)
      DO 30 J=1,3
      X(J,I)=0.0
      DO 30 K=1,3
      X(J,I)=X(J,I)+A(J,K)*XX(K)
30    CONTINUE
40    CONTINUE
      RETURN
      END

```

C
C

```

      SUBROUTINE ATX(A,X,N1,N2)

```

C
C

C THE PTR AXES ARE RETURNED TO THE ORIGINAL
C COORDINATE SYSTEM BY TAKING THE TRANSPOSE OF
C THE APPROPRIATE TRANSFORMATION MATRIX AND
C MULTIPLYING IN THE USUAL MANNER

```

      DIMENSION A(3,3),X(3,2000),XX(3)
      DO 40 I=N1,N2
      DO 10 J=1,3
10    XX(J)=X(J,I)
      DO 30 J=1,3
      X(J,I)=0.0
      DO 30 K=1,3
      X(J,I)=X(J,I)+A(K,J)*XX(K)
30    CONTINUE
40    CONTINUE
      RETURN
      END

```

C
C

```

      SUBROUTINE TEST(X,N,SENSE,NPT,PT,ITEST,A)

```

C
C

C THE TEST ROUTINE SEARCHES THROUGH AN ANGLE OF
C 90 DEGREES IN STEPS OF 5 DEGREES FOR POSSIBLE
C SOLUTIONS AND THEN COMPUTES THE VECTOR COMPONENTS OF THE
C P AND T AXES

```

      DIMENSION ANG(2000),X(3,2000),SENSE(2000),PT(3,2000),A(3,3)
      SRAD=0.01745329252
      ITN=N-2*ITEST

```

C ITN IS A VALUE EQUAL TO THE TOTAL NUMBER OF
C OF FIRST MOTIONS MINUS TWO TIMES THE NUMBER
C ERRORS ALLOWED
C THE TWO IS NEEDED SINCE ONE ERROR RESULTS IN
C THE TOTAL, COMPUTED BELOW, TO BE TWO DATA POINTS
C LESS THAN N (THE NUMBER OF FIRST MOTIONS)

```

      DO 600 I=1,N

```

```

600 ANG(I)=ATAN(X(1,I)/X(2,I))
C ANG REPRESENTS THE FIRST MOTION DATA IN THE
C PLANE Z = 0
C ANG IS COMPUTED FOR TWO REASONS
C (1) TO FORM PART OF THE SCORING METHOD AND
C (2) TO ALLOW THE DATA TO BE ROTATED EASILY
DO 605 IA=1,91,5
TOT=0.0
DO 610 I=1,N
610 TOT=TOT+SIGN(1.0,ANG(I))*SENSE(I)
IF(ABS(TOT).LT.ITN) GO TO 20
C THE VALUE OF TOTAL (TOT) IS FOUND BY THE SENSE
C OF MOTION (+1 OR - 1) AND BY THE VECTOR COMPONENT
C SIGNS IN THE SAME QUADRANT
C IF ALL THE FIRST MOTIONS LIE IN THE PROPER QUADRANTS
C WITH THE CORRECT C OR D THEN TOT = N
C THE ABSOLUTE VALUE OF TOT IS THEN CHECKED AGAINST
C ITN AND IF TOT < ITN NO SOLUTION IS FOUND AND THE
C THE DATA ARE ROTATED 5 DEGREES AND CHECKED AGAIN
NPT=NPT+1
IF(NPT.GE.250) RETURN
SONG=(SIGN(1.0,TOT)*45.0-IA+1)*SRAD
C IF THE TOTAL IS GREATER THAN OR EQUAL TO ITN
C THEN A SOLUTION IS FOUND AND THE NUMBER OF P AND
C T AXES (NPT) IS INCREMENTED BY 1 AND THEN 2 FROM
C THE ORIGINAL VALUE OF NPT IN ORDER TO STORE THE
C THE SOLUTIONS IN THE ARRAY (PT)
PT(1,NPT)=SIN(SONG)
PT(2,NPT)=COS(SONG)
PT(3,NPT)=0.0
NPT=NPT+1
PT(1,NPT)=SIN(SONG-90.0*SRAD)
PT(2,NPT)=COS(SONG-90.0*SRAD)
PT(3,NPT)=0.0
C THE VECTOR POSITIONS FOR THE P AND T AXES
C ARE COMPUTED
NPTM1=NPT-1
CALL ATX(A,PT,NPTM1,NPT)
C THE PROPER TRANSFORMATION MATRIX IS PRESERVED
C FROM THE MAIN ALLOWING THE P AND T AXES TO BE
C TRANSFORMED BACK TO THE ORIGINAL COORDINATE
C SYSTEM BY UTILIZING THE TRANSPOSE ROUTINE ATX
20 CONTINUE
C AT THIS POINT THE FIRST MOTION DATA ARE
C REDEFINED IN RADIAN MEASURE AND MAPPED
C INTO THE LOWER HEMISPHERE IF NOT ALREADY
C THAT FORM
DO 605 I=1,N
ANG(I)=ANG(I)+(5)*SRAD
IANG=ANG(I)/(1.570796327)
605 ANG(I)=ANG(I)-IANG*3.141592654

```

```
C   ANG IS THEN INCREMENTED AGAIN AND THE TEST IS MADE  
C   OVER UNTIL ALL OR NO SOLUTIONS ARE FOUND
```

```
    RETURN  
    END
```

```
C  
C
```

```
    SUBROUTINE BA(B,A)
```

```
C  
C
```

```
C   THIS SUBROUTINE TAKES TWO 3 X 3 MATRICES AND  
C   MULTIPLIES THEM TOGETHER
```

```
    DIMENSION B(3,3),A(3,3),AA(3)  
    DO 10 I=1,3  
    DO 12 J=1,3  
    AA(J)=A(J,I)  
12  A(J,I)=0.0  
    DO 10 J=1,3  
    DO 10 K=1,3  
10  A(J,I)=A(J,I)+B(J,K)*AA(K)  
    RETURN  
    END
```

BIBLIOGRAPHY

- Amick, D.C. and P. Talwani (1977). A closer look at the geology in the vicinity of Lake Jocassee, S.C. in light of the recent seismicity, 49th annual meeting of the East. Sec. Seis. Soc. Am. (abstract).
- Benson, A.F. and C.H. Fogle (1974). Intensity survey of Lincoln County, McCormick County, South Carolina, earthquake of August 2, 1974, Earthq. Not., 45, 27-29.
- Bollinger, G.A. (1972). Historical and recent seismic activity in South Carolina, Bull. Seis. Soc. Am. 62, 851-864.
- Bollinger, G.A. (1973). Seismicity and crustal uplift in the southeastern United States, Am. Jour. Sci., 273-A, 396-408.
- Bollinger, G.A. (1975). A catalog of southeastern United States earthquakes 1752 through 1974, Dept. of Geo. Sci. Vir. Polytech and State Univ., Research Division Bulletin 101.
- Bollinger, G.A., C.J. Langer and S.T. Harding (1976). The eastern Tennessee earthquake sequence of October through December, 1973, Bull. Seis. Soc. Am., 66, 525-547.
- Bridges, S.R. (1975). Evaluation of Stress Drop of the August 2, 1974 Georgia-South Carolina Earthquake and Aftershock Sequence. Georgia Institute of Technology, Master's Thesis, 103 pages.
- Brune, J.N. (1961). Radiation pattern of Rayleigh waves from the Southeast Alaska earthquake of July 18, 1958, Publ. Dom. Obs. Ottawa, 24, 373-383.
- Brune, J.N. and C.R. Allen (1967). A low-stress-drop low-magnitude earthquake with surface faulting: The Imperial, California earthquake of March 4, 1966, Bull. Seis. Soc. Am., 57, 501-514.
- Byerly, P. (1926). The Montana earthquake of June 28, 1925, Bull. Seis. Soc. Am., 16, 209-263.
- Carver, David, L.M. Turner, A.C. Tarr (1977). South Carolina Seismological Data Report. U.S.G.S. Open file Rept. 77-429.
- Cattermole, J.M. (1962). Geology of the Maryville Quadrangle, Tennessee, U.S. Geol. Survey Geol. Quad. Map GQ-163.

- Champion, J.N., JR. (1975). A Detailed Gravity Study of the Charleston, South Carolina Epicentral Zone. Georgia Institute of Technology, Master's Thesis, 97 pages.
- Chandra, Umesh (1971). Combination of P and S data for the determination of earthquake focal mechanism, Bull. Seis. Soc. Am., 61, 1655-1673.
- Chinnery, M.A. (1964). The strength of the earth's crust under horizontal shear stress, J. Geophys. Res., 69, 2085-2089.
- Cooke, C.W. (1936). Geology of the Coastal Plain of South Carolina, U.S. Geol. Sur. Bull., 867.
- Denman, H.E., Jr. (1974). Implications of Seismic Activity at the Clark Hill Reservoir. Georgia Institute of Technology, Master's Thesis.
- Dillinger, W.H., A.J. Pope and S.T. Harding (1972). Determining maximum likelihood body wave focal plane solutions, Geophys. J. Roy. Astr. Soc., 30, 315-329.
- Dunbar, D.M. (1977). Seismic Velocity Model of the Clark Hill Reservoir. Georgia Institute of Technology, Master's Thesis.
- Fletcher, J.P., M.L. Sbar, and L.R. Sykes (1974). Seismic zones and travelttime anomalies in eastern North America related to fracture zones active in the early opening of the Atlantic (abstract), EOS Trans. AGU, 55, 497.
- Fogle G.H., R.M. White, A.F. Benson, L.T. Long, G.F. Sowers (1976). Reservoir induced seismicity at Lake Jocassee, northwestern South Carolina, Law Engineering Testing Company, Marietta, Georgia.
- Galitzin, B. (1909). Zur Frage der Bestimmung des Azimuts der Epizentrums eines Bebens. Assoc. Intern. de Seismologic, pp.132-141.
- Garland, G.D. (1971). Introduction to Geophysics Mantle Core Crust. W.B. Saunders Company, Philadelphia, Pa.
- Gilbert, F. and G.J.F. MacDonald (1961). Free oscillations of the Earth I Toroidal oscillations, J. Geophys. Res., 65, 675-693.
- Herrmann, R.B. (1975). A student's guide to the use of P and S wave data for focal mechanism determination, Earthquake Notes, 46, 29-39.
- Hirasawa, T. (1966). A least squares method for the focal mechanism determination from S wave data; Part I, Bull. Earthq. Res. Inst., 44, 901-918.

- Honda, H. (1957). The mechanism of the earthquakes, Sci. Repts. Tohoku Univ., Ser 5: Geophys. Suppl. 9, 1-46.
- Honda, H. (1961). The generation of seismic waves. Publ. Dom. Obs. Ottawa, 24, 329-334.
- Hooker, V.E. and C.F. Johnson (1969). Near surface horizontal stresses, including the effects of rock anisotropy, U.S. Bur. Mines Rept. Inv. 7224, 29pp.
- Hsiao, Helmut Y.A. (1977). The Stress Amplification Mechanism for Intraplate Earthquakes Applied to Southeast United States. Georgia Institute of Technology, Master's Thesis.
- Kasahara, T. (1963). Computer program for a fault-plane solution, Bull. Seis. Soc. Am., 53, 1-13.
- Keilis-Borok, V.I., ed., Bessonova, E.N., Gotsadez, O.D., Kirillova, I.V., Kogan, S.D., Kikhtikova, T.I., Malinovskaya, L.N., Pavlova, G.I.; and A.A. Sorskii (1957). Investigation of the mechanism of earthquakes, English translation published by American Geophysical Union.
- Keilis-Borok, V.I., Pistetskii-Shapiro, I.I., Pisarenko, V.F. and T.S. Zhelankina (1972). Computer determination of earthquake mechanism; Computational Seismology, ed. V.I. Keilis-Borok, Plenum Publishing Corp., New York.
- Knopoff, L. (1961). Analytical calculation of the fault plane problem, in A Symposium on Earthquake Mechanism, Publ. Dom. Obs., 24, 309-315.
- Long, L.T. (1974). Earthquake sequences and "b" values in the southeast United States, Bull. Seis. Soc. Am., 64, 267-273.
- Long, L.T., Denman, H.E., Hsiao, H., and G.E. Marion (1976). Gravity and seismic studies in the Clark Hill Reservoir Area, Georgia Geological Society, Guidebook 16, pp.33-41.
- Long, L.T. and S.A. Guinn (1976). The Dalton, Georgia earthquake of February 4, 1976, Earthquake Notes, East. Sec. Seis. Soc. Am., vol. 47, no. 4, p.5.
- Long, L.T. and J.W. Champion, Jr. (1977). Bouguer gravity map of the Summerville-Charleston, South Carolina epicentral zone and tectonic implications, U.S. Geol. Sur. Prof. Paper No.1028, in preparation.
- Love, A.E.H. (1903-1904). The propagation of wave-motion in an isotropic elastic solid medium. Proc. London Math. Soc., Ser 21, 291-344.

- Mansfield, W.C. (1936). Some deep wells near the Atlantic coast in Virginia and the Carolinas, U.S Geol. Sur. Prof. Paper 186, 159-161.
- Marion, G.E. (1977). A Spectral Analysis of Microearthquakes that Occur in the Southeastern United States. Georgia Institute of Technology, Master's Thesis, 154 pages.
- McKee, J.H. (1974). A Geophysical Study of Microearthquake Activity near Bowman, South Carolina. Georgia Institute of Technology, Master's Thesis, 65 pages.
- McKenzie, D.P. (1969). The relation between fault plane solutions for earthquakes and the directions of the principle stresses, *Bull. Seis. Soc. Am.*, 59, 591-601.
- Mendiguren, J.A. (1969). Study of focal mechanism of deep earthquakes in Argentina using non linear particle motion of S waves, *Bull. Seis. Soc. Am.*, 59, 1449-1473.
- Money maker, B.C. (1954-1972). Earthquakes in Tennessee and nearby sections of neighboring states, *Jour. Tenn. Acad. Sci.*, no.29, 30, 32, 33, 47.
- Nankano, H. (1923). Notes on the nature of forces which give rise to earthquake motions, *Central Meteor. Observ. Japan, Seismol. Bull.*, 1, 92-130.
- Nuttli, O.W. (1961). The effect of the earth's surface on the S wave particle motion, *Bull. Seis. Soc. Am.*, 51, 237-246.
- Oliver, J.E. and B. Issacks (1972). Seismicity and tectonics of the eastern United States, *Earthq. Not.*, XLIII, NO.1, 30pp.
- Paris, T.A. (1976). The Geology of the Lincolnton 7.5' Quadrangle. Georgia Institute of Technology, Master's Thesis, 191 pages.
- Pho, H.T. and L. Behe (1972). Extended distances and angles of incidence of P waves, *Bull. Seis. Soc. Am.*, 62, 885-902.
- Pooley, R.N., Meyer, R.P. and G.P. Woolard (1960). Yamacraw Ridge, Pre-Cretaceous structure beneath South Carolina-Georgia Coastal Plain, *Bull. Am. Ass. Petrol. Geol.*, 44, 1254-1255.
- Pope, A.J. (1972). Fiducial regions for body wave focal plane solutions, *Geophys. J.R. Astr. Soc.*, 30, 331-342.
- Raisz, Erwin (1970). Physiography. Goode's World Atlas, thirteenth edition, Rand McNally Co., pp.60-61.

- Rodgers, John (1970). The Tectonics of the Appalachians. Wiley and Sons, 271 pages.
- Sbar, M.L. and L.R. Sykes (1973). Contemporary compressive stress and seismicity in eastern North America; an example of intraplate tectonics, *Geol. Soc. Am. Bull.*, 84, 1861-1882.
- Scheffler, P.K. (1976). The McCormick County, South Carolina, Earthquake of August 2, 1974: Geological and Geophysical Investigations. University of South Carolina, Master's Thesis, 65 pages.
- Scheidegger, A.E. (1964). The tectonic stress and tectonic motion direction in Europe and western Asia as calculated from earthquake fault plane solutions, *Bull. Seis. Soc. Am.*, 54, 1519-1528.
- Secor, D. (1974). Detailed geology of Clark Hill epicentral area, unpublished.
- Staub, W.P. and V.C. Johnson (1970). Gravity survey of Knox County, Tennessee, *Tenn. Div. Geol. Bull.*, 70, 74-75.
- Stauder, William S.J. (1962a). S-wave studies of earthquakes of the north Pacific, part I: Kamchatka, *Bull. Seis. Soc. Am.*, 52, 527-550.
- Stauder, William S.J. (1962b). The focal mechanism of earthquakes, *Adv. Geophys.*, 9, 1-76.
- Steketee, J.A. (1958). Some geophysical applications of the elasticity theory of dislocations, *Can. Jour. Phys.*, 36, 1168-1198.
- Stevens, A.E. (1967). S wave earthquake mechanism equations, *Bull. Seis. Soc. Am.*, 58, 1071-1082.
- Street, R.L., Herrmann, R.B. and O.W. Nuttli (1974). Earthquake mechanics in the Central United States, *Science*, 186.
- Taber, Stephen (1914). Seismic activity in the Atlantic Coastal Plain near Charleston, South Carolina, *Bull. Seis. Soc. Am.*, 4, 108-160.
- Talwani, Pradeep (1976). Earthquakes associated with the Clark Hill Reservoir, South Carolina--a case of induced seismicity, *Engineering Geology*, 10, 239-253.
- Tandon, A.N. and H.N. Srivastava (1975). Focal mechanisms of some recent Himalayan earthquakes and regional plate tectonics, *Bull. Seis. Soc. Am.*, 65, 963-969.

- U.S. Engineer District, Savannah Corps of Engineers, Savannah, Georgia (1977). Geological and Seismological Evaluation of Earthquake Hazards at the Richard B. Russell Project.
- Udias, A. and D. Baumann (1969). A computer program for focal mechanism determination combining P and S wave data, Bull. Seis. Soc. Am., 59, 503-519.
- Udias, A (1964). A least squares mechanism determination using S wave data, Bull. Seis. Soc. Am., 54, 2037-2047.
- Warner, J. (1969). Fortran IV program for construction of PI diagrams with the Univac 1108 computer, Computer Contr., 33, Kansas State Geol. Sur.
- Wallace, R.E. (1968). Earthquake of August 19, 1966, Varto area, eastern Turkey, Bull. Seis. Soc. Am., 58, no.1, 11-45.
- Watkins, J.S. (1964). Regional geologic implications of the gravity and magnetic fields of a part of eastern Tennessee and southern Kentucky, U.S. Geol. Sur. Prof. Paper 516-A, A1-A17.
- Wickens, A.J. and J.H. Hodgson (1967). Computer reevaluation of earthquake mechanism solutions 1922-1962, Publ. Dom. Obs., 33, 560.
- Woolard, G.P. Bonini, W.E. and R.P. Meyer (1957). A seismic refraction study of the subsurface geology of the Atlantic Coastal Plain and continental shelf between Virginia and Florida, University of Wisconsin, 128 pp.
- Wyss, M. and J.N. Brune (1968). Seismic moment, stress and source dimensions for earthquakes in the California-Nevada region, J. Geophys. Res., 73, 4681-4694.